Evaluating Determinants of Mitochondrial Mutagenesis and their Intersections with Cell Fate

William Valente

A dissertation

submitted in partial fulfillment of the

requirements for the degree of

Doctor of Philosophy

University of Washington

2018

Reading Committee:

Jason Bielas, Chair

Marshall Horwitz

Peter Rabinovitch

Program Authorized to Offer Degree:

Molecular and Cellular Biology

University of Washington

Abstract

Evaluating Determinants of Mitochondrial Mutagenesis and their Intersections with Cell Fate

William Valente

Chair of the Supervisory Committee:
Jason Bielas
Department of Pathology

Mitochondria are critical components of cellular metabolism as mediators of oxidative phosphorylation. As semi-autonomous organelles, mitochondria possess their own DNA (mtDNA) which encodes elements of the electron transport chain (ETC). Aberrations in the mitochondrial genome are associated with neurodegenerative diseases, metabolic syndromes, cancer, and pathologies of aging; although establishing direct links between cause and consequence of mtDNA mutagenesis has remained elusive. In this thesis, I sought to directly test two possible mechanisms of somatic mitochondria mutagenesis and to characterize the effects of a model of reduced mtDNA mutation upon cell fate. First, I evaluated extrinsic genotoxic exposures, in either the form of established nuclear mutagens benzo[a]pyrene or N-ethyl-nitrosourea, for their effects on mtDNA frequency with newly developed droplet digital PCR assays. Here I found that these classic nuclear mutagens damage mtDNA, but are not capable of significant mtDNA mutation induction. Next, I evaluated the cellular effects resulting from expression of a mitochondrial-targeted form of the antioxidant enzyme catalase, which has featured in a murine model of increased lifespan which also demonstrated attenuated mtDNA mutation frequency. Finally, I addressed the hypothesis that metabolic byproducts of oxidative

metabolism, reactive oxygen species (ROS), can influence mtDNA mutagenesis. I demonstrate, using genetically-encoded proteins with spatiotemporal control of ROS production, that ROS induce mtDNA damage and mutation. The results of this work have potentially broad-ranging impacts upon mitochondrial mutagenesis research, translational efforts to characterize tumor progression, and models of cellular aging.

TABLE OF CONTENTS

LIST OF FIGURES

LIST OF TABLES

ACKNOWLEDGEMENTS

The work presented in this thesis could not have been accomplished alone. I have enjoyed significant support from friends, family, mentors, co-workers, and co-authors throughout my graduate studies: to them I can scarcely extend sufficient gratitude.

To my friends, I thank you for reminding me that life exists outside of lab. Whether skiing, hiking, or even grabbing a beer, you offered support, advice, and inspiration. I would especially like to thank my fellow MSTP who started this academic journey with me, especially Ken Chen, Mike Doud, Paul Lindau, Aaron “Butters” Seo, and Natalie Vandeven.

To my parents and siblings, my successes are yours. You instilled the values and aspirations that brought me to where I am today. Your encouragement and reassurance strengthen my resolve during tough times.

To my mentor Jason Bielas and committee members David Hockenbery, Marshall Horwitz, Mary-Claire King, and Peter Rabinovitch, the passion and intellect you apply to science are an inspiration. My research and my growth as a scientist

To Henk Viljoen, who gave me my first lab position and many other scientific firsts, those opportunities have shaped me as a scientist and person.

To my fellow lab members, especially Nolan Ericson and Becca Martin, I cannot express how much I appreciate the camaraderie, scientific context, research direction, and sincere discussion you have given.

Chapter 1. INTRODUCTION

The following chapter draws from published work (1), particularly the chapter: "Mitochondrial Mutagenesis in Cancer" by William Valente & Jason Bielas in Mitochondria and Cell Death (pp. 131-148) .

"[T]he chromosomes are in no sense rulers [*Beherrscher*] of the cytoplasm's work; they render it assistance" (*sie sind seine Hilfsmittel*) (Correns 1937, 128, citing V. Grégoire) .

1.1 The Mitochondrial Genome

Decades before the first electron micrographs discovered mitochondrial DNA (mtDNA) in 1963 (2), geneticists fiercely debated whether the nucleus maintained a monopoly on heredity (3). According to the contemporary theory of 'cytoplasmic inheritance' (4), a prelude in some aspects to mitochondrial genetics, "[t]he transmission of cytoplasmic characters exists in some cases due to plastids, in others probably due to plasmagenes and to viruses. In still other cases, a general quality of the cytoplasm, such as a characteristic degree of hydration of the plasmon colloids, a particular degree of viscosity or osmotic value may be transmitted purely maternally"(4). Conclusive evidence of maternal inheritance of mtDNA in mammals would wait until 1974 (5), and fourteen years thereafter until mtDNA mutations were first implicated in the etiology of human diseases (6, 7). Since those discoveries, appreciation for both mtDNA variation in disease pathogenesis and the organelle's role in many cellular processes has steadily grown.

The likely product of an early endosymbiotic event, mitochondria are indispensable to eukaryotes, as the circular mitochondrial genome encodes essential elements of cellular respiration. These genes underscore both the status of mitochondria as semi-autonomous

organelles and their importance to oxidative metabolism, as they encode a mitochondrial-specific repertoire of 22 tRNA, 2 rRNA, and 13 polypeptide constituents of the electron transport chain (ETC). At 16,569 base-pairs, the human mitochondrial genome may be dwarfed by the comparably expansive nuclear genome, but the host of mitochondrial disorders ascribed to hereditary mtDNA polymorphisms demonstrate the health consequences of aberrant mtDNA (8). As well, variants in mtDNA are associated with neurodegenerative disorders, metabolic syndromes, cancer, and aging (9). However, establishing whether mtDNA mutations are active players or neutral passengers in these pathological states has proven difficult. The lack of scientific consensus for the mechanisms of somatic mitochondrial mutagenesis compounds this challenge, which provides the impetus for much of the work described in this thesis.

1.2 Detecting and Describing Mitochondrial DNA Variation

No doubt, the distinct, non-Mendelian genetics of mtDNA complicate its study: extensive variation exists at the cell, tissue, and organismal levels. A single human cell can house hundreds of mitochondria, each bearing several copies of the mitochondrial genome. The existence of a single intracellular sequence identity is denoted by the term ‘homoplasmy’; conversely, ‘heteroplasmy’ implies multiple, distinct sets of mtDNA in a given cell or tissue. Homoplasmy, until recently, was considered the normal state of healthy cells. However, with advancements in mtDNA mutation detection technology, mtDNA subpopulations are ubiquitously identified in cells and tissues, eroding the previous concept of homoplasmy (10, 11).

The technological limitations found in early studies drastically affected the measurement resolution of mtDNA mutation studies, which erroneously described the mitochondrial genome as homogenous sequences within an individual. In contrast, current-day assays of mtDNA sequence and mutation frequency have enhanced sensitivity that can detect mutant mtDNA at

frequencies of 1 mutant in 10^8 base-pairs or less (12-15). With these refined techniques, surveys of mitochondrial genomes have revealed widespread heteroplasmy, indicating 'homoplasmy' is dependent on assay measurement resolution (10, 11, 16).

Of particular consideration amongst these newer techniques, the Digital Droplet Random Mutation Capture (dRMC) and Digital Deletion Detection (3D) assays (12, 17) (Figure 1.1), modifications of the previous RMC methodology (14), are employed extensively throughout this thesis. For both dRMC and 3D, rare mutation-bearing molecules are selectively enriched through

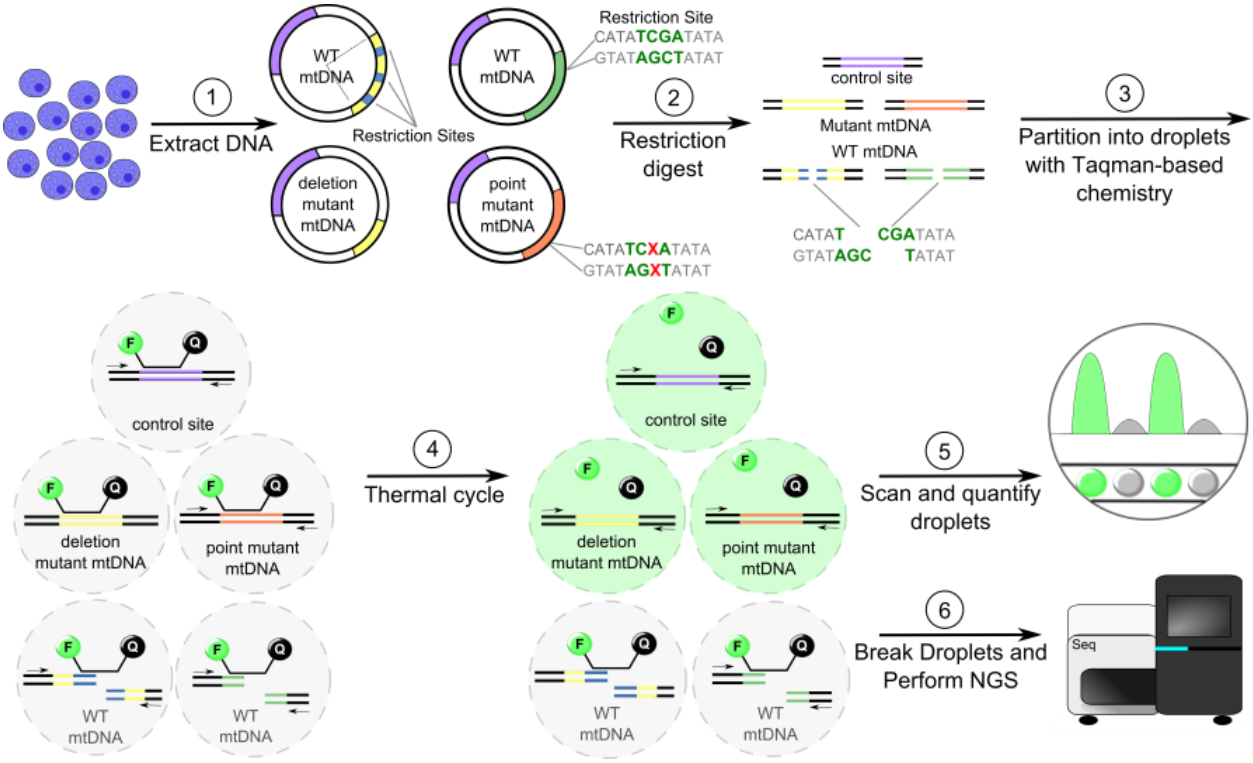

Figure 1.1 Overview of 3D and dRMC for deletion and point mutation detection. (1) DNA is extracted. (2) DNA is digested by a restriction endonuclease. Copies of mtDNA that are wild-type at TaqI endonuclease sites (WT) will be digested, whereas mutant mtDNA will be resistant to cleavage. A control region devoid of the chosen restriction site(s) is used to quantify total mtDNA copies interrogated. (3) Digested DNA is added to a PCR mastermix with locus-specific primers which flank the digest site and Taqman probes, and then partitioned into thousands of 1 nL droplets in an oil immersion. Mutant mtDNA and the control region are substrates for amplification, whereas the WT mtDNA at the mutational target is not. (4) Droplets are thermal cycled to amplify target DNA as well as release the Taqman probe fluorophore from its quencher through Taq polymerase's inherent exonuclease activity. The ongoing rounds of amplification displace and cleave more probe, accumulating fluorescence. (5) Post-amplification, droplets are passed through an adapted flow cytometer, where they are detected and quantified. Mutation frequencies are calculated by dividing the mutant concentration by the concentration of the control region. (6) Droplets may alternatively be broken open and sequenced.

endonucleolytic destruction of wild-type target sites prior to emulsion PCR in droplets with TaqMan fluorescent probes. Reactions screen ~10^7 mitochondrial genomes per sample to acquire an accurate appraisal of mutation frequency.

Measurements with these newer, more accurate techniques can describe subclonal mutations in mtDNA which reflect the mechanism and extent of mutagenesis. In contrast to clonal mutations, rare (also referred to as 'spontaneous' or 'random') mutations arise in cell divisions after the establishment of a clonal population, and exist in only a portion of the cell population. Rare mutation frequency, or *mutation load*, reflects the *mutation rate* and is dependent on the number of cell divisions after the founding of a clonal population. The frequency of rare mtDNA mutations is 2 – 3 orders of magnitude greater than that of nuclear DNA (approximately 1 x 10^{-6} mutations/base-pair in mtDNA). The capacity to quantify mtDNA variation at or below the resting rare mutation frequency is of particular importance to evaluation of models and proposed mechanisms of mtDNA mutagenesis.

1.3 Extant Models of mtDNA mutagenesis

Those factors influencing the generation and frequency of somatic mtDNA mutations may be distilled into three main mechanisms; namely, selective pressure, genomic drift, and induction. Research on these models is most consistently explored in the biological contexts of carcinogenesis and aging metabolism.

1.3.1 *Selective Pressure*

The majority of the somatic mutations observed in cancers are non-synonymous variants when observed in protein coding regions (18). Additionally, the proportion of protein-altering mutants is much greater in somatic mutations compared to early developmental or inherited polymorphisms (19). This finding raises interest in defining how selective pressure could be involved in mtDNA mutagenesis during tumor progression.

Mutation frequencies, and the observed distributions of specific mutation types, for inherited variants and somatic DNA mutations are drastically different. Evidence suggests germline transmission of mtDNA is under strong purifying selection (20). In transmitted mtDNA, mutation frequencies are higher at 3rd codon positions, explained by the variably specific mRNA:anticodon interactions at this position during peptide synthesis (21). These results seemingly contrast with the supposed pro-tumorigenic effects of mtDNA mutations observed in many cancers.

In the protein-coding regions of tumor mtDNA, negative selective pressure against mutation is either relaxed or may be positive (22-24). However, negative selection is almost universally present on large deletions. Cell survival depends on mitochondrial function, and mutations with adverse implications for cellular bioenergetics will likely be selected against based on cellular fitness (19, 25, 26). For example, a meta-analysis of studies describing the prevalence of the age-associated mitochondrial 'common deletion' in breast cancer, which removes 7 peptide-coding genes, revealed it is under significant negative selection pressure compared to normal tissue (27). 'Common deletion' prevalence is inversely correlated with advancing colorectal cancer stage (28), indicating it may pose fitness challenges to neoplasms during tumor progression.

In contrast, many single gene mutations seemingly facilitate aggressive and resilient cancer phenotypes that conceivably increase cancer cell fitness. Complex I mutant tumors, with a heteroplasmic frame-shift in *ND5*, have shown enhanced colony formation and *in vivo* tumor growth when injected into nude mice (29). A homoplasmic point mutation in the ATP synthase subunit 6 (ATP6), typically associated with inherited mitochondrial encephalomyopathy, conferred apoptotic resistance to a human ovarian cancer cell line (23). Notably, expression of

wild-type *ATP6* abrogated growth advantages in the mutant cells, and expression of mutant *ATP6* in a wild-type background accelerated tumor growth and diminished respiration (23). Much of the enrichment for mutant mtDNA in cancers appears predicated on functional consequences of these mutations, implying selection primarily occurs at the cellular level at a point when mutations have aggregated in sufficient concentration to alter tumor phenotype.

In an investigation of tumor-specific variants within five tumor types present in The Cancer Genome Atlas (TCGA), paired normal and tumor tissues were assayed for mutations (18). In protein coding regions, non-synonymous mutations represented 86% of somatic mutations, yet only 31% of inherited variants; and of the non-synonymous variants, only 3% of inherited versus 50% of somatic mutations were predicted to have high impact on protein function. This suggests somatic mtDNA point mutations in cancers represent a marked departure from the constraints of germline polymorphisms, existing under separate selection pressures and/or distinct conditions of mutation susceptibility.

1.3.2 *Genomic Drift*

Mutations in mtDNA, even pathogenic mutations, are relatively common in the human population at low levels (30, 31). Tumor mtDNA mutants, in models lacking selection bias, can originate from low-level heteroplasmic mutants (31-33). Given the stem cell-like nature of many tumors, the many cellular divisions preceding transformation may allow for stochastic isolation and enrichment of a unique mtDNA genome without any need for growth advantages or tumorigenic phenotypes derived from that mtDNA mutant (32). In mathematical models of this phenomenon, random processes predict that the majority of tumors (58%) will harbor homoplasmic mtDNA mutations given the growth parameters of many tumors. Patient-derived samples support this model with instances of germ-line mutant mtDNA expanding to

homoplasmic abundance in head and neck squamous cancer (34). However, mtDNA mutations' random drift in tumorigenesis has been called into question recently (26).

Sequencing datasets offering comparisons across tumors show predominantly relaxed negative selection for somatic mtDNA mutations relative to the germline, but possible positive selection at residues of high functionality (35). A large cohort analysis observed strong negative selection pressure on truncating mtDNA mutations and on tRNA, especially within anticodon sequences (36). Despite the many descriptions of individual mtDNA mutations facilitating cancers with ostensible fitness benefits, selection pressures within tumors are predominantly negative or neutral for many mtDNA mutations (20, 26, 36), and positive selection has not been demonstrated in a large study (> 1000 patients) (35).

1.3.3 *Induction, or damage to the mitochondrial genome*

The primary mtDNA mutations observed in cancer and normal tissues are C → T and T → C transitions, with higher proportion of the former on the heavy strand and the latter on the light strand (36). The mtDNA leading strand during replication is the heavy strand. The strand-biased distribution suggests mutations could be coupled to events during replication. Lending credence to this assertion, C → T transitions are consistent with base mis-pairing after deamination of cytosine, a reaction 140-fold faster in single-stranded DNA (37).

In addition to endogenous sources of mutagens, namely ROS, the mitochondrial genome is noted for its sensitivity to damage by environmental toxins (38, 39) and genotoxic agents employed in chemotherapy (40-44). By extension, nuclear carcinogens are proposed to play a role in the genesis of mtDNA mutations. In early reports derived from observations in buccal epithelium swabs of patients with smoking-associated lung carcinomas, the frequency of mtDNA mutations was significantly elevated over normal tissue (45, 46). However, these results have

attracted scrutiny (47), and the inability to observe mtDNA mutational susceptibility in smokers (48) has since obscured the possible role of tobacco-derived carcinogens in mtDNA mutagenesis. In a recent study of oral squamous cell carcinoma in Taiwanese patients, neither smoking status nor areca quid chewing had a significant effect on the presence of mutations across the mitochondrial genome (48). Considering other classic nuclear mutagens, there has been some suggestion that UV exposure may precipitate neoplastic change and mtDNA mutation in squamous carcinoma of the skin (49). A mutation in mtDNA derived from murine skin cancer produced enhanced cellular growth kinetics, but whether UV irradiation or the transformation process caused the mutation is unclear (50). Thus far few studies link known nuclear mutagens to increased mitochondrial mutagenesis (51, 52). Thus it appears, despite the elevated spontaneous mitochondrial genome mutation frequency relative to nDNA, mtDNA is remarkably resistant to induced mutation when exposed to established nDNA mutagenic compounds (36, 53).

1.4 METABOLISM, ROS, AND MUTAGENESIS

In a previous study on colorectal tissue performed by my advisor's group (13), quantification of mutation load within mtDNA revealed an average three-fold lower burden in patient-matched carcinoma tissue compared to normal tissue. These results were surprisingly different from observations of nuclear DNA mutation load in tumors, which demonstrates > 100-fold increase in random mutation frequency compared to matched normal tissue (54). The mtDNA mutation spectrum in normal, adenoma, and carcinoma tissues showed certain mutations occurred at similar frequency among tissues, but a significantly lower frequency of C:G → T:A mutations explained the majority of the discrepancy in observed mutation frequency. This transition mutation is associated with deamination of cytosine, an event linked to oxidative damage (55).

The predominant source of oxidative damage to mtDNA is the Electron Transport Chain (ETC) processing reduced energy metabolites derived from the Tricarboxylic Acid (TCA) cycle

(56). A shift in metabolism, favoring glycolysis over OXPHOS, is a hallmark of many tumor cells (57). Profiling the intermediate energy metabolites of glycolysis and OXPHOS in the studied colorectal tissues revealed that citrate, a TCA cycle intermediate that correlates with mitochondrial respiration, was decreased in cancer, whereas lactate, the end-product of anaerobic glycolysis, was increased. Mutation frequency of all samples plotted against the ratio of citrate to lactate revealed a non-zero slope, consistent with the hypothesis that a large portion of mtDNA mutation derives from oxidative damage. These findings provided inspiration for portions of the work undertaken in **Error! Reference source not found.** and Chapter 4.

Mutagenesis of mtDNA by ROS, as suggested in the colorectal carcinoma findings, is a facet of the "Mitochondrial Theory of Aging" (MToA) (58). Within the framework of MToA, ROS production with the mitochondrial matrix is a normal byproduct of respiration that induces mutations in proximate mtDNA. These mutations lead to aberrant gene products and dysfunctional mitochondrial processes, including OXPHOS. Completing the circuit, defective respiration produces increased ROS, which feed the cycle of mutation and dysfunction. This theory, while contentious (59), is not without support. Expression of a mitochondrial-targeted transgene containing catalase (mCAT), an enzyme responsible for the reduction of hydrogen peroxide into water and oxygen, demonstrated extended lifespan in mice. In addition to increased longevity, mCAT mice have lower mtDNA frequencies. Consistent with attenuated ROS as a mechanism of mutation reduction in colorectal carcinoma, mtDNA mutation spectra in mCAT mice echo the reduced C→T mutation burden found in colorectal carcinoma compared to normal

tissues (Figure 1.2).

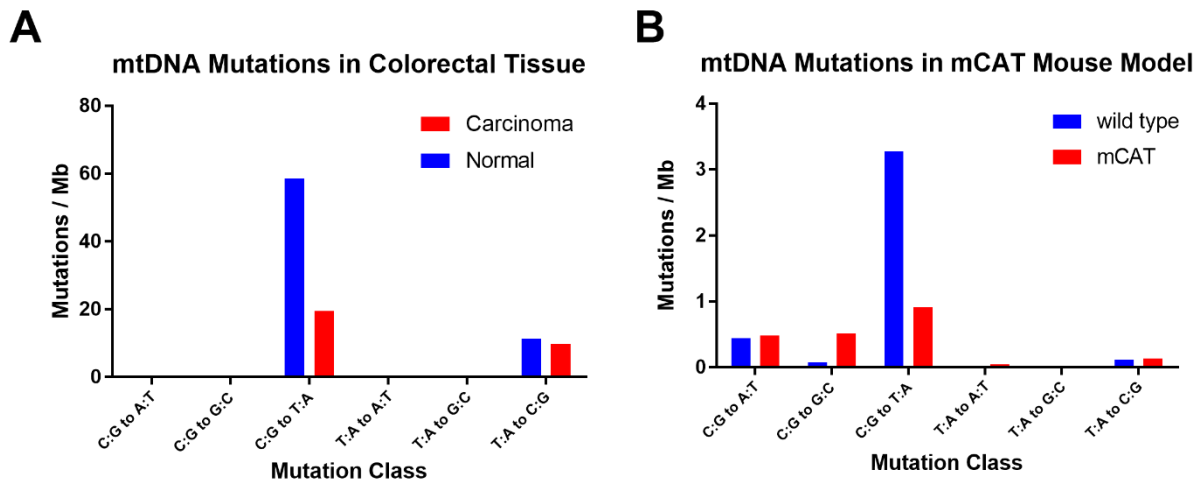

Figure 1.2 Similar mtDNA mutation spectra in colorectal carcinoma and mCAT mice compared to normal or wildtype. (A) Mutation spectrum of colorectal carcinoma along with matched normal colon tissue (13). The decrease in mtDNA mutation in colorectal cancer is attributed to a reduction in C:G→T:A transitions. (B) Mutation spectra of cardiac tissue from mCAT mice (long-lived mice expressing a mitochondrial-targeted catalase that reduces the reactive oxygen species hydrogen peroxide to water and oxygen, decreasing mtROS) and wild-type mice (adapted from (60)). Mirroring the comparison between carcinoma and normal tissue, mCAT mice compared to wild-type exhibit a reduced mutation frequency and a marked decrease in C>T mutations, suggesting a common mechanism of mutation repression, namely ROS damage.

While the mCAT mouse model provides evidence that mtDNA mutations result from oxidative damage, it has recently been suggested that the spectrum of mtDNA mutation characterized by high quantities of C→T mutations and low abundance of G→T mutations is inconsistent with oxidative damage, and that mtDNA mutations arise primarily from polymerase errors (61, 62). Semantics, and perhaps a limited consideration of the full expanse of oxidative damage to mtDNA thwarts consensus of what constitutes the mutational spectrum of oxidative damage. Quantification of a single lesion (8-oxoGuanine, 8-oxoG) and its resultant mutation (G→T), is commonly assumed to reflect total oxidative damage to DNA (62, 63). Unfortunately, this practice fails to capture the complexity or diversity of oxidative damage to mtDNA (Figure 1.3). Oxidative mtDNA damage manifests as a wide range of lesions (64-66), which vary greatly

in mutagenicity (67-69), and thus the frequency of base substitutions does not directly correspond with base-specific, ROS-induced lesion abundance (Figure 3). Differing lesion-specific repair capacity and ability of the mtDNA polymerase, pol γ, to bypass a given lesion determine how often mutation occurs (70). 8-oxoG, while the most studied lesion, is less prevalent in mtDNA than other oxidative lesions (67, 68) and only mildly mutagenic to mtDNA due to redundant and highly active repair pathways (71) and a high likelihood of stalling pol γ (72) rather than mutation. Additionally, an *in vitro* study describing pol γ incorporation fidelity opposite 8-oxoG observed polymerase inhibition 95% of the time, and that the remaining 5% resulted in correct insertion of cytosine (73).

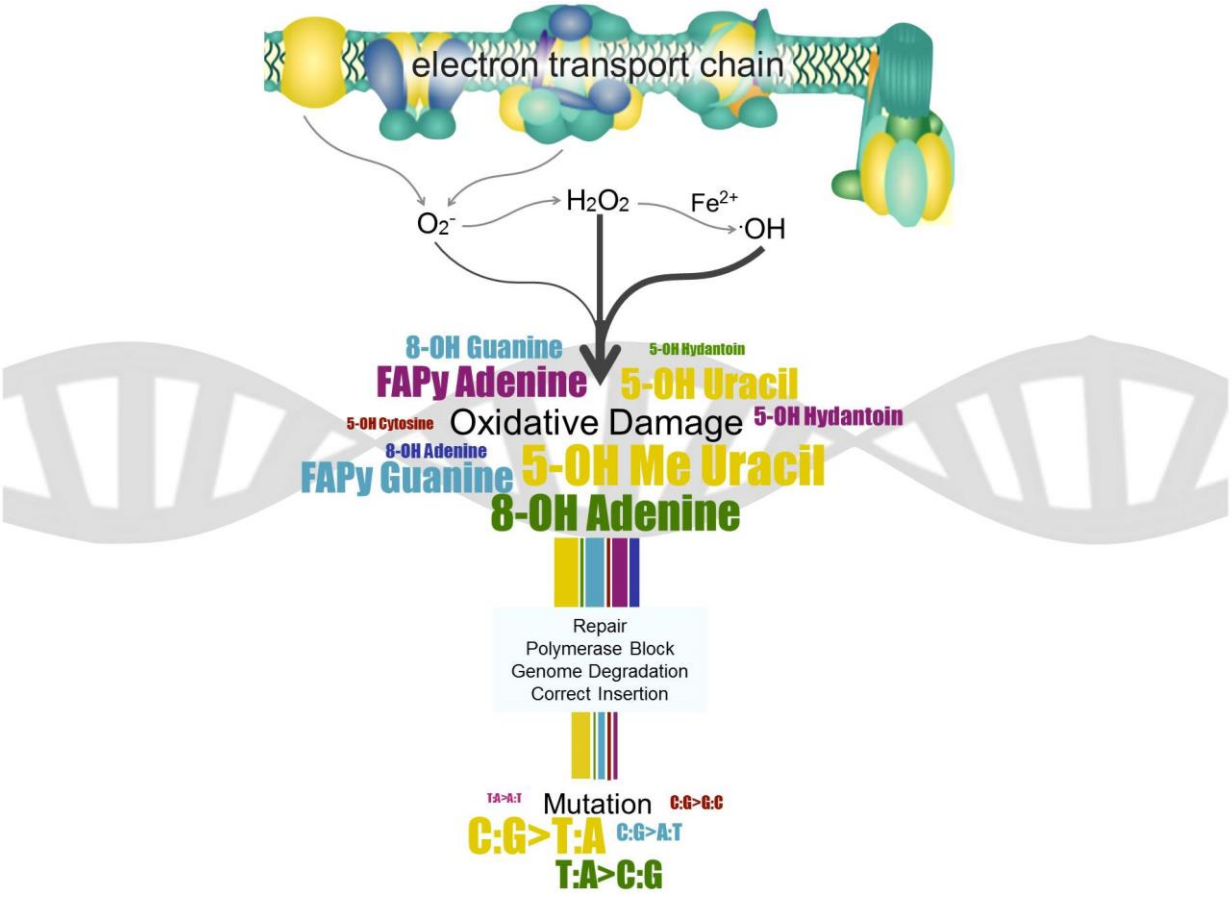

Figure 1.3**. Oxidative lesions in mtDNA and their associated mutation spectra.**

Superoxide generated from the electron transport chain is poorly reactive with DNA, but is readily converted to the more reactive hydrogen peroxide (74). Hydrogen peroxide in conjunction with Fe^{2+} participates in Fenton chemistry to produce the most DNA-reactive species: the hydroxyl radical (relative DNA activity indicated by arrow thickness). These species induce a wide variety of mtDNA lesions which are colored based on resultant mutation and sized based on relative abundance. Disparate capacities for repair, polymerase bypass efficiency, and ability to trigger genome degradation all impact lesions' relative mutagenicity, resulting in divergent spectra for mutation and precursor lesions (55, 66, 69, 70, 72, 75, 76).

1.5 Thesis Outline

This thesis describes efforts to determine the mechanisms of somatic mitochondrial mutagenesis in mammalian systems. In Chapter 2, I relate an investigation into the effects of classical mutagens on murine mitochondrial genomes. The results of that study informed the direction of continued investigation into the primary drivers of mitochondrial mutagenesis. In Chapter 3, I include my work describing the effects of reduced mitochondrial ROS on aspects of mtDNA mutagenesis, metabolism, and cell fate. In Chapter 4, I detail my efforts to evaluate the hypothesis that mitochondrial ROS promotes mtDNA mutation.

Chapter 2. RESISTANCE OF MITOCHONDRIAL DNA TO INDUCED MUTATION

A version of the following work was published as:

William Valente, Nolan Ericon, Alexandra Long, Paul White, Francesco Marchetti, Jason Bielas. Mitochondrial DNA Exhibits Resistance to Induced Point and Deletion Mutations. Nucleic Acids Research. 2016. 44(18):8513-8524.

Jason Bielas and Francesco Marchetti conceived the initial approach. Jason Bielas, Francesco Marchetti, Paul White, and I designed the research plan. Paul White and Francesco Marchetti provided samples. Alexandra Long performed animal care and treatments, as well as initial DNA extraction and lacZ mutation evaluations. Nolan Ericson and I performed ddPCR mutation quantification of mtDNA mutations. I designed and implemented all quantitative long-range PCR for lesion frequency determination, ddPCR quantification of nDNA mutations, and statistical analyses. Jason Bielas and I wrote the manuscript with input from all authors.

2.1 ABSTRACT

The accumulation of somatic mitochondrial DNA (mtDNA) mutations contributes to the pathogenesis of human disease. Currently, mitochondrial mutations are largely considered results of inaccurate processing of its heavily damaged genome. However, mainly from a lack of methods to monitor mtDNA mutations with sufficient sensitivity and accuracy, a link between mtDNA damage and mutation has not been established. To test the hypothesis that mtDNA-damaging agents induce mtDNA mutations, we exposed Muta^{TM}Mouse mice to benzo[a]pyrene

(B[a]P) or N-ethyl-N-nitrosourea (ENU), daily for 28 consecutive days, and quantified mtDNA point and deletion mutations in bone marrow and liver using our newly developed Digital Droplet Random Mutation Capture (dRMC) and Digital Deletion Detection (3D) assays. Surprisingly, our results demonstrate mutagen treatment did not increase mitochondrial point or deletion mutation frequencies, despite evidence both compounds increase nuclear DNA mutations and demonstrated B[a]P adduct formation in mtDNA. These findings contradict models of mtDNA mutagenesis which assert the elevated rate of mtDNA mutation stems from damage sensitivity and abridged repair capacity. Rather, our results demonstrate induced mtDNA damage does not readily convert into mutation. These findings suggest robust mitochondrial damage responses repress induced mutations after mutagen exposure.

2.2 INTRODUCTION

Maternally inherited mutations in the mitochondrial genome cause a diverse array of disorders, all of which are associated with defects in oxidative energy metabolism (77). Furthermore, emerging evidence implicates the accumulation of somatic mutations in mitochondrial DNA (mtDNA) as drivers of other complex traits, including neurodegenerative diseases, pathologies of aging, and cancer (9, 78-83). Yet, the mechanisms by which these mutations arise and contribute to the etiology of disease are poorly defined.

mtDNA readily reacts with exogenous chemicals (39, 84-86), exhibiting lesion frequencies that are many hundreds of fold higher than those in nuclear DNA (nDNA) in the same cells following exposure . Thus, damage to mtDNA may underlie the vast majority of pathogenic mitochondrial mutations. Furthermore, the disparate induction of DNA damage that results between the nuclear and mitochondrial genomes may be due to the fact that many genotoxic substances preferentially concentrate within mitochondria (39, 87). Other contributing

factors that have been implicated in the magnitude of mtDNA damage include: a disputed protective function of mtDNA-packaging proteins (88-90), the proximity of mtDNA to reactive oxygen species (ROS) produced during oxidative phosphorylation , and the inherent susceptibility of mtDNA to adduct formation with genotoxic agents (85). As such, it is commonly theorized that mtDNA's inherent susceptibility to induced damage underlies its high rate of mutation, which is two to three orders of magnitude greater than nDNA (38, 41, 43, 91-93). However, to our knowledge, this premise, i.e., that mtDNA is more susceptible to induced mutation, has never been tested.

Direct evidence linking lesion burden to mtDNA mutation remains scarce or contradictory (51, 53, 94-96), as previously existing assays have lacked sufficient accuracy and sensitivity to quantify *de novo* mtDNA mutations (97). Earlier mtDNA mutation detection technologies inherently suffer from assay-induced errors mediated by polymerase infidelity on damaged templates and by cloning artifacts (97, 98). As such, we sought to improve upon these shortcomings by developing the Digital Droplet Random Mutation Capture (dRMC), a novel adaptation of the RMC assay (14), and Digital Deletion Detection (3D) (12) to track the accumulation of point and deletion mutations in mtDNA, respectively. In these approaches, enrichment for mutant mtDNA with restriction endonucleases precedes single molecule amplification, effectively eliminating issues with polymerase fidelity (12-14). dRMC and 3D couple the accuracy and increased throughput of droplet digital PCR (ddPCR) with the reporting specificity of molecular probe-based Taqman™ chemistry for accurate quantification of mtDNA mutation frequency at unprecedented sensitivity (12-14). With dRMC and 3D, it is possible to evaluate not only single point mutations, but also large deletions. To test the hypothesis that the high mutation rate of mtDNA stems from its well-documented sensitivity to DNA damage, we

exploited the enhanced sensitivity of these assays to investigate the consequences of mutagen exposure on mtDNA mutagenesis *in vivo,* and the results are interpreted in the context of nuclear DNA mutation frequency in the same tissue samples.

2.3 Materials and Methods

Animal treatment

Twenty to twenty-four week-old Muta^{TM}Mouse males were dosed via oral gavage in a single exposure or daily for 28 days with B[a]P dissolved in olive oil (75 mg/kg body weight in the single-exposure trial, 25, 50, or 75 mg/kg body weight/day in the subchronic trial). Fourteen to sixteen week-old males were dosed for 28 days with ENU dissolved in water (5 mg/kg body weight/day). B[a]P and ENU were obtained from Sigma-Aldrich Canada (Oakville, ON). Each dose group, including vehicle control, contained four animals for the single-exposure study and five animals for the subchronic exposure study. Mice in the single-exposure study were anesthetized with isofluorane prior to cervical dislocation 24 hours following B[a]P exposure. Tissues, including liver and bone marrow, were isolated, flash-frozen in liquid nitrogen, and stored at -80°C until use. In the 28-day studies, mice were euthanized three days after the final treatment in the same manner as the single-exposure study, and tissues were obtained as described above. Mice were maintained under conditions approved by the Health Canada Ottawa Animal Care Committee. Food and water were available *ad libitum* for the duration of the experiment. The *lacZ* mutant frequencies in animals from the 28-day exposure to B[a]P have been described in Lemieux et al 2011 , however, here we present the *lacZ* data only from those mice where we conducted mtDNA analysis (those that had sufficient sample DNA quantity or quality).

Genomic DNA isolation

Bone marrow. Bone marrow cells were isolated and lysed according to previously published methods (99, 100). Briefly, to collect bone marrow, femurs were flushed with PBS (Invitrogen Canada, Burlington, ON), the solution was briefly centrifuged, and the pellet was stored at –80°C. Cells were homogenized in 5 mL lysis buffer (1 mM Na_2EDTA, 100 mM NaCl, 20 mM Tris-HCl, pH 7.4), supplemented with 1% SDS (w/v) and proteinase K (1 mg/mL, Invitrogen Canada, Burlington, ON). The lysate was then incubated at 37°C overnight with gentle shaking. Genomic DNA was isolated the following day, using the phenol/chloroform extraction procedure described previously (101, 102). Isolated DNA was dissolved in 50-100 µL TE buffer (10 mM Tris pH 7.6, 1 mM EDTA) and stored at 4°C until use. DNA was quantified using a NanoPhotometer™ (Implen, Westlake Village, CA, USA).

Liver. Liver tissue was thawed and homogenized on ice using a motor-driven conical tissue homogenizer in 5 mL TMST buffer (50 mM Tris pH 7.6, 3 mM magnesium acetate, 250 mM sucrose, 0.2% (v/v) Triton X-100). The liver homogenate was centrifuged for 6 min at 800×g (4°C), the supernatant was discarded, and the pellet was washed twice more with TMST buffer as before. The pellet was suspended in 5 mL lysis buffer (10 mM Tris pH 7.6, 10 mM EDTA, 150 mM NaCl, 1% (w/v) SDS and 1 mg/mL proteinase K (≥20 Units/mg). This suspension was incubated overnight at 37°C with gentle shaking. DNA was isolated and stored as described above.

TaqMan probe and primer design

The following primer/probe sets were used with murine total DNA for mtDNA mutation detection (designed using assembly GCA_000001635.6 for *mus musculus*). Control site: 5'-GAC ACA AAC TAA AAA GCT CA -3′ (forward primer), 5′- TAA GTG TCC TGC AGT AAT GT -3′ (reverse primer), and 5′-6FAM- CCA ATG GCA TTA GCA GTC CGG C -BHQ-1-3′

(probe). ND5 site: 5′- CCC ACT GTA CAC CAC CAC ATC AA -3′ (forward primer), 5′- TGT TGG CTG AGG TGA GGA TAA GCA -3′ (reverse primer), and 5′-6FAM- AAC CTG GCA CTG AGT CAC C -MGB-NFQ-3′ (probe). 12S rRNA site: 5′- GAC AGC TAA GAC CCA AAC TGG GAT -3′ (forward primer), 5′- CAT TGG CTA CAC CTT GAC CTA ACG -3′ (reverse primer), and 5′-6FAM- ACC GCC ATC TTC AGC A -MGB-NFQ-3′ (probe). Common deletion site: 5′- AGG CCA CCA CAC TCC TAT TG -3′ (forward primer), 5′- AAT GCT AGG CGT TTG ATT GG -3′ (reverse primer), and 5′-6FAM- AAG GAC TAC GAT ATG GTA TAA -MGB-NFQ-3′ (probe). RNaseP site for nuclear DNA quantification: 5'-GTG CTG CAG AAA GGG TAA GC-3' (forward primer), 5'-CCA TCG GCA AAC AGT TAC AA-3' (reverse primer), and 5'-VIC-TGG AAT ACT TTG TCC CAG CA-MGB-NFQ-3' (probe).

For *lacZ* mutation detection, primers were designed to the reference sequence GenBank:V00296.1. Control site: 5'- TAC GAT GCG CCC ATC TAC AC -3' (forward primer), 5'-CAA ATT CAG ACG GCA AAC GA -3' (reverse primer), and 5'-6FAM-CCT TCC TGT AGC CAG CTT TCA T-MGB-NFQ-3'(probe); TaqI site: 5'-TAC GCG TAG TGC AAC CGA AC -3' (forward primer), 5'-AAG CCT GAC TGG CGG TTA AA-3' (reverse primer), and 5'-6FAM-TGC AAA AAT CCA TTT CGC TGG T-MGB-NFQ -3'(probe).

For mitochondrial:nuclear copy number ratio analysis, primers were designed using the assembly GCA_000001635.6 for *mus musculus*, as above, with mitochondrial copies quantified using the control primer set and nuclear DNA copies quantified using primers directed toward the murine *RPP30* gene: 5'- CTC ACC AAA AAC AAA AAC AGC C -3' (forward primer), 5'- CTT TTG TCC CTC CCA CTT TGG -3' (reverse primer), and 5'-VIC-TGG AAT ACT TTG TCC CAG CA-MGB-NFQ-3' (probe).

Primers were designed using Primer3 specifications to limit off-target amplification within the murine genome (especially within nuclear mitochondrial segments ,NUMTs, which are transpositions of mtDNA into the nucleus), and their specificity was confirmed using UCSC in silico PCR (http://rohsdb.cmb.usc.edu/GBshape/cgi-bin/hgPcr) and NCBI primer-BLAST (103). Additionally, melt peak analysis was performed in real-time PCR experiments along with agarose gel separation of PCR products to ensure single product amplification.

Mitochondrial DNA Mutation Detection

To measure point mutations in mouse mtDNA, we adapted the Random Mutation Capture (RMC) assay for the droplet digital PCR (ddPCR) platform, as detailed in the subsections below. Deletions were quantified in mtDNA extracted from mouse tissues using the Digital Deletion Detection (3D) method described previously by Taylor et al. (12).

TaqI Digest. Rare mutation-bearing molecules were selectively enriched through endonucleolytic destruction of wild-type target sites. First, a 100 µL digestion reaction mixture was prepared containing 1 µg of genomic DNA, 1 µL (100 U) of TaqI (New England Biolabs, Ipswich, MA, USA), and TaqI reaction buffer (Fermentas, Vilnius, Lithuania). The reaction mixture was incubated at 65°C for 10 h, with an additional 100 U of TaqI added to each reaction every hour. After each TaqI addition, samples were thoroughly mixed and briefly centrifuged to ensure efficient digestion. Prior to ddPCR, complete cleavage of wild-type TaqI sites was verified by PCR amplification of the target regions followed by post-PCR restriction digest and agarose gel electrophoresis.

Droplet digital PCR (ddPCR). The final concentration of digested DNA was adjusted to yield less than ~3500 positive molecules per µL, which is within the range of linearity for the Poisson calculation (104). Reaction mixtures (25 µL) contained ddPCR Master Mix (Bio-Rad, Hercules,

CA, USA), 250 nM TaqMan probe, 900 nM of each appropriate flanking primer, and 0 – 100 ng of TaqI-digested DNA. Reaction droplets were made by applying 20 μL of each reaction mixture to a droplet generator DG8 cartridge (Bio-Rad) for use in the QX100 Droplet Generator (Bio-Rad). Following droplet generation, 38 μL of the droplet emulsion was carefully transferred to a Twin.tec semi-skirted 96-well PCR plate (Eppendorf, Hamburg, Germany), which was then heat-sealed with a pierceable foil sheet. To amplify the fragments, thermal cycling was carried out using the following protocol: initial denaturation step at 95°C for 10 min, followed by 40 cycles of 94°C for 30 s, and 58°C for 1 min. The thermally cycled droplets were analyzed by flow cytometry in a QX100™ Droplet Digital™ Reader (Bio-Rad) for fluorescence analysis and quantification of mutation frequencies.

Analysis of fluorescence amplitude and quantification. Following normal thermal cycling, droplets were individually scanned using the QX100™ Droplet Digital™ PCR system (Bio-Rad). Positive (mutation-bearing) and negative droplets were distinguished on the basis of fluorescence amplitude using a global threshold. The number of mutant genomes per droplet was calculated automatically by the accompanying software (QuantaSoft, Bio-Rad) using Poisson statistics as described elsewhere (105). Quantification of point mutation frequency requires ddPCR amplification using two primer sets. The first primer set flanks the test region and measures the concentration of mutation-bearing molecules. The second primer set flanks a region in the mitochondrial genome that bears no restriction recognition sites. This control set measures the concentration of all mtDNA genomes. Because de novo point mutations are so rare, reactions using the different primer sets must be run using different dilutions of the digested DNA, and the results are normalized against undiluted concentrations during downstream calculations. Mutation frequency per base pair is calculated by taking the ratio of the normalized

concentrations of mutation-bearing mtDNA molecules to the total mtDNA molecules screened, divided by the number of bases per target site. Reactions that yielded < 5 positive droplets per well were scored conservatively as having no positives above background, though in rare cases technical replicates were pooled to achieve higher droplet counts (104). At least two technical repeats were performed per biological sample, and the average result presented.

Nuclear mutation assessment with dRMC

The methodology for quantifying nDNA mutations follows that for mtDNA mutations (as above) with a few changes: input DNA was scaled to 10 μg per mouse sample; twenty one-hour rounds of TaqI digestion were required for this amount of DNA; and ddPCR cycling parameters consisted of an initial denaturation step at 95°C for 10 min, followed by 40 cycles of 94°C for 30 s, and 60°C for 1 min.

Mitochondrial:nuclear DNA copy number ratio

ddPCR reactions were performed with TaqI-digested genomic DNA as above, using the mitochondrial control primer/probe set (within the *ATP6* gene) for mtDNA copy quantification, and the RNAseP (RPP30) primer/probe set for nDNA copy quantification (both detailed above), with an initial denaturation step at 95°C for 10 min, followed by 40 cycles of 94°C for 30 s, and 60°C for 1 min. After droplet processing, mtDNA:nDNA copy number ratio was calculated by dividing the concentration of mtDNA molecules detected by the nDNA molecules determined by ddPCR.

Quantitative Long-Range Real-Time PCR

The induced lesion frequency of B[a]P in the single-exposure mice was quantified using long-range quantitative real-time PCR amplification, as described previously (106). 1 μg of each DNA sample for mitochondrial amplification was digested with NotI prior to amplification, as this was

seen to increase amplification efficiency (107). No NotI sites are found in the target amplicons. Primers for mouse mtDNA short (mtDNA control primers above) and long (forward 5'-CCA CCG CGG TCA TAC GAT TA-3', reverse 5'-CGA TGT CTC CGA TGC GGT TA-3' 11.9 kb) amplicons, and mouse nDNA short (nDNA control primers) and long (forward 5'- CGC CGC CTT GCC CTC GTC T-3', reverse 5'-AGC TCC GCA AAT TCG CCT ACA C-3' 12.5 kb, localized to the lambda transgene) amplicons were used to amplify DNA isolated from mouse liver and bone marrow in reaction mixtures of 0.05 U/μL JumpStart™ AccuTaq™ polymerase (Sigma), JumpStart™ AccuTaq™ polymerase buffer (working concentrations of 50 mM Tris-Hcl, 15 mM ammonium sulphate, pH 9.3, adjusted with NH_4OH, 2.5 mM $MgCl_2$, and 1% Tween-20), 500 μM dNTP mix (Promega), and 1 uL of a 1:8 dilution of EvaGreen® in water. Full-strength EvaGreen® inhibited long-range product formation. Samples containing 50 – 200 ng of DNA were amplified in triplicate using a C1000 series CF96® Real-Time PCR Detection System (Bio-Rad) with detection in the SYBR® Green fluorescence channel. Cycling parameters for the 12 kb mtDNA and nDNA fragments were as follows: initial denaturation at 96°C for 30 seconds, followed by 40 cycles of denaturation at 94°C for 15 seconds and extension at 65°C for 16 minutes. A final extension step of 30 minutes at 65°C was performed after cycling, prior to a melting curve analysis to verify correct product amplification – a ramp from 58°C to 96°C where fluorescence amplitude was measured at 0.5°C intervals – with subsequent sample cooling to 4°C. Short-range amplicons were amplified as above, though with extension periods of 1 minute during cycling and a 3 minute final extension, at 58°C and 62°C for mtDNA and nDNA primer sets, respectively. Primers were designed with the aid of NCBI's primer-BLAST (103) and UCSC In-Silico PCR (http://rohsdb.cmb.usc.edu/GBshape/cgi-bin/hgPcr), as with the

primer/probes used in ddPCR. Standard curves and melt temperature analysis are included in Supplemental Figures 7-10.

Determination of induced lesion frequency. Lesion frequency was calculated using methods similar to those previously described (106, 107). Amplification products were quantified from the EvaGreen® fluorescence amplitude, with regression analysis (CFX Manager, Bio-Rad) and a standard curve for each sample set, which was performed simultaneously with sample amplification using the same prepared reagent mix along with no template controls. Assuming a random distribution of lesions within the amplicon, the Poisson equation [$f(x) = e^{-\lambda}\lambda^x/x!$] for undamaged templates is $f(0) = e^{-\lambda}$. The average lesion frequency for each amplicon (λ) is calculated by dividing the normalized (long-range over short-range ratio of input copies determined by standard curve) amplification in DNA extracted from treated mice by the same in DNA from untreated mice (thus lesion frequency is equivalent to $-\ln\left(\frac{\left(\frac{Long\ Amplicons}{Short\ Amplicons}\right)_{treated}}{\left(\frac{Long\ Amplicons}{Short\ Amplicons}\right)_{controls}}\right) \times \frac{10000bp}{Length(Long\ Amplicon)}$. Values reported reflect the average of individual samples assayed in triplicate, and then pooled for lesion frequency (n = 4-5 for each group).

lacZ mutation evaluation

The frequency of *lacZ* transgene mutants in genomic DNA isolated from liver and bone marrow was assessed using the phenyl-β-D-galactopyranoside (P-Gal) positive selection assay as previously described . λgt10*lacZ* DNA was rescued from genomic DNA using the Transpack™ lambda packaging system (Agilent, Mississauga, ON). Packaged phage particles were then mixed with the host bacterium (*Escherichia coli lacZ*$^-$, *galE*$^-$, *recA*$^-$, pAA119 with *galT* and *galK*) , plated on minimal medium containing 0.3% (w/v) P-Gal and incubated overnight at

37°C. Total plaque-forming units (pfu) were measured on concurrent titer plates that did not contain P-Gal. Mutant frequency is expressed as the ratio of mutant pfu to total pfu.

Statistical analysis

All reported results represent at least three biological replicates with 2 technical replicates. Error reported represents s.e.m. Concentration- and dose-response data were analyzed using both non-parametric (e.g. chi-square and Fisher's exact tests) and parametric methods (e.g., analysis of variance, ANOVA; Welch's t-test). Non-parametric methods are frequently employed to analyze experimental datasets where the response variable is a discrete dichotomous outcome (i.e., mutant versus normal). The non-parametric analyses of *lacZ* mutant frequency employed 2 x 2 or 2 x 4 contingency tables with chi-square and Fisher's exact tests to assess the degree of association between treatment and response at each dose/concentration. In addition, a one-way Cochran-Armitage test was employed to determine whether increasing doses or concentrations yielded an increasing likelihood of recovering mutant copies of *lacZ*. The parametric methods analyzed frequency values (mutant *lacZ* per 10^5 plaque forming units, mtDNA mutation frequencies, and mtDNA damage), and employed one-way ANOVA (B[a]P treatment samples, 4 treatment groups) or unpaired t-test with Welch's correction (for the two ENU treatment groups) to investigate the relationship between dose/concentration and mutant frequency (MF). Mutation frequencies in mtDNA and lesion frequencies in mtDNA and nDNA were Poisson transformed during analysis from droplet and RT-PCR data, respectively, and thus are not compatible with chi-square tests. For each one-way ANOVA, a one-tailed, post-hoc Dunnett's test was employed to subsequently compare responses at individual doses/concentrations to matched controls. Values of $p < 0.05$ were considered statistically significant.

2.4 RESULTS

We used benzo[*a*]pyrene (B[a]P) to investigate the relationship between induced mtDNA damage and mutation. B[a]P is an established mutagen that has been shown to induce 40 to 90 fold more lesions in mtDNA than in nDNA (38, 39). B[a]P is present in a wide range of combustion products, including tobacco smoke, coal tar, and vehicular exhaust (87), and requires metabolic activation by cytochrome P450 isozymes, followed by epoxide hydrolase, to form mutagenic metabolites (e.g., benzo(*a*)pyrene-7,8-diol-9,10-epoxide, BPDE), which form bulky helix-distorting lesions by covalently modifying DNA .

To maximize the likelihood of mtDNA damage, we implemented a 28-day sub-chronic dosing regimen, which included three concentrations of B[a]P (25, 50, or 75 mg/kg body weight/day). As B[a]P requires metabolic conversion to a DNA-reactive substance (i.e., BPDE) , we elected to study mtDNA mutagenesis in the liver, a well-known site of this activation (108-110). Additionally, to assess the impact of mutagen treatment in a highly proliferative tissue, bone marrow was also included in our study. Both tissues have been shown to be exceptionally sensitive to DNA-damaging agents in nuclear and mitochondrial DNA , including B[a]P-induced damage . Moreover, previous work has shown that B[a]P significantly increases mutations in nuclear DNA , at similar doses, and in the same tissues tested as in the present study (100). However, the potential effect of B[a]P exposure on the induction of mtDNA mutations *in vivo* has not been examined.

To this end, we extracted DNA from liver and bone marrow cells to explore the possible effect of B[a]P treatment on mtDNA mutagenesis using the dRMC assay, which builds upon the RMC methodology , and 3D assay (12, 14). The dRMC and 3D assays (Figure 2.1) have been

used to quantify point mutations and deletion mutations in both humans and mice (14, 60, 111) (validation results presented in Supplemental Figure A.1).

2.4.1 *Effect of B[a]P exposure on the frequency of mtDNA point mutation*

Whole-cell DNA was extracted from frozen bone marrow and liver for mtDNA mutation analysis from B[a]P-exposed and control mice after 28 days of daily treatment and 3 post-exposure rest days. In bone marrow mtDNA isolated from B[a]P-treated mice, the mutation burdens, ordered by increasing daily dose of B[a]P, were 3.8 ± 1.1, 4.2 ± 1.2, $3.8 \pm 1.4 \times 10^{-6}$ bp and 2.6 ± 0.5, 2.4 ± 0.6, $2.0 \pm 1.0 \times 10^{-6}$ bp (Figure 2A), for the 12S rRNA region and ND5 site, respectively. In untreated mice, bone marrow mtDNA mutation frequencies were $3.5 \pm 0.7 \times 10^{-6}$ bp and $1.7 \pm 0.2 \times 10^{-6}$ bp, at the 12S and ND5 sites, respectively. No significant increases, or dose-dependent changes (ANOVA, multiple-comparisons corrected t-test), were observed between control (Figure 2.2A) and treatment groups.

mtDNA isolates from the liver of B[a]P-treated mice displayed mutation frequencies, ordered by increasing dose, of 2.3 ± 0.5, 2.4 ± 0.1, $2.5 \pm 0.2 \times 10^{-6}$ bp and 2.0 ± 0.8, 2.1 ± 0.9, and $2.0 \pm 0.7 \times 10^{-6}$ bp for 12S rRNA and ND5 sites (Figure 2B), respectively. The mutation frequency of untreated liver mtDNA at the 12S rRNA and ND5 sites were $2.6 \pm 1.0 \times 10^{-6}$ bp and $2.2 \pm 1.00 \times 10^{-6}$ bp. As with bone marrow, liver mtDNA mutation frequency was unaffected by B[a]P exposure. Thus, in both tissues, B[a]P exposure did not affect the frequency of point mutations in mtDNA.

2.4.2 *Incidence of mtDNA deletions following mutagen exposure*

The bulky adducts induced by B[a]P may underlie the lack of conversion into mtDNA point mutations, as the strand-distorting lesion produced by B[a]P strongly inhibits mitochondrial

replication and thus lesion bypass (112). Polymerase stalling, however, has been hypothesized to cause deletion mutations (112, 113). The observed lack of point mutation induction (Figure 2.2) in mtDNA may be predicated upon blocked replication instead of error-prone polymerase bypass or DNA repair processes. Thus, we speculated that this would lead to polymerase stalling at the sites of damaged bases and, potentially, induce the formation of large mtDNA deletions.

To examine this possibility, we employed the 3D assay (12) to quantify mtDNA deletions following exposure to B[a]P (Figure 2.1). 3D can evaluate the presence of deletions in the mitochondrial genome, such as the 'common deletion': a 3.8 kb region in mouse mtDNA that shows preferential excision and end-joining due to sequence microhomology (27, 114). The frequency of mtDNA deletions in our control mice was 1.1 ± 0.4 and 111.4 ± 31.0 deletions per 10^7 genomes for bone marrow and liver, respectively. These values are complementary to those found in previous studies for similarly aged mice, where liver showed the highest frequency of deletions (114). Deletion frequencies in treated mice, ordered by increasing doses of B[a]P were: 1.1 ± 0.50, 0.9 ± 0.40, and 1.1 ± 0.2 copies per 10^7 genomes in bone marrow (Figure 2.3A); and, 71.4 ± 15.5, 47.6 ± 14.3, and 84.1 ± 33.2 deletions per 10^7 genomes, in liver (Figure 3B). As with point mutations, B[a]P exposure did not significantly change the frequency of deletions at any dose or in either tissue (ANOVA, multiple comparisons adjusted t-test).

2.4.3 *B[a]P adducts in mtDNA and nDNA*

Although the induction of mtDNA damage induced by B[a]P is extensively described , the unexpected lack of mutation induction in mtDNA following B[a]P exposure prompted us to address the possibility that damage was not induced in our test animals. To quantify the potential induction of B[a]P induced damage, we extracted DNA from bone marrow and liver tissues 24 hours post-treatment with an acute dose of 75 mg B[a]P/kg body weight. As adducts formed by

B[a]P inhibit polymerase extension , we quantified their presence via long-range quantitative PCR (87, 115). This sensitive assay quantifies lesions that inhibit polymerase extension, and is not specific to one species of DNA adduct or lesion. B[a]P induced 0.29 ± 0.10 lesions per 10 kb (Figure 2.4A, $p < 0.05$, one-tailed Welch's t-test) and 0.26 ± 0.09 lesions per 10 kb (Figure 2.4B, $p < 0.05$, one-tailed Welch's t-test) in bone marrow and liver mtDNA, respectively. DNA samples were also processed for nDNA lesions using quantitative PCR directed to portions of the *lacZ* transgene. B[a]P induced 1.27 ± 0.40 lesions per 10 kb (Supplemental Figure A.2A, $p < 0.01$, one-tailed Welch's t-test) and 0.66 ± 0.11 lesions per 10 kb (Supplemental Figure A.2B, $p < 0.05$, one-tailed Welch's t-test) in bone marrow and liver nDNA, respectively. Thus, the lack of induced point and deletion mutations in the mitochondrial genome following 28 days of daily B[a]P exposures cannot be explained by the absence of damage induction. A single exposure of 75 mg B[a]P/kg body weight introduced 29 lesions per 10^6 bp in mtDNA with the potential to stall or inhibit polymerase extension. Yet despite the abundance of B[a]P-induced DNA lesions, no significant induction of mutation is observed in the mitochondrial genome following 28 days of daily B[a]P exposures.

2.4.4 *Nuclear B[a]P-induced mutagenesis*

Mutation and damage burdens in mtDNA are typically described with comparisons to nDNA. Therefore, we sought to place the observed mitochondrial resistance to mutation in the context of the nuclear genome. We had selected B[a]P as our test mutagen, as previous reports had demonstrated preferential B[a]P adduct formation in mtDNA compared to nDNA (39). As such, we had hypothesized the mitochondrial genome would be more sensitive to B[a]P-induced mutation than the nuclear genome. In our evaluation of induced nDNA mutation and damage, we utilized the Muta^{TM}Mouse transgenic rodent, which harbors a stably integrated *lacZ* transgene

incorporated into a recoverable lambda phage shuttle vector. The shuttle vector can readily be recovered by packaging in phage particles that are subsequently used to infect galactose-sensitive bacteria (116, 117). In the presence of P-gal, only those phages that receive a mutant *lacZ* can form plaques, allowing quantification of the mutant frequency in the nDNA (99, 118). The mutant frequency in untreated animals was $4.3 \pm 0.9 \times 10^{-5}$ in bone marrow, and $6.3 \pm 0.6 \times 10^{-5}$ in liver. Contrary to our observations in the mitochondrial genome, B[a]P exposure resulted in a dose-dependent increase in nuclear mutant frequencies in both tissues, with 203 ± 35.8, 344 ± 75.0, and 679 ± 59.8 mutants $\times 10^{-5}$ in bone marrow and 26 ± 4.8, 96 ± 14.5, and 219.0 ± 59.8 mutants $\times 10^{-5}$ in liver samples (Figure 2.5A, $p \leq 0.0001$ in bone marrow; Figure 2.5B, $p \leq 0.001$ in liver, chi-square test). Additionally, we were able to confirm increased mutant frequencies using a nuclear version of the dRMC that quantifies mutations within the *lacZ* transgene. Mutation frequencies in untreated animals were $2.9 \pm 1.7 \times 10^{-6}$ bp in bone marrow and $1.6 \pm 0.4 \times 10^{-6}$ bp in liver tissues, whereas mutation frequency in mice exposed to 75 mg/kg body weight/day B[a]P was $35.2 \pm 14.4 \times 10^{-6}$ bp in bone marrow and $29.5 \pm 8.3 \times 10^{-6}$ bp in liver (Supplementary Figure A.3, $p \leq 0.05$ for bone marrow and liver, one-tailed Welch's-adjusted t-test). These results show a clear differential response between mtDNA and nDNA to B[a]P-induced mutagenesis.

2.4.5 *Evaluation of ENU as a mitochondrial DNA mutagen*

To explore whether the resistance of mtDNA to mutagenesis is unique to chemicals that induce bulky adducts, we investigated the potential of *N*-ethyl-*N*-nitrosourea (ENU) to induce mtDNA mutation. ENU is an alkylating agent that acts by transferring its ethyl group to oxygen or nitrogen radicals in nucleic acids (119). This primarily induces base mis-pairing and misincorporation by replicative polymerases without substantial stalling, which we hypothesized

would encourage polymerase bypass errors rather than inhibit replication (120). Similar to our protocol for B[a]P exposure, we employed a 28 day, sub-chronic dosing regimen of 5 mg/kg body weight/day of ENU. As with the B[a]P-treated cohort, we evaluated mitochondrial point mutations and large deletions with dRMC and 3D, and quantified nDNA mutagenesis. In bone marrow, control and ENU-treated mouse mtDNA, point mutation frequencies were: $4.6 \pm 1.5 \times 10^{-6}$ bp vs. 4.5 ± 0.5 for the 12S rRNA locus; and, $1.6 \pm 0.3 \times 10^{-6}$ bp vs. $1.9 \pm 0.4 \times 10^{-6}$ bp for ND5 site (Figure 2.6A). In liver, these frequencies were: $7.9 \pm 4.8 \times 10^{-6}$ bp vs. 14.8 ± 4.8 for the 12S rRNA site; and $3.2 \pm 0.4 \times 10^{-6}$ bp, and $4.4 \pm 1.19 \times 10^{-6}$ for the ND5 site (Figure 2.6B). Thus, mirroring our B[a]P results, the mtDNA point mutation frequency was not significantly altered at either mtDNA target and in either tissue after ENU exposure (bone marrow: $p = 0.97$, 12S rRNA locus; $p = 0.90$, ND5 locus; and in liver: $p = 0.29$, 12S rRNA locus; $p = 0.09$, ND5 locus, Welch's unpaired t-test). 3D quantification of mtDNA 'common' deletions revealed 1.6 ± 0.3 and 1.5 ± 0.3 deletions per 10^7 genomes in untreated and treated bone marrow, respectively (Figure 2.7A). In liver, these frequencies were 12.5 ± 3.8 deletions per 10^7 genomes and 20.4 ± 5.5 (Figure 2.7B). In summary, regardless of the tissue of origin, ENU did not induce mtDNA point or deletion mutations.

2.4.6 *Nuclear ENU-induced mutagenesis*

Similar to our observations with B[a]P, quantification of nuclear mutants following ENU exposure showed, as expected, that ENU significantly induced mutant frequencies in both bone marrow and liver tissues. Specifically, we observed *lacZ* mutant frequencies of $5.0 \pm 1.2 \times 10^{-5}$ in the untreated mice bone marrow, whereas 155.0 ± 11.1 mutants $\times 10^{-5}$ were recovered from the ENU-treated mice. In liver, we quantified 3.0 ± 0.7 mutants $\times 10^{-5}$ in the untreated cohort, and 27.0 ± 3.3 mutants $\times 10^{-5}$ from their ENU-exposed counterparts (Supplemental Figure A.4).

The *lacZ* dRMC assay performed on these samples confirmed mutation induction by ENU in the nuclear genome. In these mice, mutant frequency of untreated animals was $1.1 \pm 0.8 \times 10^{-6}$ bp in bone marrow and $1.6 \pm 0.7 \times 10^{-6}$ bp in liver tissues, whereas mutation frequency in mice exposed to 5 mg/kg body weight/day ENU was $15.5 \pm 4.6 \times 10^{-6}$ bp in bone marrow and $10.2 \pm 4.67 \times 10^{-6}$ bp in liver (Supplementary Figure A.5, $p \leq 0.05$ for bone marrow and liver, one-tailed Welch's-adjusted t-test). As with the results of B[a]P exposure, these findings show a clear difference in the sensitivity of mtDNA and nDNA to ENU-induced mutagenesis. Intriguingly, although mtDNA copies per nuclear genome were unaffected by either B[a]P or ENU exposure in bone marrow (B[a]P, $p = 0.37$; ENU, $p = 0.40$, both Welch's-adjusted t-test), recovered liver tissue posted increased mtDNA copy number in B[a]P-exposed mice (ANOVA, $p = 0.06$; 0 vs 75 mg/kg bw/day $p = 0.03$, Welch's-adjusted t-test) and decreased mtDNA copy number in ENU-exposed mice ($p = 0.03$, Welch's-adjusted t-test), suggesting tissue- and compound-specific responses to mutagens that do not produce changes in the relative abundance of mtDNA copies (Supplemental Figure A.6).

2.5 Discussion

Diverse theories have emerged to explain the remarkably greater frequency of somatic mutations in mtDNA, as compared to the nuclear genome (9, 33, 81, 121). One popular model, which developed from observations of increased damage burdens in mtDNA following genotoxin exposures (38-40, 84, 93), posits that this damage readily drives mutagenesis and thus mutation accumulation (65, 122). This paradigm expands foundational concepts in nuclear mutagenesis to the mitochondrial genome: i.e., unrepaired DNA lesions, when encountered during replication, can promote error-prone trans-lesion synthesis or block polymerase extension,

which result in point and deletion mutations (123). In essence, this model proposes the susceptibility of mtDNA to damage largely underlies its high rate of mutation.

However, testing the validity of this hypothesis has remained impractical, as the accurate quantification of *de novo* mtDNA mutations has been hampered by technical limitations (59); notably, the inability to distinguish true mutations from DNA damage (97, 124). To overcome this and other impediments to accurate mutation quantification, we employed our droplet digital PCR assays, dRMC and 3D, to ascertain the degree to which exposure to damaging agents influences the frequency of mitochondrial and nuclear mutagenesis. In the dRMC assay, the frequency of DNA mutations is evaluated per base pair by leveraging the fact that single base mutations in the 4-bp recognition motif of TaqI restriction enzyme (5'-TCGA-3') are sufficient to shield sites from endonuclease activity. In the 3D assay, TaqI sites present in wild-type mtDNA are removed by deletion events, maintaining the deletion-bearing genome as a substrate for amplification and subsequent detection. The dRMC and 3D assays permit accurate resolution of a single point (13, 125) or deletion (12) mutations, respectively, in a background of hundreds of millions of wildtype genomes, and enabled our investigation into mtDNA mutagenesis.

To test the hypothesis that DNA-damaging compounds induce mtDNA point and deletion mutations, we first exposed mice to one of two model mutagens, B[a]P or ENU. The bulky adduct created by BPDE, the active metabolite of B[a]P, can stall both mitochondrial (112) and nuclear replication (126) and was expected to initiate mtDNA mutagenesis, similarly to the nuclear genome; in a study of human mitochondrial DNA polymerase γ (pol γ) tolerance of B[a]P adducts, polymerase extension ceased after error-prone incorporation of a single base-pair adjacent to the adduct (112). In contrast to B[a]P, ENU-induced damage is often bypassed by DNA polymerases, but the alkylated base modification alters DNA-polymerase interactions and

can result in polymerase misincorporation during trans-lesion synthesis in the nucleus (127). In concert with these compounds' proven mutagenic effects in nDNA, previous studies have demonstrated that the mitochondrial genome is a focal point for B[a]P (38, 39, 87) and ENU (40, 93) adduct formation. Therefore, following mutagen exposure we anticipated robust conversion of DNA damage to mutation and a rise in the mtDNA mutation frequency, which would drastically exceed the level of induced mutation in the nucleus. However, against expectations, our results demonstrate that this was not the case. Rather, although sub-chronic exposures to B[a]P or ENU increase mutations in nDNA, they did not increase mtDNA mutagenesis, suggesting that DNA adducts are not readily converted into mutations in the mitochondrial genome.

These results could imply that adducts are managed through efficient DNA repair. Though the list of DNA repair pathways identified in the mitochondrion is greatly expanded from earlier assertions (128), deficiencies in lesion processing capability persist and may shape uniquely mitochondrial responses to DNA damage. For example, although a considerable amount of data asserts the susceptibility of mtDNA to adduct formation and damage (38, 41, 43, 92, 93), there is no known nucleotide-excision repair (NER) pathway in mitochondria for resolving bulky adducts such as those produced by B[a]P (128, 129). No clear mitochondrial DNA repair mechanism has been identified to alleviate these lesions. As for management of ENU-induced DNA alkylation damage, mitochondrial versions of mismatch repair (MMR) (130, 131), base-excision repair (BER) (132, 133), and alkylation-specific DNA repair enzymes have been described (134). Thus, it remains possible that mitochondria safeguard against converting DNA lesions into mutation via robust mechanisms for mtDNA repair.

In addition to DNA repair, studies have proposed that selective destruction of mitochondrial genomes eliminates the potential for mutation conversion from damaged mtDNA (135, 136). Such degradation would be reflected via a decrease in mitochondrial genomes copy number. In support of targeted degradation of damaged mtDNA, mitochondrial genome copy-number was reduced in the liver tissues of ENU-exposed mice; although bone marrow samples from the same mice exhibited no differences between treated and untreated cohorts. Exposure to B[a]P produced a dose-dependent *increase* in liver mtDNA copy-number, while copy-number was unchanged in bone marrow. Thus our results do not support a role for targeted degradation of damaged of mitochondrial genomes in mtDNA mutation repression, though the activities of such a pathway might be masked by other phenomena.

For example, it is possible that upon encountering B[a]P-induced lesions, terminal pausing of pol γ produces incomplete extension products of linear mtDNA, which, if not repaired, are likely targeted for destruction (136). If these linear products include the control region amplified by our primers, and they are not degraded, they would serve as template for our mtDNA:nDNA copy number assay and thus inflate the mtDNA:nDNA ratio. Contrasting the dynamic liver mtDNA:nDNA ratios, our analysis observed bone marrow tissues had no mtDNA copy-number changes in either mutagen exposure cohort. While these results may hint at mechanisms for mutation avoidance in mtDNA, as our results are inconsistent across mutagen and tissue type, we can draw no unifying conclusions. Thus, untangling a pathway by which mtDNA avoids mutation following damage remains an intriguing area of future investigation.

As mtDNA adducts do not appear to contribute appreciably to the induction of point and deletion mutations, the generation of mtDNA mutations must be ascribed to other sources. We demonstrate that B[a]P and ENU exposures produced no significant increases in mtDNA point

mutation or deletion frequencies, while inducing mutation in nDNA. Regardless of the mechanism by which damage-induced mutagenesis in the mitochondrial genome is suppressed, these findings highlight that the elevated frequency of somatic mtDNA mutation is not likely a byproduct of broad DNA damage sensitivity (51, 58). Thus, as exogenous damage to the mitochondrial genome appears to be a negligible source of induced point and deletion mutations, the majority of mutations induced in mtDNA are likely consequences of endogenous sources of error (137). Indeed, the most reliable models of increased mtDNA mutation frequency employ functional mutants of pol γ (79, 138). The burden of mtDNA mutations in mice deficient in the proofreading domain of pol γ, so-called 'mutator mice', can be hundreds- to thousands-fold higher than wild-type littermates (139). Curiously, the mutation spectrum of mtDNA in mutator mice is inconsistent with the expected spectra of pol γ misincorporation on undamaged template DNA (60, 70), and expression of a mitochondrial-targeted human catalase in these mice, which reduces the reactive oxygen species (ROS) hydrogen peroxide, also reduced their mutation frequency (60). Thus, although synthesis by pol γ is fairly accurate on undamaged template *in vitro* (70, 72), the presence of naturally-occurring mitochondrial ROS may contribute to the elevated spontaneous mutation frequency of the mitochondrial genome (65). Byproducts of mitochondrial metabolism, reactive oxygen species are recurrently associated with organismal aging and mtDNA mutagenesis (79, 81, 140, 141). Recent appraisals of the mitochondrial mutation spectrum in aging and in models of attenuated oxidative damage repair, although, have concluded that oxidative damage imparts minimal contributions to mtDNA mutation frequency (61, 62). Importantly, these assertions rely upon a narrowly-defined, unverified consensus signature of oxidative damage and induced mutagenesis in mitochondria. The lesions generated by reactive oxygen species range in severity from the subtle, 8-oxo-dG, to the obvious, strand

breaks (142); consequently, the imputed mutation 'signature' of oxidative DNA damage has developed as the amalgam of results derived from mutagenesis studies using defined lesions, often pursued *in vitro*, and not necessarily in the context of the mitochondrial replisome (55, 75, 143-145). Given the varied lesions formed by oxidative DNA damage (142), a direct assessment of mutation frequency and spectrum in mtDNA following oxidative damage is warranted, as these results may identify lesions which contrast in mutagenic potential with the adducts induced in our system. Additionally, the ostensible capacity of pol γ for lesion recognition and aborted synthesis (52, 73, 112, 138, 146, 147) appears a probable mechanism for mutation suppression in mtDNA. Future studies examining the factors that repress the conversion of mtDNA damage to mutations may elucidate these mechanisms, and could identify interventions to augment their activity, hopefully with advances for our understanding of pathologies in which somatic mtDNA mutations are implicated, such as aging and cancer (9, 148).

2.6 FIGURES

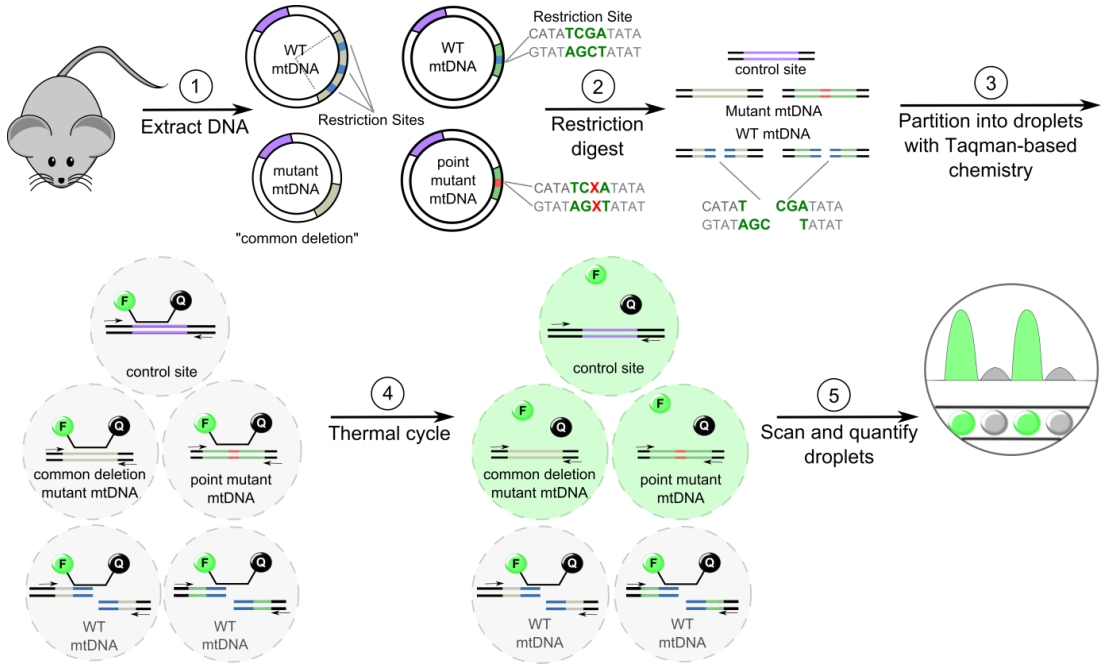

Figure 2.1. Illustrated overview of the 3D and dRMC assays for the quantification of mitochondrial mutations. (1) Whole cell DNA is extracted. (2) mtDNA is incubated with *Taq*I restriction endonuclease, which recognizes 5'-TCGA-3' sites. mtDNA that are wild-type at *Taq*I sites (WT, blue), will be cleaved, whereas mtDNA

with a mutation in the mutation target site (red) will be resistant to cleavage. A control region devoid of *Taq*I site(s) (purple) is used to quantify total mtDNA copies interrogated. (3) Digested DNA is added to a PCR mastermix with site-specific primers which flank the mutational target and Taqman probes, and then partitioned into thousands of 1 nL droplets in an oil immersion. The control region and mtDNA with mutations in the target site act as substrates for amplification, whereas mtDNA which are WT at the mutational target are not. (4) Droplets are thermal cycled to amplify target DNA as well as release the Taqman probe fluorophore from its quencher through *Taq* polymerase's inherent exonuclease activity. The ongoing rounds of amplification displace and cleave more probe, accumulating fluorescence. (5) Post-amplification, droplets are detected and their fluorescence is quantified. Frequency is calculated by dividing the mutant concentration by the concentration of the control region.

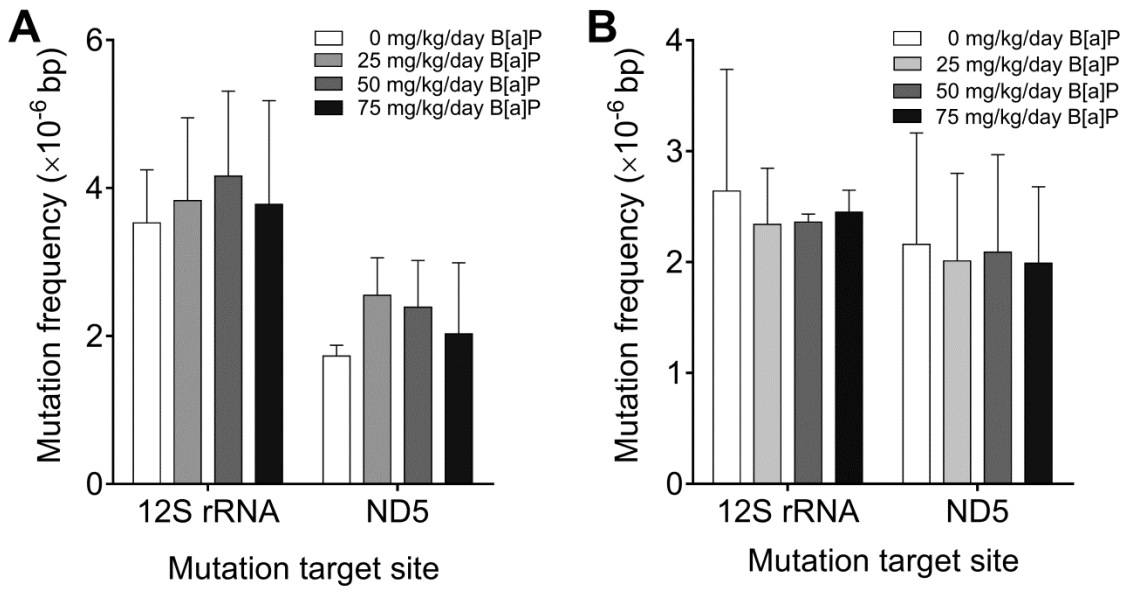

Figure 2.2 B[a]P treatment does not increase the frequency of mitochondrial point mutations. Mice were treated daily with B[a]P or vehicle for 28 consecutive days and tissues collected three days later. After DNA extraction, mutation frequency per bp (± s.e.m.) was determined via dRMC within the 12S rRNA and ND5 genes in mouse mtDNA. B[a]P did not induce mutations in (A) bone marrow (p = 0.66, 12S rRNA locus; p = 0.21, ND5 locus; one-way ANOVA) or (B) liver isolates of mice treated (p = 0.98, 12S rRNA locus; p = 0.98, ND5 locus; one-way ANOVA).

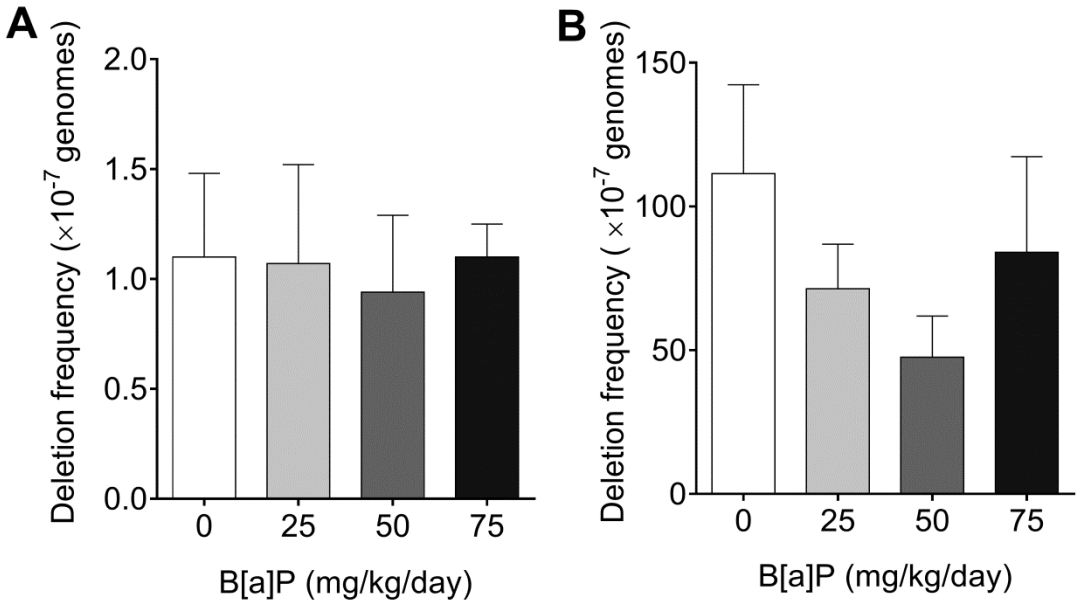

Figure 2.3 B[a]P treatment does not induce mitochondrial deletions. Following 28 days of treatment with B[a]P no significant induction of deletion mutation frequency, (± s.e.m.) per mitochondrial genome was determined via 3D in (A) bone marrow (p = 0.94; one-way ANOVA) and (B) liver mtDNA(p = 0.37; one-way ANOVA).

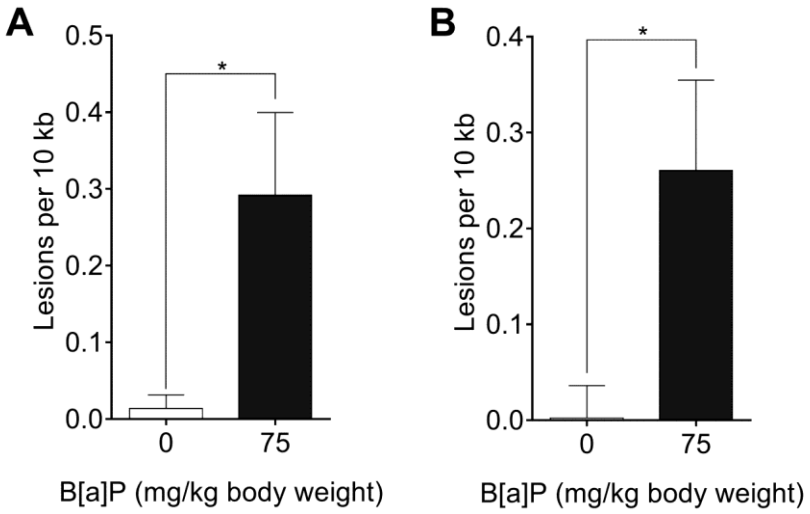

Figure 2.4 B[a]P treatment induces mtDNA adducts. The presence of lesions (± s.e.m.) in mouse bone marrow and liver mtDNA was enumerated by quantitative PCR. Mice were treated with a single, acute dose of B[a]P at either 0 or 75 mg/kg body weight. DNA was extracted from bone marrow and liver tissues 24 hours after treatment. B[a]P induces significant adduct burden in each tissue mtDNA (* indicates $p < 0.05$; one-tailed Welch's t-test). (A) Lesions formed in bone marrow. (B) Lesions formed in liver.

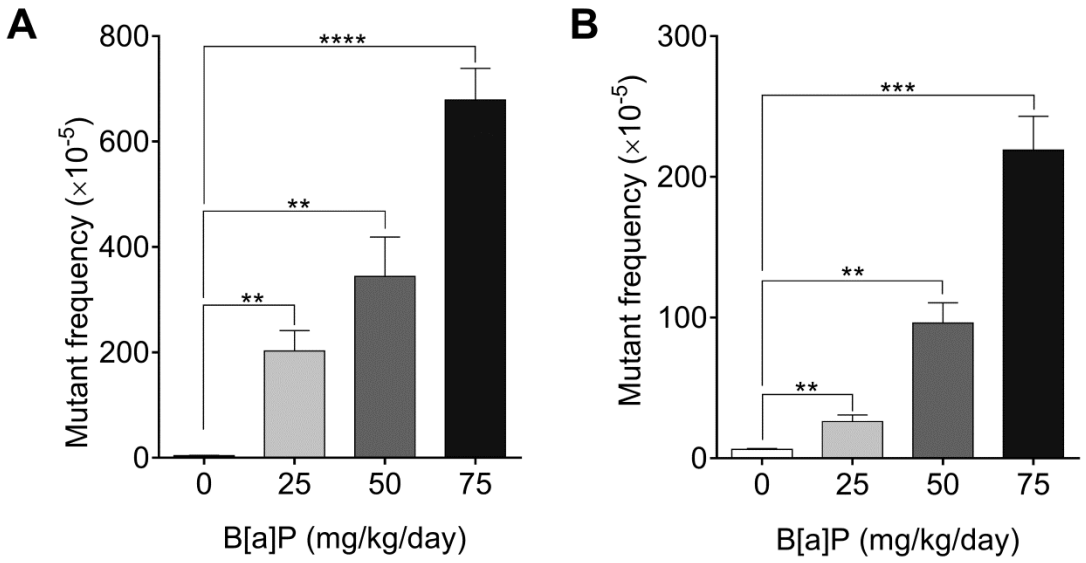

Figure 2.5 B[a]P treatment results in a dose-dependent increases in the frequency of nuclear DNA transgene (lacZ) mutants. After 28 days of daily treatment with B[a]P, DNA was extracted from mouse tissues 3 days post-exposure. Mutant frequency (± s.e.m.) in mouse nuclear DNA displayed significant, dose-dependent increases (**, $p < 0.01$; ***, $p < 0.001$; ****, $p < 0.0001$; Welch's-adjusted t-test). (A) Nuclear mutant frequency induced in bone marrow isolates ($\chi^2 = 4898$, $p = < 0.0001$; Fisher's Exact, $p = < 0.0001$). (B) Nuclear mutant frequency induced in liver nuclear DNA ($\chi^2 = 897.2$, $p = < 0.0001$; Fisher's Exact, $p = < 0.0001$).

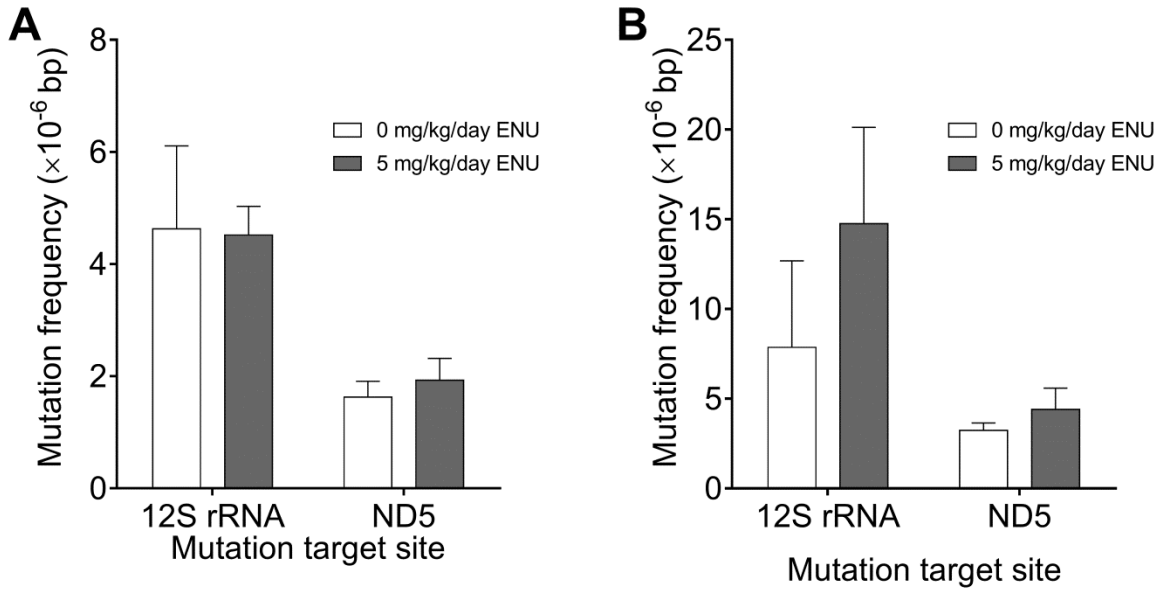

Figure 2.6 Subchronic ENU treatment does not increase the frequency of mitochondrial point mutations. Mice were treated daily with vehicle or 5 mg/kg ENU for 28 consecutive days. Three days following treatment, DNA was extracted from bone marrow and liver. Mutation frequency per bp mtDNA (± s.e.m.) was determined via dRMC at TaqI restriction sites within the 12S rRNA and ND5 genes in mouse mitochondrial DNA. (A) Bone marrow mutation frequency ($p = 0.97$, 12S rRNA locus; $p = 0.90$, ND5 locus; Welch's unpaired t-test). (B) Liver mutation frequency ($p = 0.29$, 12S rRNA locus; $p = 0.09$, ND5 locus; Welch's unpaired t-test).

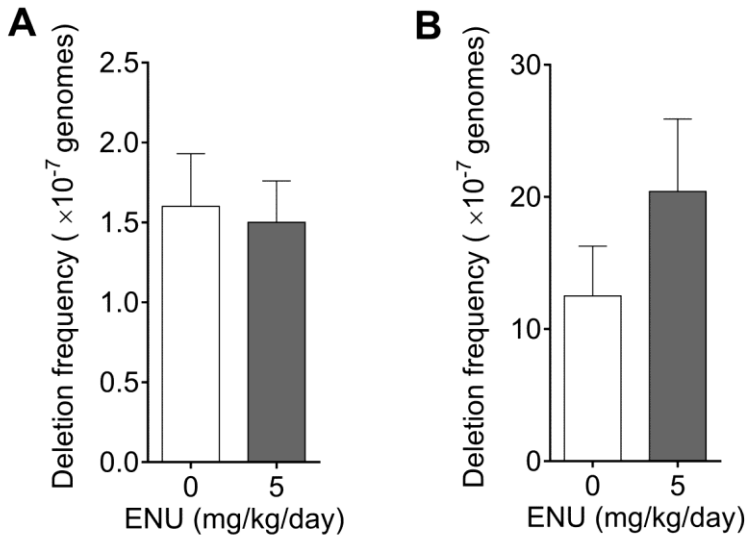

Figure 2.7 Subchronic ENU treatment does not induce deletions in mouse bone marrow and liver mtDNA. Deletion frequency per mitochondrial genome (± s.e.m.) was determined via 3D. (A) Bone marrow deletion frequency in mice treated with ENU (p = 0.82, two-tailed Welch's unpaired t-test). (B) Liver deletion frequency in mice treated with ENU (p = 0.09, two-tailed Welch's unpaired t-test).

Chapter 3. REDUCED MITOCHONDRIAL REACTIVE OXYGEN SPECIES ATTENUATES APOPTOTIC SIGNALING

The following work is unpublished. Jason Bielas and I designed the study. Mariola Kulawiec provided confocal microscopy of mCAT cells and generated the initial mCAT retroviral constructs. Joell Solan prepared the microarray slides and assisted with western blotting. Taran Gujral and Stella Shin prepared the reverse phase protein arrays. I performed tissue culture and cell manipulation experiments, data analysis, and wrote the manuscript.

3.1 ABSTRACT

The metabolic shift in many cancers to de-emphasize oxidative phosphorylation for enhanced glycolysis is consistent with the hypothesis that metabolic byproducts of oxidative metabolism, namely reactive oxygen species (ROS), influence the generation of mtDNA mutation. Here we test the hypothesis that a reduction in mitochondrial ROS conveys survival benefits to cancer cells as well as reduced mtDNA mutations. To accomplish this, we express a mitochondrial-targeted antioxidant enzyme, catalase (mCAT) in colorectal carcinoma cell line HCT116. mCAT expression reduces ROS and promotes resistance to cell stressors, including conventional chemotherapeutics. Changes to cellular transcription and translation offer insight into the mechanism of this enhanced cell survival, with evidence for altered NF-kB signaling and BCL2 family member activity in mCAT cells. The findings we describe may present a novel marker of aggressive neoplasms with reduced mitochondrial ROS and support targeted manipulation of mitochondrial metabolism as an adjunct to traditional approaches in cancer therapy.

3.2 INTRODUCTION

Otto Warburg's seminal finding of tumor cells' predominantly glycolytic metabolism in the abundance of oxygen, 'aerobic glycolysis', was accomplished in 1930 (57). In the intervening

years, far greater attention has been paid to increased glycolysis in tumors than the reduced reliance on oxidative phosphorylation, to the detriment of our understanding of the consequences of this metabolic shift in cancer. Whether OXPHOS activity enter into the host of factors that determine cancer cell survival is of particular importance to our understanding of the biological repercussions of this characteristic shift. There is evidence that increased glycolysis provides cancer cells with an acquired resistance to apoptosis, but this is poorly understood (149). One suggested pro-tumorigenic effect of OXPHOS downregulation is the reduction of metabolic byproducts of oxidative metabolism.

ROS are predominantly generated as byproducts of respiration. Electrons leak during transfer between elements of the ETC, and can interact with molecular oxygen to produce superoxide. This highly reactive oxygen radical is attenuated by mitochondrial enzymes, such as manganese superoxide dismutase (Mn-SOD), which partition superoxide into diatomic oxygen and hydrogen peroxide (H_2O_2), another ROS (150). Emerging evidence shows hydrogen peroxide regulates many adaptive responses in cancer cells (151, 152), and thus presents an intriguing target of investigation for its association with pro-glycolytic tumor metabolism. In support of an association between attenuated ROS and adverse patient outcomes, past studies found that antioxidant adjuvants for cancer chemotherapy decreased tumor responses, furthered disease development, and increased patient mortality (153, 154). Antioxidants, long heralded for their ability to reduce oxidative damage to nuclear DNA and thus the nuclear genetic instability integral to cancer progression (155), may provide newly transformed cancer cells the fitness advantage of apoptotic resistance and enable unchecked proliferation.

Here we evaluate the roles of reduced OXPHOS and mitochondrial ROS in cell survival, to test they hypothesis that mitochondrial ROS can modify cell fate in response to pro-apoptotic

stimuli. To do so, we examine the effects of mitochondrial-targeted expression of human catalase (mCAT) on cell survival, a model with previous demonstrations of longevity and reduced mtDNA mutagenesis (60, 81).

3.3 Materials and Methods

Chemicals

Chemicals involved in cell treatment or detection of stress included 30% hydrogen peroxide solution (Sigma), 5-Fluorouracil (Fisher Biosciences), DMSO (Sigma), and sodium dichloroacetate (DCA, Acros Organics).

Cell Culture

Human colorectal carcinoma cell line HCT116 was acquired through American Type Culture Collection (ATCC). HCT116 SCO2-/- were a generous gift of Dr. Paul Hwang (Translational Medicine Branch, National Heart, Lung, and Blood Institute, National Institutes of Health, Bethesda). Human breast adenocarcinoma cell lines MCF7 and MDA-MB-231 were kind gifts from Dr. Peggy Porter (Fred Hutchinson Cancer Research Center, Seattle, WA, USA). All cell lines and their stably transfected derivatives, except HCT116 SCO2-/-, were cultured at 37°C in a humidified, 5% CO_2 incubator at 19% O_2 in DMEM (Gibco) supplemented with 10% fetal bovine serum (FBS), 1 U/mL penicillin, 1 µg/mL streptomycin, and 2 mM L-glutamine (Sigma). HCT116 SCO2-/- cells were cultured in McCoy's 5A media supplemented as above, and incubated in 1.5% oxygen; other conditions remained the same.

Plasmids and Transfection

The retroviral GFP expression vector (pBMN-I-GFP, "Mock") and transgene-bearing pBMN-mCAT-I-GFP ("mCAT") vectors were gracious gifts of Dr. Peter Rabinovitch (University of Washington, Seattle, WA, USA). The mCAT transgene is comprised of an N-terminal

mitochondrial localization sequence (MLS) derived from the human ornithine transcarbomylase (OTC) gene, and the cDNA of the human catalase gene. Qiaprep Spin Miniprep Kit (Qiagen) was used to purify plasmid DNA from pelleted overnight cultures derived from single colony isolates. An Applied Biosystems (ABI) 3730xl DNA Analyzer with ABI BigDye Terminator Reagent Kit was used to sequence plasmid DNA (performed by Genomics and Bioinformatics Shared Resource, Fred Hutchinson Cancer Research Center).

The generation of retroviral vector and the production of high-titer vectors followed previously described methods (156). Briefly, the Phoenix packaging cell line derived from HEK293T cells, a kind gift of Dr. Garry Nolan (Stanford University, Palo Alto, CA, USA), was transfected with 10 μg purified retroviral vector by calcium-phosphate method. Culture supernatants containing viral particles were collected 24 h after transfection. Target cell infection was accomplished through the addition of centrifuged and filtered viral supernatant supplemented with 4 μg/mL of polybrene (Sigma) to cultures in log-phase growth for 16 hours. Three infection cycles were performed on consecutive days using freshly acquired viral supernatant. After infection, target cells were plated in fresh culture medium. The efficiency of transduction was evaluated by fluorescence microscopy. Successfully infected cells were sorted by flow cytometry (FACS-Aria, Becton-Dickinson) with standard doublet-discrimination gating and assessment of GFP fluorescence intensity by 488 nm laser excitation. At least 150,000 GFP-positive cells were sorted to found each lineage of transformed cells.

Apoptosis analyses

Propidium Iodide staining and sub-G1 population quantification

Staining followed previously published protocol (157).~100,000 cells are resuspended in 150uL PBS before the addition of 50 uL of PFA. After incubation for ~1 hr at 4C, cells are briefly spun

at 500 × g in a bucket centrifuge, with most of the supernatant removed. Cell pellets are then resuspended by the dropwise addition of 70% EtOH previously chilled to -20C. Cells are then suitable for staining with propidium iodide.

Reactive Oxygen Species quantification

Catalase assay

Enzymatic activity of catalase was measured using Amplex Red Assay kit (A22180, Invitrogen) according to the supplied protocol. Fluorescence was measured using 530- and 585-nm filters for excitation and emission, respectively, on a SpectraMax M5 plate reader (Molecular Devices).

MitoPY1

Quantification of mitochondrial hydrogen peroxide was determined by fluorescence of the hydrogen peroxide-responsive, mitochondrial-localized dye MitoPY1 ((158), purchased through Tocris Biosciences), either via microscopy or flow cytometry. Cells were grown for 24-48 hours in 24-well tissue culture plates or 8-well chamber slides prior to treatments and MitoPY1 staining. Prior to image acquisition, cells were incubated in a PBS solution of 5 µM MitoPY1 for 30 minutes at 37°C and protected from light, with 2 subsequent PBS washes. Fluorescence microscopy of MitoPY1 staining was performed with a Zeiss 700 LSM microscope at 20× magnification using the 488 nm laser line. For flow cytometry assessment of MitoPY1 fluorescence intensity, cells were detached prior to staining with 5 µM MitoPY1 and subsequently acquired with an Guava easyCyte 8HT flow cytometer (EMD Millipore).

Protein extraction and quantification

Whole-cell extracts of proteins was prepared in RIPA buffer according to standard protocol. A pure mitochondrial fraction was isolated from cell pellets using an iodoxinal gradient and ultracentrifugation according to previous protocol (159). Lysis buffers were supplemented with

cOmplete Mini Protease Inhibitor Cocktail (Sigma), 30 mM sodium fluoride (NaF, Sigma), and 2mM sodium orthovanadate (Na_3VO_4, Sigma). Protein quantification was determined with the Bio-Rad Protein Assay using the recommended experimental setup for microplate readers. Dilutions of Bovine Serum Albumin (BSA) in lysis buffer were used for standard curves. Signal acquisition and analysis were performed with a Spectramax M5 plate reader and the accompanying SoftMax Pro 5 software.

High-density antibody microarray

Lysates from HCT116 mCAT and HCT116 mock were processed using a previously described high-dimensional microarray assay (160, 161). Briefly, proteins in cell lysates and a reference human plasma were labeled with the amine-reactive dyes Cy5 and Cy3, respectively, before mixing (Amersham Biosciences). Unbound dye was removed by centrifugation with 10,000 molecular weight cutoff spin filters (Millipore). Microarray plates contained 3600 unique antibodies (printed in triplicate for a total of 10,800 spots) targeting proteins associated with cell signaling and carcinogenesis. After incubation of dye-labeled samples with the arrays, unbound proteins are washed away to leave only proteins tightly bound by the capture antibodies. Scanning performed with a GenePix 4200A microarray scanner (Molecular Devices, Sunnyvale, CA) measured average pixel intensity of Cy5 signal from sample lysates and Cy3 signal intensity from reference plasma at three separate microspots per sample. The median value of the Cy5/Cy3 ratio from the three readings was used to reduce outliers. Signal normalization proceeded as with two-channel cDNA arrays (162); subsequent analysis was performed with custom Python scripts.

Western Blot

For determination of protein expression, total cell lysates or mitochondrial extracts were prepared as stated above. Western blotting proceeded as previously described (163). Protein extracts were resolved on SDS-PAGE gels, transferred onto PVDF membranes, and incubated with murine antibodies against human HIF1α (1:1000, CST, cat), AKT (1:1000, CST, cat), phospho-JNK (1:200, SCBT), BAX (1:250, BD), BCL2 (1:100, DAKO), or ERK (1:1000, CST); or rabbit antibodies for phospho-AKT (1:1000, CST), catalase (1:1000, Athens Research and Technology), JNK (1:1000, CST), GFP (1:1000, Abcam), or phospho-ERK (1:2000, CST). Anti-β tubulin (Abcam) and anti-Atp5B (CST) antibodies were used as loading controls for catalase expression assessments (Invitrogen, Santa Cruz Bio., respectively); otherwise, samples were normalized by total protein input. Catalase localization and expression experiments used horseradish peroxidase coupled goat anti-mouse and goat anti-rabbit antibodies for chemiluminescence detection. For western blots subsequent to microarray analysis, secondary antibodies AlexaFluor 546-goat anti-mouse or Alexa Fluor 647-goat anti-rabbit were used in conjunction with an Odyssey imaging system (LI-COR Biosciences).

Reverse-phase antibody array

A description of the reverse-phase antibody array production, experimental setup, and analysis are provided in previously published work (164). In this series of experiments, lysates were produced from flash-frozen pellets of 150,000 cultured cells. Each distinct transgene-bearing cell lineage was assayed in technical duplicate for each biological replicate. Lysates were deposited and adhered to mictotiter plates before incubation with primary antibodies. Primary antibodies used in this study are from a curated selection of 48 proteins implicated in carcinogenesis, with particular emphasis on receptor tyrosine kinases and their downstream targets. An anti-actin antibody served as a normalization control. Signal from fluorescent secondary antibodies bound

to primary antibodies was quantified on a spot-by-spot basis. Differences of > 1.5-fold in median signal intensity were considered significant.

Single-cell RNA-seq and analysis

Single-cell RNA-seq adhered to manufacturer guidelines (165). HCT116 cells in log-phase growth were rinsed twice with PBS before detachment with HyQtase (Fisher Scientific). 7000 cells were targeted for each experiment. Resultant libraries were sequenced on a HiSeq 2500 sequencing system (Illumina), yielding ~150 M paired-end reads per sample.

Statistical analysis

Microarray analysis was performed as described (161). Single-cell RNA-seq analysis was accomplished with the R-based Monocle 2 software library (166). Ingenuity Pathway Analysis™ (Qiagen) was used for computing significantly altered metabolic pathways.

3.4 RESULTS

3.4.1 *OXPHOS deficient cancer cells are chemoresistant*

To first address whether reduced OXPHOS activity has a pro-survival effect on tumors, we investigated the effects of respiratory deficiency with cytochrome c oxidase assembly protein null cells (SCO2 -/-) in the colorectal carcinoma cell line HCT116. The chaperone protein SCO2 is responsible for the correct assembly of cytochrome c oxidase (COX, aka Complex IV). Cells without SCO2 have impaired biogenesis of COX and cannot complete the terminal step of the ETC; transfer of electrons to molecular oxygen. Survival of OXPHOS deficient SCO2 -/- HCT116 was addressed with exposure to common chemotherapeutic 5-fluorouracil (5-FU). The antimetabolite 5-FU promotes apoptosis primarily through two routes dependent on the *in vivo* conversion to active metabolites 5-fluoroxyuridine (F-UMP) and 5-5-fluoro-2'deoxyuridine-5'-O-monophosphate (F-dUMP). These metabolites inhibit RNA processing and thymidylate

synthase, respectively; the latter resulting in depletion of thymidine triphosphate (TTP) and subsequent inhibition of DNA synthesis. We selected 5-FU as an apoptosis inducer as it is commonly used in the treatment of colorectal carcinoma and its mechanism of action does not depend directly on OXPHOS activity or ROS homeostasis. We found that in short exposure to high-dose 5-FU, SCO2-/- HCT116 were more resilient than their isogenic parental line, demonstrated by reduced labeling with the early apoptosis indicator Annexin V (Figure 3.1A).

3.4.2 *Reduction of mitochondrial ROS desensitizes cancer cells to chemotherapy*

As ROS are a natural byproduct of oxidative metabolism, it was unclear whether ablated OXPHOS activity alone mediated the pro-survival effects of SCO2 knockout. To refine our model of chemotherapeutic resistance of SCO2-/- cells, we sought to disentangle the related effects of mitochondrial ROS generation and OXPHOS activity. To address the effects of reduced mitochondrial ROS on cancer cell survival, we utilized a modified human catalase (mCAT), which contains an N-terminal mitochondrial localization signal (MLS) to facilitate its import into the mitochondrial matrix where it can reduce endogenous, damaging hydrogen peroxide into water and oxygen. The mCAT construct is constitutively expressed in target cells following stable retroviral-mediated integration (Supplemental Figure B.1). This strategy has been employed to test aspects of the Mitochondrial Theory of Aging (59), which showed that mice harboring a mCAT transgene live significantly longer, healthier lives (81). HCT116 cells expressing mCAT show targeted catalase reduces mitochondrial hydrogen peroxide, sensitivity to hydrogen peroxide-induced cell death, and 5-FU mediated apoptosis (Figure 3.1B,C,D).

3.4.3 *Increased OXPHOS is synergistic with 5-fluorouracil*

If reduced OXPHOS can promote cell survival, we theorized that reversing the glycolytic shift could sensitize cells to chemotherapeutic agents. The formation of pyruvate, a product of

glycolysis, represents a metabolic branching point. Pyruvate decarboxylation by the pyruvate dehydrogenase (PDH) complex produces acetyl-CoA and continues the tricarboxylic acid (TCA) cycle. Alternatively, lactate dehydrogenase can process pyruvate into lactate anaerobically. Dichloroacetate, a byproduct of water chlorination, attenuates the enzymatic regulation of PDH through inhibition of pyruvate dehydrogenase kinase, PDK (167). PDK inhibits the activity of pyruvate dehydrogenase through phosphorylation, thus favoring the production of lactate over acetyl-CoA. The balance between OXPHOS and lactic acid production is approximated through the indirect measurement of cellular oxygen consumption rate (OCR) and extracellular acidification (ECAR) (diagrammed inSupplemental Figure B.2). DCA addition to media stimulates OCR and decreases ECAR in HCT116 cells (**Figure 3.2**A,B). This increased OCR/ECAR ratio was accompanied by greater production of mitochondrial ROS (**Figure 3.2**C). At a dose which produced significant increases in OCR/ECAR, DCA administration was not significantly lethal to HCT116 cells, but proved synergistic with concomitant exposure to 5-FU (**Figure 3.2**D).

3.4.4 *mCAT cells overexpress pro-survival genes compared to parental controls*

To understand the mechanism by which mCAT cells resist apoptosis, we evaluated the levels of key proteins associated with aspects of carcinogenesis using an antibody microarray (160, 161). The array consists of 3463 unique antibodies present with 137 control sites, each in triplicate, for 10800 individually represented spots per sample. Examination revealed 135 differentially expressed proteins between mCAT and those expressing a GFP-only vector (mock). As expected, catalase expression demonstrated one of the largest fold changes in mCAT over parental HCT116 (**Figure 3.3**). Pathway analysis revealed mCAT expression associated with greater translation of pro-survival members of the BCL2 family proteins, altered P53 regulatory

network, and TNF/NFκB signal cascade (**Figure 3.4**). A portion of these results within the apoptotic signaling cascade were confirmed, in part, through western blot (**Figure 3.3**). Of particular note, the ratio of BCL2 to BAX proteins shifted in the mCAT cells to a more BCL2-dominant balance, a known anti-apoptotic state (**Table 3.1**) (168, 169).

To address transcriptional regulation as a possible contributor to the pro-survival phenotype displayed by mCAT, we turned to single-cell RNA-seq. Single-cell RNA-seq allows capture of the underlying heterogeneity in transcriptional states that is lost upon bulk analysis. We profiled ~7000 mCAT and mock cells each at ~20,000 reads per cell. Overall, there were few differences between mCAT and mock across the 16,000 expressed genes, with only 1118 genes displaying significant differential expression. Genes enriched in mCAT cells included members of the interferon (IFNG, predominantly) and TNF signaling pathways (**Figure 3.5**); reduced expression was observed for targets of the mitochondrial LONP1 peptidase and the prolyl hydroxylase EGLN (**Figure 3.6**).

The agreement witnessed between the translation and transcription pathways affected by mCAT expression inspired an appraisal of the regulatory mechanisms that may underlie these findings. In concert with a cohort of phospho-specific antibodies present in the initial microarray, others from a reverse-phase protein array (RPPA) identified protein phosphorylation differences between mCAT, mock and parental HCT116 cells (**Figure 3.7**). Targets of activated protein kinase C (PKC), both MARCKS and NFκB demonstrated increased phosphorylation in mCAT. The activation of NFκB signaling, while typically associated with increased ROS, has also demonstrated increased activity with antioxidant treatment (170). Whereas PAK1 protein levels are relatively unchanged between the cell lines, the active, phosphorylated form of PAK1

(Ser199/204) is more abundant in mCAT cells. PAK1 can inactivate BAD directly through phosphorylation at Ser112; a more abundant species in mCAT cells (171).

3.5 DISCUSSION

Arbiters of apoptosis, effectors of innate immunity, and intracellular signaling elements, ROS are well-known players in a diverse repertoire of physiological roles. Their relationship with cell survival is a particular focus in oncology and gerontology (9, 58, 148, 172, 173). As mitochondria are focal points in the apoptotic signaling cascade and chief location of intracellular ROS generation, their size belies their outsized importance to cell fate. The mechanisms by which they affect cell survival remain murky, especially in the pathological context of cancer. In this manuscript, we relate efforts to describe the effects of reduced mitochondrial ROS on cell survival in the context of cancer, as well as the effects classically altered mitochondrial metabolism may play in this mechanism.

The perturbations to ROS achieved through altered respiration in SCO2-/- and mCAT cells suggest cancer survival is predicated on the local generation of ROS within mitochondria. Consistent with this finding, chemoresistant tumors demonstrate relatively greater uptake of glucose as visualized with FDG-PET imaging (174). The synergy achieved with 5-FU in combination with DCA would also support the converse of the findings shown with SCO2-/- and mCAT cells; that increased OXPHOS/mitochondrial ROS also increases sensitivity of cancer cells to apoptosis.

The mechanism by which sensitization may occur was suggested by our multi-omic approach. The increased activity of NFκB and enhanced production of pro-survival transcripts in mCAT cells offers confirmatory evidence to recent appraisals of both positive and negative regulation of NFκB by ROS. Furthermore, the apparent shift from relatively more pro- to anti-

apoptotic BCL2 family members offers a plausible mechanism for increased resilience of mCAT to cell stress. The ratio of BCL2 family members, many of which contain a conserved BH3 protein domain, commonly indicates a change in the apoptotic threshold ‘setpoint’, and can reflect sensitivity to apoptotic stimuli (169). The concomitant increases in phosphorylated, inactive BAD and phosphorylated, active PAK1 offers an attractive foundation for further study into mechanistic regulation of apoptosis by ROS. Future experimentation as to the kinetic or dynamic implications of these perturbations for the mediators of the intrinsic apoptotic pathway is warranted, perhaps through the recently developed dynamic BH3 profiling technique (175).

Our findings join others to suggest a unique, subcompartment-specific role for ROS in cell fate determination. Targeted alterations in mitochondrial ROS through mCAT expression and treatment with pro-OXPHOS DCA yielded an interconnected network of metabolism and programmed cell death. As well, our coupled transcriptomic and proteomic analysis of reduced mitochondrial ROS demonstrated conserved interactions with likely implications for targeted therapeutic interventions in carcinogenesis. Moreover, our results support investigations into concurrent modulation of mitochondrial ROS as a therapeutic enhancer in clinical approaches to cancer management.

3.6 FIGURES

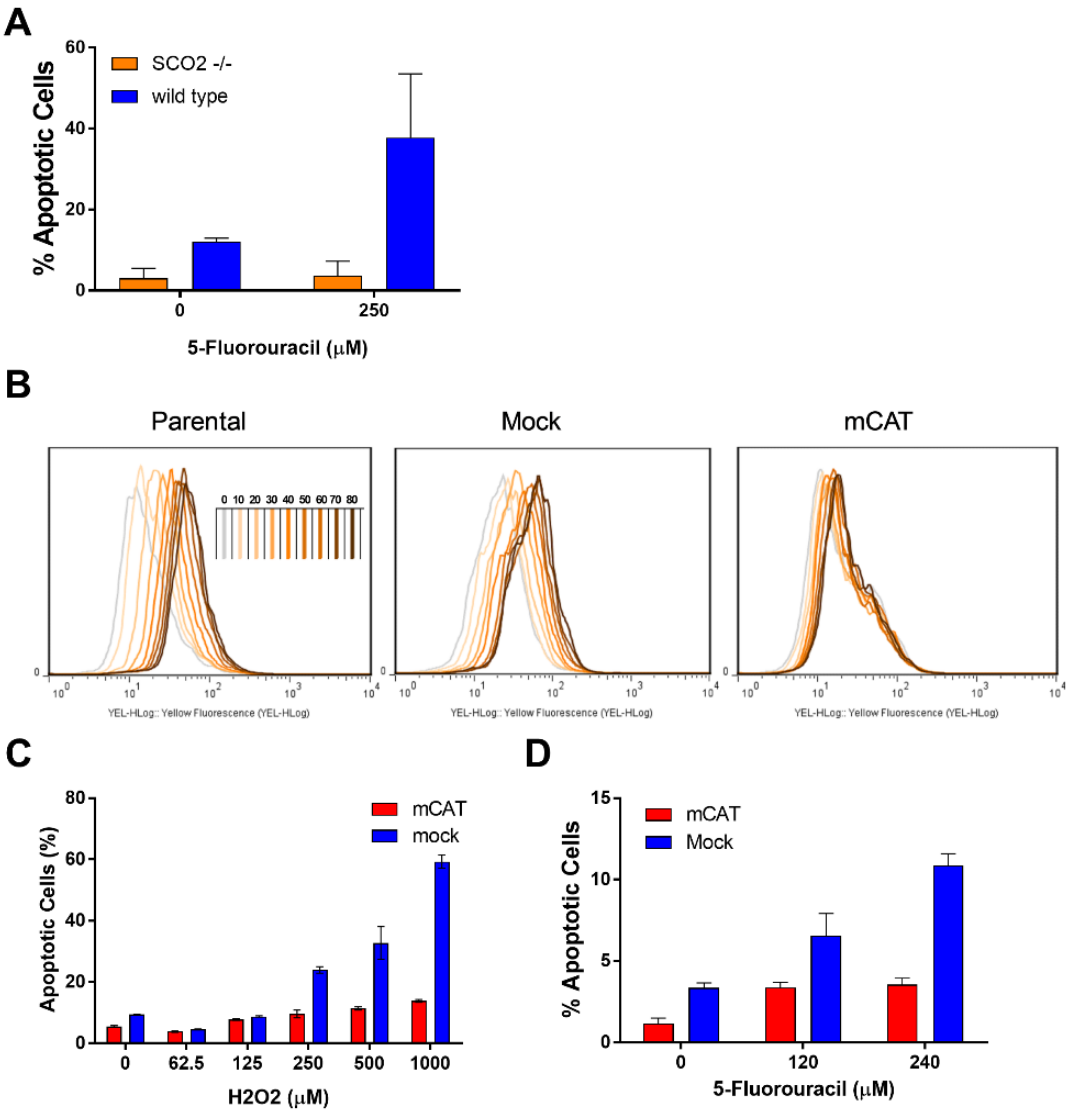

Figure 3.1 Ablated OXPHOS or reduced ROS provide survival benefits to HCT116 cells. (A) Cells were treated with 250 μM of 5-FU for 24h under 20% oxygen condition followed by media change. Floating and attached cells were harvested 48 h after media change, stained with FlowCellect Annexin Red kit from Millipore and acquired on Guava easyCyte 8HT cytometer. Analysis was done using FloJo 9.3.1 software. Early apoptotc cells (positive only for Annexin V) and late apoptotic (positive for both Annexin V and 7-AAD) were taken for graphical presentation. Values shown as mean and s.e.m.; *p*-values determined by Student's t-test. (B) HCT116 cells, parental, Mock, and mCAT, were incubated with MitoPY1, which is oxidized to produce fluorescence by mitochondrial hydrogen peroxide. After an initial 15 minutes of incubation, samples were analyzed by flow cytometery and thereafter at 10 minute intervals for 80 minutes. (C) HCT116 cells expressing either mCAT or mock were treated with hydrogen peroxide for 1 hour, after which they were allowed to recover for 24 hours. Cells were then fixed and analyzed by TUNEL assay for apoptosis. Samples were assayed in triplicate. (D) HCT116 cells were exposed to 5-Fluorouracil for 24 hours in culture, and given 24 hours to recover. Apoptosis was then assayed by TUNEL. Samples were assayed in triplicate.

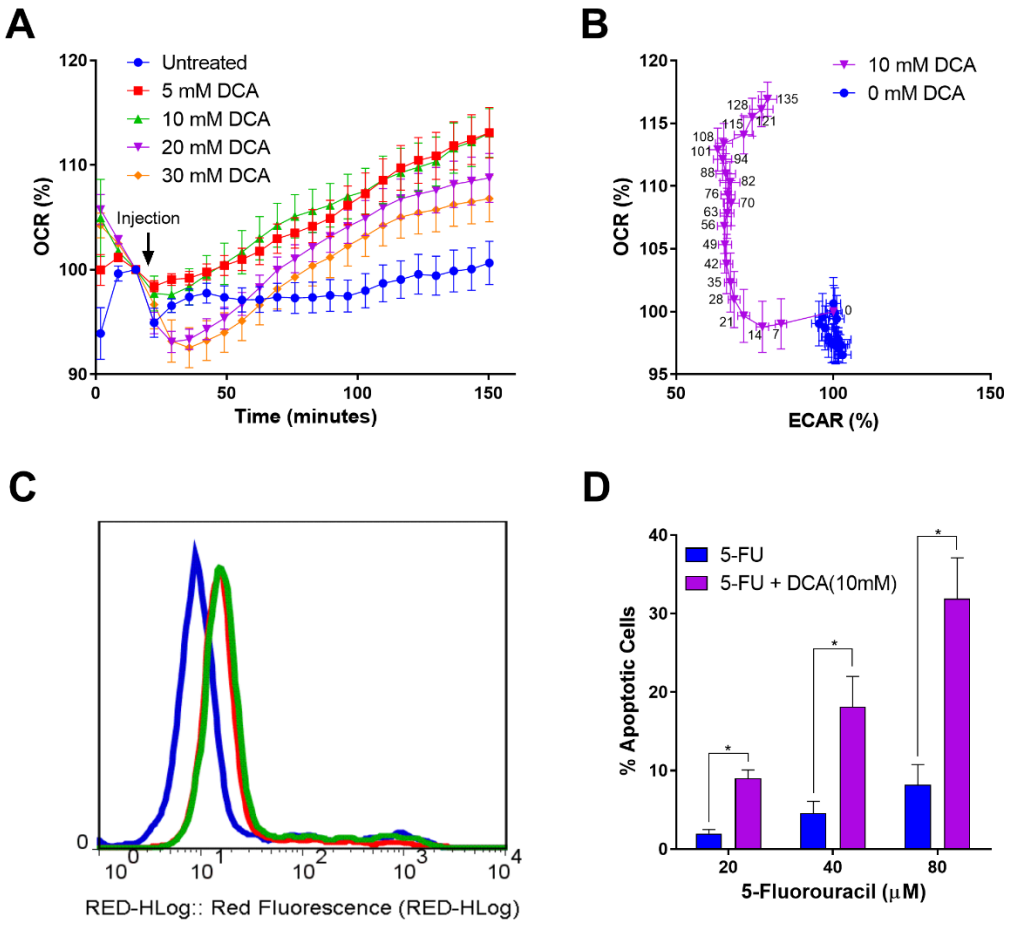

Figure 3.2 Dichloroacetate increases OXPHOS, mitochondrial ROS and apoptotic sensitivity. (A) A Seahorse XF 96 Exctracellular Flux Analyzer was used to evaluate the effects of dichloroacetate (DCA) on HCT116 cell metabolism with measurement of extracellular acidification rate (ECAR) and oxygen consumption rate (OCR), proxies for glycolytic and OXPHOS activities. Treatment with 0, 5, 10, 20, or 30 mM dichloroacetate began after 15 minutes of initial calibration, and was followed for an additional 135 minutes. Results represent the s.e.m. of 12 independent wells. (B) A comparison of untreated and 10 mM DCA effects upon OCR and ECAR. (C) Fluorescent staining of HCT116 cells with the hydrogen peroxide, mitochondrial-localized dye MitoPY1 following 24 hour treatment with 0 mM (blue), 10 mM (red) or 20 mM (green) DCA. (D) Demonstration of syngergism in the combined effects of DCA and 5-FU compared to 5-FU alone in HCT116 cells after 24 hours of treatment. Results reflect the quantification of apoptotic cells from three biological replicates baseline normalized to untreated controls, as measured by sub-G1 staining by propidium iodide.

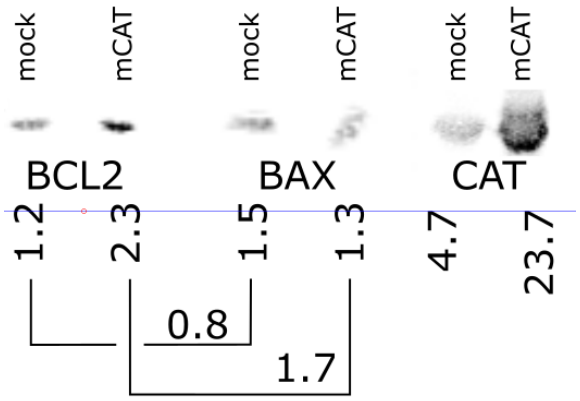

Figure 3.3 Balance in BAX and BCL2 tipped toward survival. Western blots of 20 ug whole cell protein lysate per lane. Numbers next to blots indicate relative intensities as calculated by Odyssey Imaging software. Numbers above connecting lines are the ratio between BCL2 and BAX for mCAT and mock.

Table 3.1 Members of the intrinsic apoptosis pathway affected by mCAT expression.

Protein	Function	Ratio mCAT/Mock (*p*-value)
BCL2	anti-apoptotic, inactivates BAD,BAK,BAX	2.01(0.04)
BCL2L1 (BCL-XL)	anti-apoptotic, inhibits release of mitochondrial contents	1.37 (0.0004)
XIAP	anti-apoptotic, inhibits apoptosis through ubiquitination of pro-apoptotic proteins	1.66 (<0.0001)
BAD	pro-apoptotic, competes for binding to anti-apoptotic BCL2-family proteins, liberating BAX	0.72 (0.04)
BAX	pro-apoptotic, homo-oligomerization to form pores in outer mitochondrial membrane	0.93 (0.04)

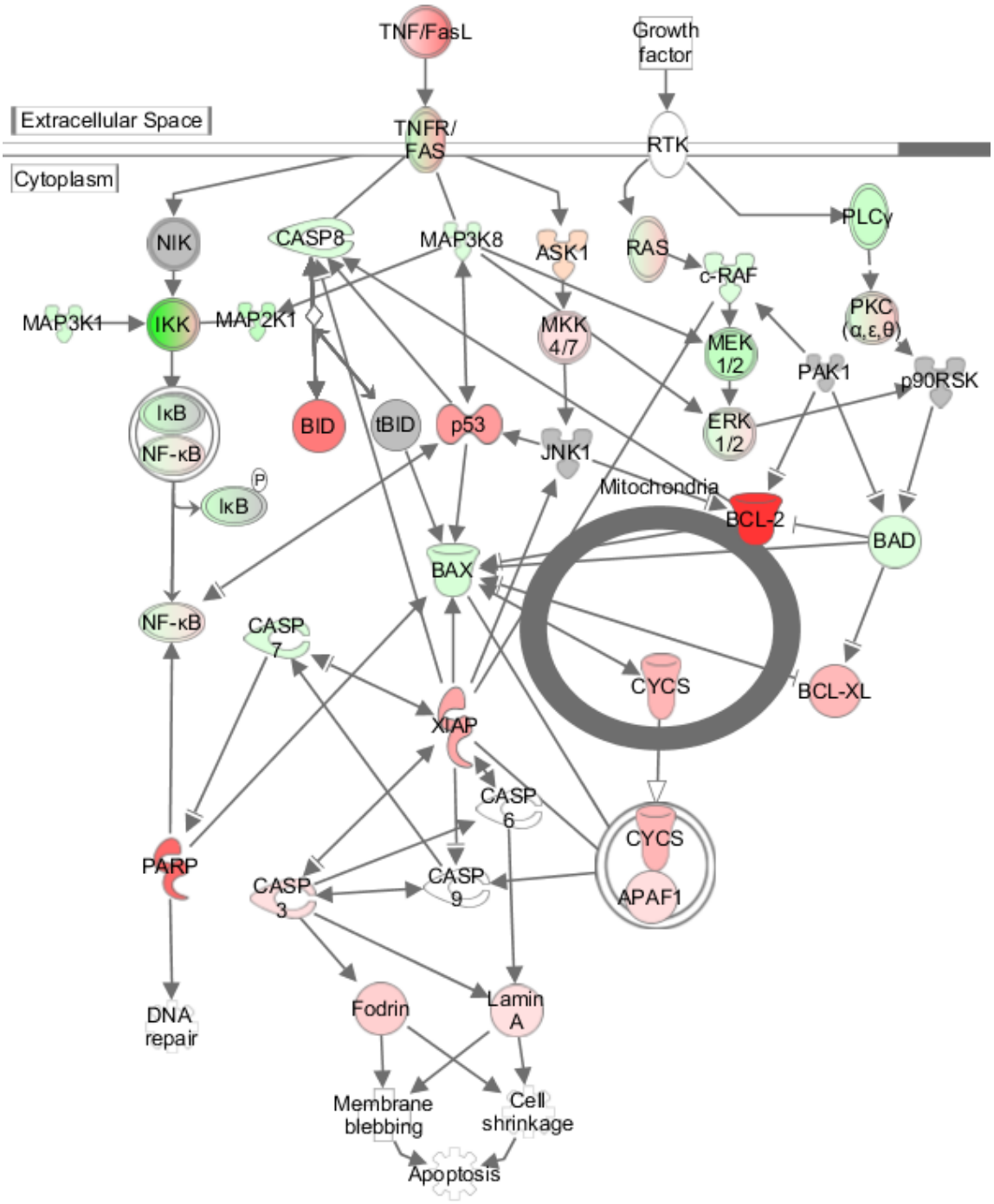

Figure 3.4 Translation differences in mCAT highlight apoptotic signal pathways. Comparisons between mCAT and mock protein lysates reveal differential translation. Extent of differential abundance denoted by color saturation, reflected the log fold change of mCAT/mock; Red: mCAT/mock > 0, Green: mCAT/mock < 0, Gray: non-significant change present. Image created with Qiaqen Ingenuity Pathway Analysis.

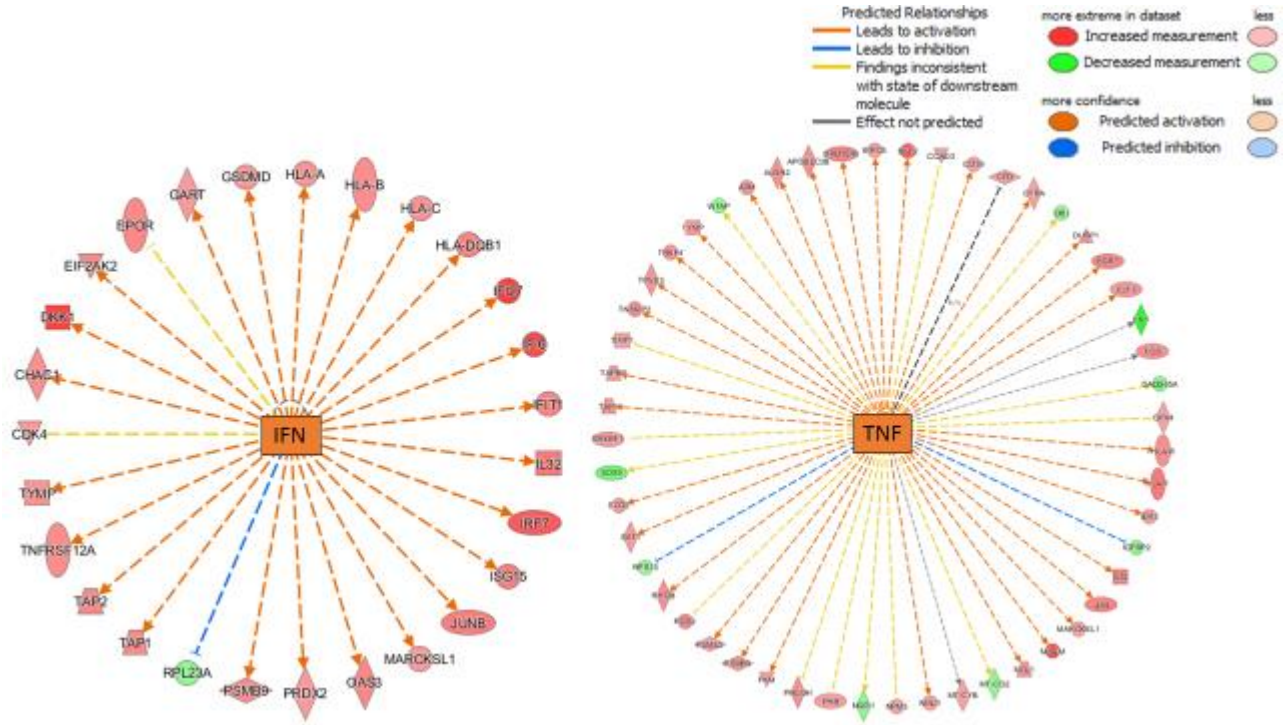

Figure 3.5 Expression of mCAT increases transcription of downstream targets in interferon (IFN) and tumor necrosis factor (TNF) signaling networks. Increased intensity of red or green reflect enrichment or relative reduction in mCAT cells, respectively. Images created from Qiagen Ingenuity Pathway Analysis.

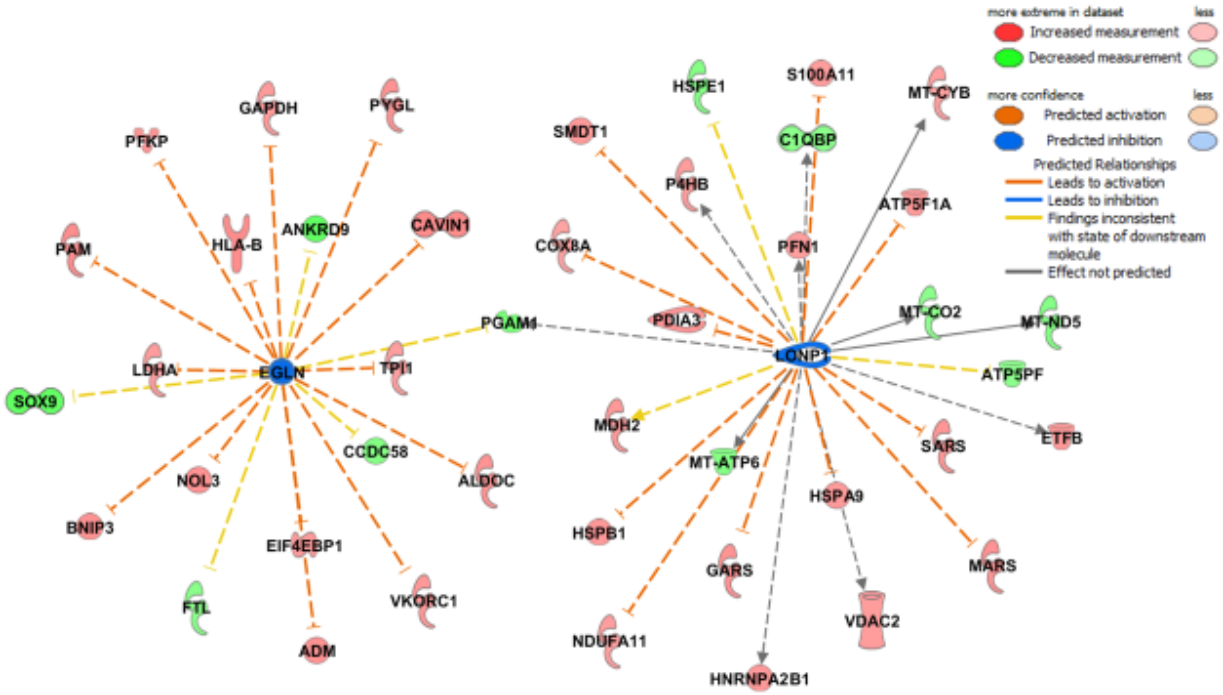

Figure 3.6 Expression of mCAT decreases transcription of targets downstream of EGLN and LONP1 interaction networks. Increased intensity of red or green reflect enrichment or relative reduction in mCAT cells, respectively Images created from Qiagen Ingenuity Pathway Analysis.

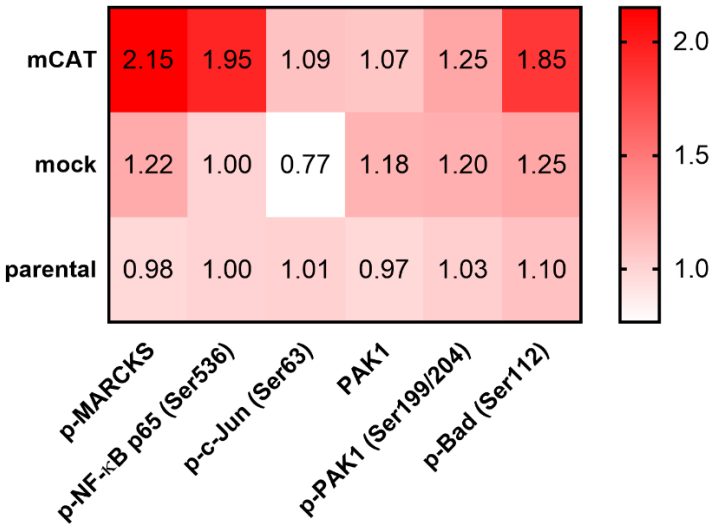

Figure 3.7 mCAT promotes differential phosphorylation in apoptotic regulatory proteins. Reverse Phase Protein Array (RPPA) results demonstrate mCAT expression alters the phospho-specific abundance of key regulators in survival pathways. Numerals represent mean fold change in abundance normalized to the median of the parental HCT116 signal. Results derived from biological duplicates in technical duplicate.

Chapter 4. INDUCTION OF MTDNA MUTAGENESIS WITH REACTIVE OXYGEN SPECIES

This chapter has not been published. Jason Bielas and I designed the study. I performed all experiments, data analysis, and wrote this section.

4.1 ABSTRACT

Aberrations in the mitochondrial genome are associated with neurodegenerative diseases, metabolic syndromes, cancer, and pathologies of aging; although establishing direct links between cause and consequence of mtDNA mutagenesis remains elusive. The mitochondrial theory of aging posits mtDNA mutations arise from genomic damage by reactive oxygen species (ROS). However, recent publications raise doubt that ROS play a prominent role in mtDNA mutagenesis, and instead implicate stochastic polymerase errors in the accumulation of mtDNA mutations seen in aging, largely based on the interpretation of mutation spectra. However, the signatures of polymerase misincorporation and oxidative damage overlap, which obscures clear interpretation of mutation spectra. Thus, we sought to directly test the hypothesis that ROS induce mtDNA mutations. To accomplish this, we produced transgenic cell lines which express either of two mitochondrial-targeted ROS generators, SuperNova or D-amino acid oxidase (DAAO). The modified fluorescent protein, SuperNova, emits superoxide (O_2^-) upon excitation, whereas the peroxisomal enzyme DAAO oxidizes non-standard D-amino acids into achiral imino acids, and in the process generates hydrogen peroxide (H_2O_2). Mitochondrial-targeted versions of SuperNova (mSN) and DAAO (mDAAO) demonstrated localized ROS production, which subsequently yielded polymerase-blocking lesions in mtDNA. Using the recently developed Digital Droplet Random Mutation Capture (dRMC) assay, we quantified point mutations in mtDNA after subchronic exposures to activated mSN or mDAAO. Both exposure regimens

exhibited significant, dose-dependent increases in mtDNA point mutations. The induction of mutation by ROS seen in this study affirms a tenet of the mitochondrial theory of aging and may serve to refocus mtDNA mutagenesis in the lens of oxidative metabolism. These findings have significant implications for the mechanistic interpretation of ROS and mitochondria interactions in models of aging.

4.2 INTRODUCTION

In models of organismal aging, reactive oxygen species (ROS) generate a self-sustaining 'vicious cycle' of oxidative DNA damage, deleterious mutation, dysfunctional protein translation, and ensuing ROS generation (58). Within this paradigm, ROS generated from metabolism initiate mitochondrial DNA (mtDNA) mutation through damage to nucleic acids. However, recent appraisals of mtDNA mutation spectra challenge the model of oxidative stress as a major contributor to mitochondrial mutagenesis, largely through interpretation of mutation signatures (61, 62).

Mutagenesis studies of defined DNA lesions or exposures have established the patterns of mutation consistent with given damage types (117, 176-178). Thus, from a given mutation spectrum, one can ostensibly infer the exposures underlying its creation. The primary mtDNA mutations observed in human tissues are C:G → T:A and T:A → C:G transitions, with a higher proportion of the former on the mitochondrial genome 'heavy strand' (leading strand during replication) and the latter on the 'light strand' (also the reference strand) (36). This strand-biased distribution suggests mtDNA mutagenesis occurs during instances of heavy and light strand separation, as in replication or transcription. Lending credence to this assertion, C → T transitions are consistent with base mis-pairing following deamination of cytosine, an oxidative reaction with 140-fold faster kinetics in single-stranded DNA (37). To attribute these mutations

to ROS is perhaps premature; to date, there have been no direct determinations of the ROS-induced mutation spectra in mitochondrial DNA, though >100 species of mtDNA lesions are proposed to follow ROS damage (142). Absent an established ROS-induced mtDNA mutation spectrum, recent efforts freely speculate oxidative damage is a poor contributor to somatic mtDNA mutagenesis (61, 62, 179).

Inconsistent with such assertions, rodents that express a mitochondrial-targeted antioxidant catalase enzyme (mCAT) display fewer mitochondrial mutations, and comparisons with their wild-type littermates reveal striking differences in the frequency of C→T mutations (81). A similar reduction in mtDNA mutation frequency and altered mutation spectrum is evident in colorectal carcinoma compared to matched normal tissues (13) . The discrepancy in mutation frequency between cancer and normal tissue was accompanied with a shift in metabolism to de-emphasize oxidative metabolism. These results inspire our hypothesis that ROS promote mtDNA mutagenesis.

To address the hypothesis that mitochondrial ROS induce mtDNA mutations, we pursued alternative, non-pharmacological manipulation of mitochondrial ROS, and engineered two separate cell lines to express mitochondrial-localized proteins D-Amino Acid Oxidase (mDAAO) and SuperNova (mSN), a red fluorescent protein (180). DAAO normally is located in the peroxisome, where it generates H_2O_2 during conversion of unusable D-enantiomer amino acids into achiral imino acids. Ectopic expression of DAAO has been previously used to investigate oxidative stress in cultured neurons (181). The mDAAO retroviral construct fuses the ornithine transcarbomylase (OTC) mitochondrial localization signal (MLS) to the N-terminus of the *Rhodotorula gracilis* DAAO. The mSN construct is similar, but includes SuperNova instead. SuperNova is a modified red fluorescent protein that produces superoxide (O_2^-) upon excitation

and can perform chromophore-assisted light inactivation (CALI) to acutely perturb target proteins (180). Together, the mDAAO and mSN constructs produce stable lines with spatiotemporal control over chronic and acute increases in mitochondrial ROS, respectively, without direct alteration of mitochondrial metabolism.

4.3 Materials and Methods

Cell culture

Human colorectal carcinoma cell line HCT116 was acquired through ATCC. All cell lines and their stably transfected derivatives were cultured at 37°C in a humidified, 5% CO_2 incubator at 19% O_2 in DMEM (Gibco) supplemented with 10% fetal bovine serum (FBS), 1 U/mL penicillin, 1 µg/mL streptomycin, and 2 mM L-glutamine (Sigma). pCMMP-mDAAO, pCMMP-MCS, and pCMMP-mSN transfected lines received 1 µg/mL puromycin throughout the study. Other chemicals used during cell treatments include: D-alanine (Sigma), calcium phosphate,

Construct generation and transfection

SuperNova/pRSETB was a gift from Takeharu Nagai (Addgene plasmid # 53234) (180). Digestion of this plasmid with BamHI and EcoRI liberated the SuperNova coding region. This product was resolved via agarose gel electrophoresis and subsequently purified from a portion of the gel (Zymogen). The pBMN-mCAT-IRES-GFP plasmid (described in Chapter 3) was digested with MfeI and SalI, with the larger fragment containing the vector backbone and ornithine transcarbomylase mitochondrial localization sequence. Ligation of the SuperNova fragment with the pBMN-MLS fragment produced the pBMN-SuperNova-IRES-GFP retroviral vector. Ligation product was transfected into DH5α E.coli cells according to manufacturer protocol (Invitrogen). The mDAAO construct was a kind gift of Dr. Rajiv Ratan (Weill Cornell Medicine, White Plains, NY, USA). The empty vector pCMMP-MCS-IRES-Puro was a gift from

Bill Sugden (Addgene plasmid # 36952) (182). pBMN-mDAAO-I-GFP, pBMN-mSN-I-GFP, and pCMMP-MCS-IRES-Puro plasmids were digested with AgeI and NotI (both New England Biosciences). Small fragments representing the mDAAO or mSN inserts were ligated with the empty backbone (from pCMMP-MCS-IRES-Puro). Transformation, colony selection, and capillary eletrophoresis sequencing proceeded as with the pBMN vectors.

The generation of retroviral vector and the production of high-titer vectors followed previously described methods (156). Briefly, the Phoenix packaging cell line derived from HEK293T cells, a kind gift of Dr. Garry Nolan (Stanford University, Palo Alto, CA, USA), was transfected with 10 μg purified retroviral vector by calcium-phosphate method. Culture supernatants containing viral particles were collected 24 h after transfection. Target cell infection was accomplished through the addition of centrifuged and filtered viral supernatant supplemented with 4 μg/mL of polybrene (Sigma) to cultures in log-phase growth for 16 hours. Three infection cycles were performed on consecutive days using freshly acquired viral supernatant. After infection, target cells were plated in fresh culture medium. The efficiency of transduction was evaluated by fluorescence microscopy and/or survival in 1 μg/mL puromycin. Cells infected with fluorescent constructs were sorted by flow cytometry (FACS-Aria, Becton-Dickinson) with standard doublet-discrimination gating and assessment of GFP fluorescence intensity by 488 nm laser excitation. At least 150,000 GFP-positive cells were sorted to found each lineage of transformed cells. Sorting of pCMMP-mSN-IRES-Puro cells based on SuperNova fluorescence yielded no viable cells. The pBMN-mSN-IRES-GFP infected cells were sorted exclusively on GFP fluorescence intensity.

Confocal Microscopy

Static images were obtained using a Zeiss 700 LSM confocal microscope. Kinetic traces were produced from images captured with a Cytation5 Multi-mode imager (BioTek).

Statistical Analysis

All reported results represent at least three biological replicates with 2 technical replicates. Error reported represents s.e.m. Mutation frequencies in mtDNA and lesion frequencies in mtDNA were Poisson transformed during analysis from droplet and RT-PCR data, respectively. For each one-way ANOVA, a one-tailed, post-hoc Dunnett's test was employed to subsequently compare responses at individual doses/concentrations to matched controls. Values of $p < 0.05$ were considered statistically significant. Analysis were performed in Graphpad Prism 7.

4.4 RESULTS

4.4.1 *A genetic approach to generation of mitochondrial ROS*

To address our hypothesis that ROS increases mtDNA mutation frequency, we pursued alternative, non-pharmacological manipulation of mitochondrial ROS. Previous attempts to mutagenize mtDNA (136) demonstrate that ROS-promoting, respiration inhibitors do not induce mtDNA mutagenesis. Additionally, non-specific applications of oxidative stress, such as exogenous H_2O_2 treatments, do not increased mtDNA mutations (136). Given these encountered difficulties to mutagenize mtDNA, we developed a genetic approach to modulation of mitochondrial ROS. We produced spatio-temporal control of ROS, without direct metabolic perturbation via two strategies: expression of mitochondrial-localized proteins D-Amino Acid Oxidase (mDAAO) and SuperNova (mSN), a red fluorescent protein. DAAO normally is located in the peroxisome, where it generates H_2O_2 during conversion of non-standard D-enantiomer amino acids into achiral imino acids. Ectopic expression of DAAO has been previously used to investigate oxidative stress in cultured neurons (181). SuperNova is a modified red fluorescent

protein that produces O_2^- upon excitation and can perform chromophore-assisted light inactivation (CALI) to acutely perturb target proteins (180). Stable transfectants expressing either mDAAO or mSN constructs were created in the colorectal carcinoma cell line, HCT116. Some previous efforts to mutagenize mtDNA have employed this cell line (136), which has a low endogenous frequency of mtDNA deletion mutations (12).

4.4.2 *ROS production by mitochondrial-localized SuperNova induces mtDNA damage*

Chromophore-assisted light inactivation (CALI) is a technique which capitalizes on the phototoxicity of certain excitable moieties by tethering or targeting them to targets of interest (183). Upon excitation, the chromophore ablates target function through, typically, intense local production of destructive ROS, as with the fluorescent proteins KillerRed or SuperNova (180, 184). The SuperNova fluorescent protein is a monomeric form of KillerRed, but which has enhanced stability and less impact upon cell survival (180). SuperNova, like KillerRed, demonstrates rapid production of predominantly O_2^- species upon excitation. Activation of mitochondrial-targeted SuperNova, mSN, demonstrated rapid production of O_2^- as measured with the superoxide-reactive, mitochondrial-targeted dye MitoSOX (Figure 4.1A).

Intense, brief light exposures can kill SuperNova-expressing cells rapidly (180). Lower intensity light, then, was anticipated to produce mitochondrial ROS without significant cell death. Single treatments of up to 30 minutes of broad-spectrum light exposures (73,000 Lux at 580 nm, 2.8W/cm^2), demonstrated no significant induction cell death 24 hours post-exposure by trypan blue exclusion (Figure 4.1B).

To assess whether superoxide produced by mSN damages mtDNA, we undertook a long-run PCR approach, which detects induced polymerase-blocking lesions (17). Induced damage

was detected with 1 minute of white light exposure, and increased with 5 minutes of exposure (Figure 4.1C). This damage was similar to a 10 J/m^2 UVC light exposure control.

The damage to mtDNA produced by 5 minutes of activated mSN was monitored over time, with most repair occurring within 24 hours, and negligible damage visible at 96 hours of recovery (Figure 4.1D).

4.4.3 *Superoxide produced by SuperNova induce mtDNA mutations*

Given the mtDNA damage induced by activated mSN, we hypothesized that repeat exposures of brief, low intensity light would promote mtDNA mutagenesis. HCT116 cells were exposed to white light for 10 days, and allowed 4 days of recovery. This was to ensure the maximal conversion of damage to mutation, and is consistent with international guidelines for recovery periods in determination of genomic instability after putative mutagen exposure (185). To quantify mtDNA point mutations, we implemented a human-specific adaptation of the previously described Digital Droplet Random Mutation Capture assay (dRMC) (17).

Mutations in the mitochondrial 12S rRNA TaqI site were quantified for parental control cells and mSN cells exposed to 0, 1, or 5 minutes of white light (Figure 4.2A). No significant changes were seen in parental cells and untreated mSN cells, although both 1 and 5 minutes of demonstrated 2.01 and 2.10-fold greater mutation frequencies than those which received no light exposures (Figure 4.2A). A similar result was also demonstrated with a less intense amber light, which necessitated longer exposure times (Figure 4.2B).

4.4.4 *mDAAO generates mitochondrial hydrogen peroxide and mtDNA damage*

The results of our SuperNova experiment indicated that acute ROS exposures are capable of mutagenizing mtDNA, but this result fails to answer whether persistent exposures to ROS are capable of inducing mtDNA mutations. It is unclear if reduced respiratory capacity associated

with aging or other mitochondrial defects produce bursts of ROS , or if they produce constant, but elevated ROS. To address whether the duration of ROS exposure could alter our results, we tested the effects of mitochondrial-localized D-amino acid oxidase (DAAO).

To address if chronic ROS exposure affects mtDNA mutagenesis, we created transgenic HCT116 cells that express a modified form of *Rhodotorula gracilis* DAAO with an added N-terminal human mitochondrial localization signal and its C-terminal peroxisomal targeting sequence removed. The DAAO enzyme converts non-standard D-amino acids to their corresponding imino acid through oxidative deamination while also generating hydrogen peroxide as a byproduct (186). Preferable to mammalian DAAO, *R. gracilis* DAAO has greater catalytic activity, lower enzyme affinity, and enhanced resistance to auto-oxidation induced inactivation (181). Detection of hydrogen peroxide proceeded with a mitochondrial-targeted redox-labile fluorescent reporter, roGFP2-Orp1 (187). Excitation of the fluorescent moiety in roGFP2-Orp1 corresponds with the oxidation status of the protein; after interaction with hydrogen peroxide, the excitation wavelength shifts from 488 nm to 405 nm (188). Thus the ratio of light emitted with 405 to the intensity with excitation at 488 nm provides a readout of steady-state hydrogen peroxide concentration (187, 188). With the addition of D-alanine and enzyme cofactor FAD to media, cells expressing mitochondrial-localized DAAO (mDAAO) generate hydrogen peroxide (Figure 4.3A). Mitochondrial hydrogen peroxide was most notable after 2 hours of incubation, with undetectable differences between treated and untreated cells at 12 hours post addition of D-alanine to culture media (Figure 4.3A). The kinetics of induced mtDNA damage proceeded similarly; in mDAAO cells treated with 3 mM D-alanine, LR-PCR detectable damage arose within 4 hours of treatment, peaked at 12 hours, and persisted for 24 hours (Figure 4.3A B).

4.4.5 *Subchronic exposure to hydrogen peroxide induces mtDNA point mutations*

Given the induction of mitochondrial ROS and genomic damage in mDAAO cells exposed to D-alanine, we next investigated if this promoted mtDNA mutagenesis. We adopted a subchronic dosing schedule for D-alanine treatment of HCT116 cells expressing either an empty vector control (multiple cloning site, MCS) or mDAAO. As with the mSN treatment regimen, cells had 4 recovery days after once-daily additions of D-alanine. After 26 consecutive days of exposure, the mtDNA mutation frequencies at the 12S rRNA and COX2 sites were determined via dRMC. We observed no significant differences between untreated and treated cells in any control cell cohort, whereas mDAAO cells exhibited dose-dependent increases in mutation frequency at both sites (p = 0.04, 0.03, test for trend, one-way ANOVA). The mDAAO cells exposed to 3 mM D-alanine displayed mutation frequencies 3.91-fold and 2.93-fold greater at the 12S and COX2 sites, respectively, than those unexposed to D-alanine (Figure 4.4A, B).

4.5 DISCUSSION

A proposed role for ROS in mtDNA mutagenesis may have its origins in the mitochondrial theory of aging (MToA) first proposed by Harman in 1972 (58). Mutation in mtDNA accumulate with age and correlate with increased cell senescence and apoptosis (58, 61, 121, 189). The MToA posits that mtDNA mutations initiate cellular dysfunction through aberrantly encoded electron transport chain (ETC) components, generating excess ROS, which cause further mtDNA damage, perpetuating a vicious cycle of mitochondrial dysfunction that ultimately culminates in cell death (58). Observations of elevated oxidative lesion burdens in mtDNA, mostly in the form of 7,8-dihydro-8-oxoguanine (8-oxoG) (67, 140) have offered support to the MToA model. As well, mice harboring a mitochondrial-targeted version of the antioxidant enzyme catalase (mCAT) demonstrate enhanced longevity and reduced mtDNA mutation frequency (60, 81). However, the MToA as initially proposed has fared poorly under the scrutiny afforded by

advanced approaches in genetic manipulation (62, 190), genomic damage detection (191), and sequencing methodologies (61, 192). Instead, more recent publications have concluded ROS play little role in mtDNA mutagenesis (61, 192).

However, whereas attenutated mitochondrial ROS demonstrates clear reductions in mtDNA mutagenesis (60, 81), there is contradictory evidence for the converse (51, 61, 136, 179). To resolve the role of ROS in mtDNA mutagenesis, we endeavored to directly test the hypothesis that ROS induce mtDNA mutations. We find that, indeed, ROS induce mtDNA point mutations.

Technical advances to mtDNA mutation detection technologies and our targeted approached to mitochondrial ROS modulation are likely contributors to our positive findings. In contrast to cloning and standard sequencing approaches to mutation detection, the Digital Droplet Random Mutation Capture assay (dRMC) enumerates rare mutations without PCR-introduced errors (14, 17, 124, 193). Importantly, the effects of thermal degradation on DNA templates (194) likely generated in some mutation detection methods (137, 195) diminish the sensitivity and reliability of these methods. As well, the stably incorporated ROS generators featured in our experimental design differ significantly from previous experimental approaches to mutagenize mtDNA.

Unlike exogenous oxidant additions (136) or removal of antioxidant defenses (62, 196), mitochondrial-targeted SuperNova and DAAO offer spatiotemporal control of increased mitochondrial ROS. The presence of antioxidant enzymes in the cytosol diminish the efficacy of exogenous treatment with hydrogen peroxide, whether by bolus addition or sustained generation (e.g. xanthine oxidase, glucose oxidase with their respective substrates) (133, 197). The diffusion gradient of hydrogen peroxide across biological membranes can approach 650-fold across the plasma membrane (198). Consequently, the outer and inner mitochondrial membranes likely

impart significant barriers to entry of hydrogen peroxide into the mitochondrial matrix. A more targeted approach to generation of ROS, respiration inhibitors such as rotenone, antimycin A, and cyanide promote mitochondrial ROS production and collapse of the mitochondrial transmembrane potential. However, the evidence for activation of mitochondrial degradation and reduced mutation accumulation by impaired oxidative metabolism and mitochondrial dynamics (199, 200) indicates mitochondrial poisons are unlikely to promote mtDNA mutation.

In contrast to induced mutation, the mCAT mouse model provides convincing evidence that C→T mutations result from oxidative damage. However, it has recently been suggested that the spectrum of mtDNA mutation, characterized by high quantities of C→T mutations and low abundance of G→T mutations is inconsistent with oxidative damage, and that mtDNA mutations arise primarily from polymerase errors (61, 62). However, limited consideration of the full expanse of oxidative damage to mtDNA stymies consensus of what constitutes the mutational spectrum of oxidative damage. Quantification of a single lesion, 8-oxoG and its resultant mutation (G→T), is commonly assumed to reflect total oxidative damage to DNA (62, 63). Unfortunately, this practice fails to capture the complexity or diversity of oxidative damage to mtDNA. Oxidative mtDNA damage manifests as a wide range of lesions (64-66), which vary greatly in mutagenicity (67-69), and thus the frequency of base substitutions does not directly correspond with base-specific, ROS-induced lesion abundance (Figure 3). Differing lesion-specific repair capacity and ability of the mtDNA polymerase, pol γ, to bypass a given lesion determine how often mutation occurs (70). 8-oxoG, while consistently enumerated as an indicator of oxidative DNA damage (63), is less prevalent in mtDNA than other oxidative lesions (67, 68) and only mildly mutagenic to mtDNA due to redundant and highly active repair pathways (71) and a high likelihood of stalling pol γ (72) rather than mutation. Additionally, an

in vitro study describing pol γ incorporation fidelity opposite 8-oxoG observed polymerase inhibition 95% of the time, and that the remaining 5% resulted in correct insertion of cytosine (73).

Although 8-oxo-G lesions are a widely used measurement of oxidative DNA damage, the most abundant lesions following oxidative DNA damage are cytosine derivatives (69). One-electron and radical species-mediated oxidation of cytosine typically occurs at the 5,6-unsaturated bond of cytosine to form unstable intermediary structures. Importantly, oxidation at this position enhances the rate of the ensuing dehydration and deamination reactions by 5-6 orders of magnitude over basal hydrolysis to produce both oxidized cytosine and uracil species (69, 75, 76, 201). These oxidized bases, such as 5-hydroxymethyl uracil and 5-hydroxyuracil (68), are precursors of C→T transitions, the most common oxidative damage-induced mutation (69). However, C→T transitions and their precursor lesions have also been attributed to spontaneous (hydrolytic) damage and pol γ errors during replication (70), but the spectrum of pol γ errors (70) is not consistent with the decrease in C→T transitions seen in colorectal cancer and mCAT mice (70, 72). Furthermore, although deaminated cytosine lesions can arise from base oxidation and hydrolysis, hydrolytic cytosine deamination is sufficiently slow at physiological conditions that it is undetectable *in vitro* (37), whereas *oxidative* cytosine deamination is substantially quicker. Oxidative cytosine deamination is most likely to occur to single-stranded DNA and can thus account for the C→T strand bias seen on the replicative lagging strand of mtDNA (36, 61). This ROS-mediated mutational mechanism is also consistent with the decrease in C→T transitions seen in mCAT mice (60, 81).

In our approach, the damage to mtDNA was determined by long-range PCR. This technique, while adventitious in its ease, is not without caveats. Unlike HPLC-MS/MS or other

highly specific techniques, the identity of the damaged species is undetermined. Identification of the particular lesion types may be possible with pre-incubation of sample DNA with repair enzymes, such as APE1, UNG1, or Fpg (197). These enzymes have a limited repertoire of lesions they recognize; conceivably, combinations of enzymes in an incubation step prior to LR-PCR could limit the list of possible damages present in mtDNA. Variations on this approach have shown dramatic increases in mtDNA damage following singlet oxygen exposure (197). Experimental validation of lesion types following ROS exposure, while not evaluated in this study, represents an understudied arena of inquiry with distinct implications for biomarker development. Moreover, an amended understanding of the lesions present in mtDNA with newer, more accurate techniques is likely to resolve the ongoing debate over the extent to which polymerase misinsertion events or forced errors determine mtDNA mutation.

Our finding that ROS are capable of inducing mutations in mtDNA may serve as a counterpoint to recent works by other groups. However, the assertion that mitochondrial ROS are minor contributors to mtDNA mutagenesis may be true for healthy states or normal aging; yet, in times of cell stress wherein mitochondrial ROS are elevated, our results suggest that mutagenesis will increase. Future mechanistic approaches to evaluation of these concerns is warranted. As well, current work is poised to characterize the spectrum of ROS-induced mtDNA mutations, with likely consequences for previous and future endeavors to describe context-dependent mutagenesis in mtDNA. Given the results of our current studies, it seems there's still life left in the mitochondrial theory of aging.

4.6 FIGURES

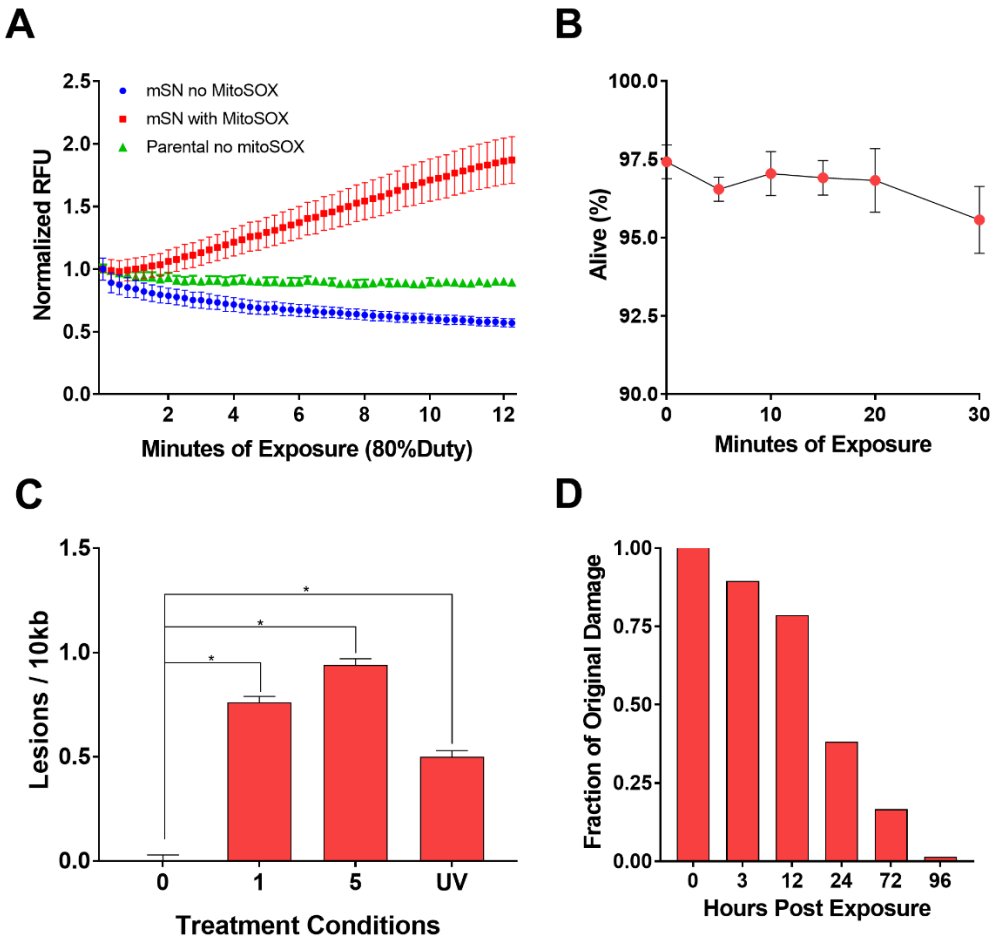

Figure 4.1 Mitochondrial-targeted SuperNova produces ROS and mtDNA damage. (A) Exposure of HCT116 mSN cells to intense, excitatory LED light promotes the generation of mitochondrial superoxide. MitoSOX dye increases fluorescence upon interaction with superoxide dye. Both SuperNova and MitoSOX register in the 'RFP' channel; apparent photobleaching (blue) contrasts with mSN cells pre-incubated with MitoSOX. Untreated HCT116 parental cells served as a control. Images were captured every 15 seconds, with 12 seconds of intervening excitation. Results reflect the average of 4 individual wells. (B) mSN viability 24 hours following exposure to medium-intensity white light for the indicated times. N = 4. (C) Quantity of polymerase-blocking lesions in mtDNA from mSN cells exposed to white light for the indicated minutes of exposure or 10 J/m^2 UVC light. N =3. (D) Normalized fraction of DNA lesions in mtDNA of mSN cells exposed to 5 minutes of white light, as in (C).

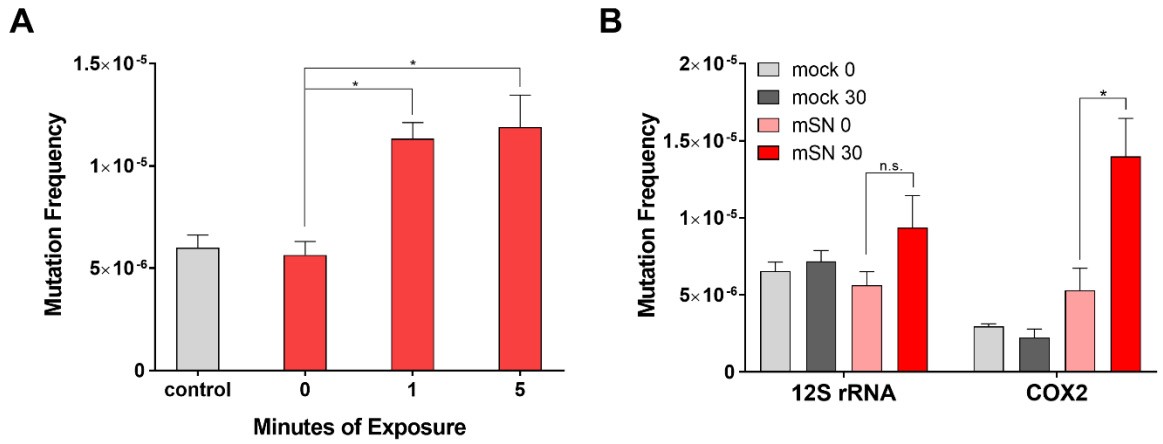

Figure 4.2 Exposure to activated mSN increases rare mtDNA point mutation frequency. (A) HCT116 parental (grey) or mSN-expressing (red) were exposed to 0, 1, or 5 minutes white light once daily for 10 consecutive days before a 4 day recovery period. Results are the point mutation frequency as determined by dRMC for the 12S rRNA TaqI site (locus 1216). Significant differences are seen for 1 and 5 minutes exposures ($p = 0.03$, 0.02, respectively; Student's two-tailed t-test). (B) HCT116 expressing mock or mSN constructs were exposed to 0 or 30 minutes amber light once daily for 10 consecutive days before a 4 day recovery period. Results are the point mutation frequency as determined by dRMC for the 12S rRNA (locus 1216) or COX2 (locus 8006) TaqI sites. Significant differences are seen at the COX2 site ($p = 0.02$, Student's two-tailed t-test). N = 3 biological replicates with the average of their technical duplicates and s.e.m. presented.

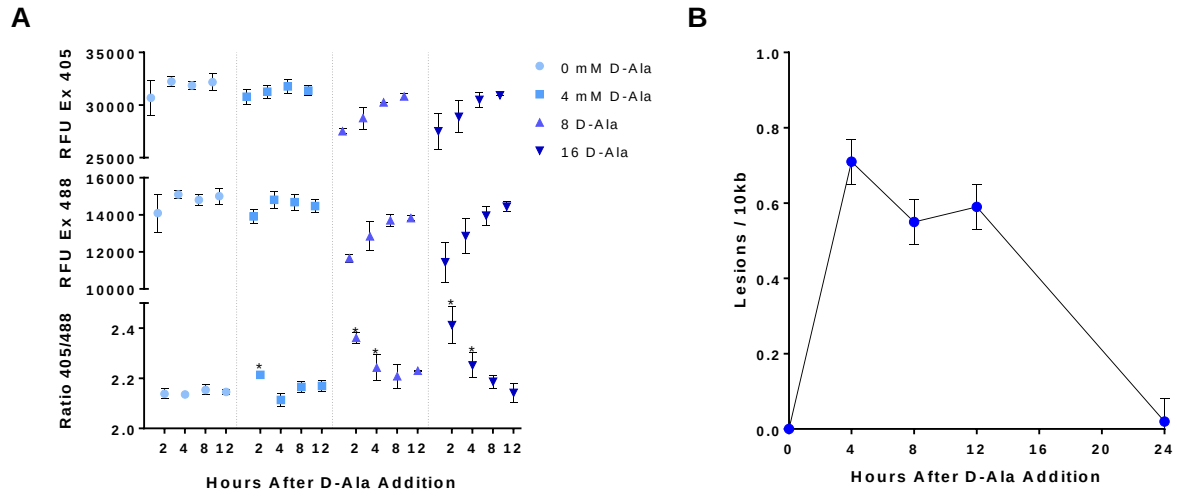

Figure 4.3 Mitochondrial DAAO generates hydrogen peroxide and mtDNA damage.(A) D-alanine treatment in HCT116 mDAAO which express mito-roGFP2-Orp1, a matrix-localized ratiometric fluorescent detector of hydrogen peroxide. The roGFP2-Orp1 construct can be excited by either 405 nm or 488 nm, in a redox-depended manner; roGFP2-Orp1 oxidized by hydrogen peroxide is excited by 405 nm light and peak excitation of reduced roGFP2-Orp1 is achieved with 488 nm light. Ratio of intensities in emitted light following excitation by 405 nm or 488 nm reflects the steady-state abundance of local hydrogen peroxide. N = 4 with s.e.m. $p < 0.05$ for multiple-comparisons-adjusted t-test. (B) HCT116 mDAAO cells treated with either 0 or 3 mM D-alanine were collected at various times after initial exposure. Results represent the lesion frequency as determined by long-range PCR in mtDNA, comparing treated and untreated samples. N = 2, mean with error.

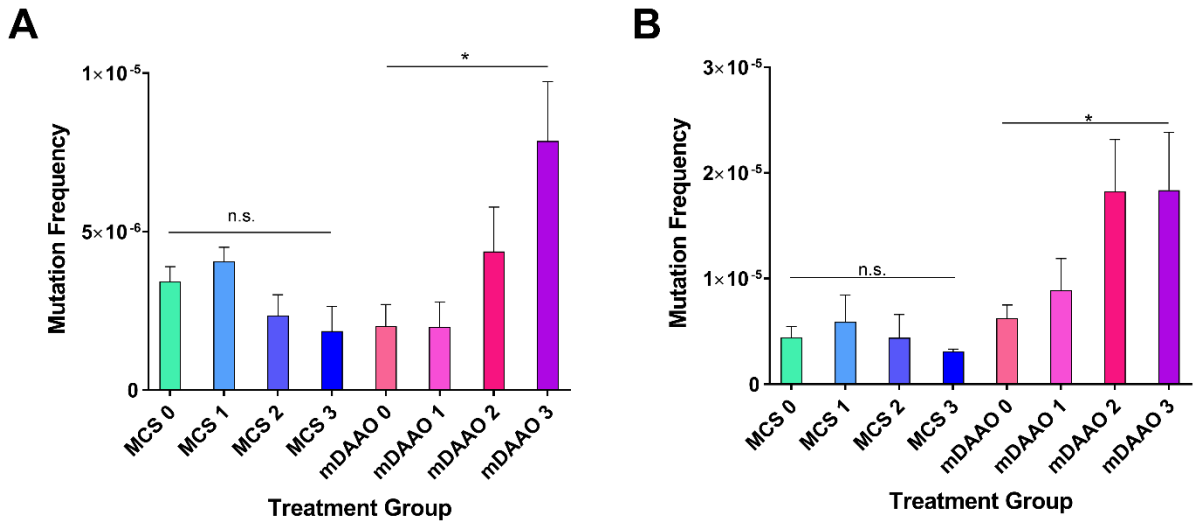

Figure 4.4 Subchronic D-ala treatment increases mtDNA point mutations with mDAAO. Mutation frequency at the 8006 locus in HCT116 cells (Right, +/- s.e.m.). 'MCS' denotes results from cells expressing empty vector. 'mDAAO' denotes cells expressing the targeted DAAO construct. Numbers beside "MCS" and "mDAAO" reflect the dose in mM of D-alanine that was freshly applied on consecutive days for 26 days. Samples were collected after 4 rest days, N = 4.

Chapter 5. CONCLUSIONS AND FUTURE DIRECTIONS

The work detailed in this thesis addresses aspects of long-standing questions in the fields of mitochondrial genetics, aging, and oncology, and lays the foundation for future studies. In answering these questions, I aided in the development and application of novel methodologies and constructs to measure mutation frequency determination, quantify mitochondrial ROS production, and exert spatiotemporal control of ROS. The implementation of these tools will provide better understanding of the modifiers of mtDNA integrity and sequence, cellular fate decisions, and intracellular ROS signaling networks.

We designed our study of genotoxic exposures in mice to address the pervasive belief that susceptibility to interactions with DNA-damaging agents dictates mtDNA mutagenesis and explains its relatively higher frequency of mutation compared to nuclear DNA. These experiments were a proving ground for the dRMC and 3D methodologies developed to address the lack of sensitive mutation detection assays that are also resilient to erroneous mutation calls from damage conversion to “mutation” during PCR. The dRMC and 3D techniques provided critical advances to the throughput and sensitivity of point mutation and deletion detection at defined loci. Through the analysis of mutation data generated by these techniques, we determined B[a]P and ENU fail to induce mtDNA mutations whereas they are potent inducers of nuclear DNA mutations. This negative finding directed my subsequent investigations; the failure of exogenously applied mutagens to increase mtDNA mutation pivoted our attentions toward possible endogenous sources of mtDNA mutagenesis.

Of the very few successful methods for alteration of the mtDNA mutation frequency in which the host organism remains proficient in mtDNA repair pathways, mitochondrial-targeted catalase simultaneously addresses the mitochondrial theory of aging (14, 58, 60, 81). The mCAT

construct, when expressed in mice, increases lifespan and delays pathologies of aging. Additionally, while not reported in the same publication as the lifespan findings (81), mCAT mouse tissues demonstrate reduced mtDNA point mutation frequencies compared to their wild-type littermates. This finding prompted initial inquiries into the properties of cells that can mitigate the accumulation of mtDNA mutations and mitochondrial metabolic byproducts.

Intriguingly, cells expressing mCAT demonstrated reduced sensitivity to pro-apoptotic exposures that had no immediately obvious mitochondrial component to their mode of action. To elucidate the mechanism of this attenuated apoptosis signaling, we pursued multiple lines of inquiry. Initial results from a protein microarray offered the first insights that mitochondrial-localized proteins of the BCL2 family may play a role in the mCAT pro-survival phenotype. The BCL2 family member proteins mediate intrinsic apoptosis through interactions at the mitochondrial outer membrane, and a connection extends between BCL2 protein overexpression and resistance to oxidative cell death (202). Reverse Phase Protein Array (RPPA) and Western Blot results further highlighted the differential regulation of pro-survival proteins in mCAT cells. Transcript-level data from single-cell RNA-seq demonstrated an enrichment for modulation in pathways involved in the inflammatory response, namely increased interferons alpha and gamma (IFNA, IFNG) and tumor necrosis factor (TNF). These expression differences are consistent with the pro-survival phenotype in mCAT cells, and demonstrate this active suppression of cell death signals even in unstressed conditions. Although, imperative to any future research along this vein will be the quantification of changes to gene products in mCAT cells with response to stressors. Those actors which show differential regulation in time-resolved measurements are much more likely to be causally related to modified mitochondrial ROS. Such work would help bridge efforts to translate these findings into clinical research. As well, any intersections of the mCAT

phenotype with the more recently described forms of cell death regulation, like ferroptosis (203), necroptosis (204), or parthanatos (205), may prove particularly useful for characterizing the mechanism by which mCAT exerts its anti-apoptotic effects. Dynamic relationships among the identified pathway members represents a likely fruitful source for future investigation. Temporal changes to anti- and pro-apoptotic factors may elucidate the mechanisms of cancer cell chemoresistance and extended organismal lifespan. Furthermore, as mCAT represents a reduction in mitochondrial ROS burden, a demonstration of the converse finding, that *increased* mitochondrial ROS *increases* apoptotic signaling, is a particularly useful exercise. The SuperNova and DAAO constructs afford such an opportunity for future investigation.

The mitochondrial-targeted constructs of DAAO and SuperNova serve as counterpoints to the reduced mitochondrial ROS modeled with mCAT expression. Additionally, where traditional nuclear mutagens were insufficient to induce mtDNA mutations, both mDAAO and mSN constructs demonstrate ROS increase mtDNA mutation frequency. The paradigm tested with B[a]P and ENU in mice, of damage-induced mtDNA mutation, viewed through the lens of the successful induction of mutations with mDAAO and mSN would suggest mtDNA mutagenesis is restricted by the types of lesions induced by damaging agents, and underscore the importance of oxidative lesions to this process. The uneven distribution of mutation types in mtDNA (13) is consistent with the hypothesis that a select set of DNA damage types can produced mtDNA mutations. Whether mDAAO and mSN promote diverse or limited sets of mutation types is currently unknown, although this is the subject of current investigation. The application of error-corrected Next Generation Sequencing methods (206) to mDAAO and mSN samples after their respective treatment regimens may demonstrate not only increased mutations, but may reveal regional or subtype specificity in the induction of mutations throughout the entire mitochondrial

genome. Whether the results demonstrated with mDAAO and mSN indicate a form of the Mitochondrial Theory of Aging will arise a phoenix from the former remains conjecture. Nonetheless, the clear demonstration of induced mutagenesis with oxidants indicates revisions to models of mtDNA mutagenesis are likely in the future.

The work described here sets the stage for future research into the complex interplay between mitochondrial mutagenesis, metabolism, and cell fate. Development of the dRMC and 3D assays, and the implementation of genetic tools such as mCAT, mDAAO, and mSN afford a precision to the investigation of mitochondrial biology that is likely to reap further rewards for our understanding of the mechanisms of organismal aging and cancer progression.

BIBLIOGRAPHY

1. Hockenbery DM. Mitochondria and Cell Death: Springer New York; 2016.
2. Nass MMK, Nass S. INTRAMITOCHONDRIAL FIBERS WITH DNA CHARACTERISTICS. I Fixation and Electron Staining Reactions. 1963;19(3):593-611. doi: 10.1083/jcb.19.3.593.
3. Sapp J. Beyond the Gene: Cytoplasmic Inheritance and the Struggle for Authority in Genetics: Oxford University Press; 1987. 282 p.
4. Caspari E. Cytoplasmic Inheritance. In: Demerec M, editor. Advances in Genetics: Academic Press; 1948. p. 1-66.
5. Hutchison Iii CA, Newbold JE, Potter SS, Edgell MH. Maternal inheritance of mammalian mitochondrial DNA. Nature. 1974;251:536. doi: 10.1038/251536a0.
6. Wallace DC, Singh G, Lott MT, Hodge JA, Schurr TG, Lezza AM, Elsas LJ, 2nd, Nikoskelainen EK. Mitochondrial DNA mutation associated with Leber's hereditary optic neuropathy. Science. 1988;242(4884):1427-30. Epub 1988/12/09. PubMed PMID: 3201231.
7. Holt IJ, Harding AE, Morgan-Hughes JA. Deletions of muscle mitochondrial DNA in patients with mitochondrial myopathies. Nature. 1988;331(6158):717-9. Epub 1988/02/25. doi: 10.1038/331717a0. PubMed PMID: 2830540.
8. MITOMAP: A Human Mitochondrial Genome Database 2014 [cited 2014 October 31]. Available from: http://www.mitomap.org.
9. Taylor RW, Turnbull DM. Mitochondrial DNA mutations in human disease. Nature reviews Genetics. 2005;6(5):389-402. Epub 2005/04/30. doi: 10.1038/nrg1606. PubMed PMID: 15861210; PMCID: PMC1762815.
10. Ye K, Lu J, Ma F, Keinan A, Gu Z. Extensive pathogenicity of mitochondrial heteroplasmy in healthy human individuals. Proceedings of the National Academy of Sciences. 2014;111(29):10654-9. doi: 10.1073/pnas.1403521111.
11. Payne BA, Wilson IJ, Yu-Wai-Man P, Coxhead J, Deehan D, Horvath R, Taylor RW, Samuels DC, Santibanez-Koref M, Chinnery PF. Universal heteroplasmy of human mitochondrial DNA. Hum Mol Genet. 2013;22(2):384-90. Epub 2012/10/19. doi: 10.1093/hmg/dds435. PubMed PMID: 23077218; PMCID: PMC3526165.
12. Taylor SD, Ericson NG, Burton JN, Prolla TA, Silber JR, Shendure J, Bielas JH. Targeted enrichment and high-resolution digital profiling of mitochondrial DNA deletions in human brain. Aging cell. 2014;13(1):29-38. Epub 2013/08/06. doi: 10.1111/acel.12146. PubMed PMID: 23911137; PMCID: PMC4068027.
13. Ericson NG, Kulawiec M, Vermulst M, Sheahan K, O'Sullivan J, Salk JJ, Bielas JH. Decreased Mitochondrial DNA Mutagenesis in Human Colorectal Cancer. PLoS Genet. 2012;8(6):e1002689. doi: 10.1371/journal.pgen.1002689.
14. Vermulst M, Bielas JH, Loeb LA. Quantification of random mutations in the mitochondrial genome. Methods. 2008;46(4):263-8. Epub 2008/10/25. doi: 10.1016/j.ymeth.2008.10.008. PubMed PMID: 18948200; PMCID: PMC2615251.
15. Schmitt MW, Kennedy SR, Salk JJ, Fox EJ, Hiatt JB, Loeb LA. Detection of ultra-rare mutations by next-generation sequencing. Proceedings of the National Academy of Sciences. 2012;109(36):14508-13. doi: 10.1073/pnas.1208715109.
16. He Y, Wu J, Dressman DC, Iacobuzio-Donahue C, Markowitz SD, Velculescu VE, Diaz Jr LA, Kinzler KW, Vogelstein B, Papadopoulos N. Heteroplasmic mitochondrial DNA mutations in normal and tumour cells. Nature. 2010;464(7288):610-4. doi: http://www.nature.com/nature/journal/v464/n7288/suppinfo/nature08802_S1.html.
17. Valente WJ, Ericson NG, Long AS, White PA, Marchetti F, Bielas JH. Mitochondrial DNA exhibits resistance to induced point and deletion mutations. Nucleic acids research. 2016;44(18):8513-24. Epub 2016/08/24. doi: 10.1093/nar/gkw716. PubMed PMID: 27550180; PMCID: PMC5062989.
18. Larman TC, DePalma SR, Hadjipanayis AG, Network TCGAR, Protopopov A, Zhang J, Gabriel SB, Chin L, Seidman CE, Kucherlapati R, Seidman JG. Spectrum of somatic mitochondrial mutations in five cancers. Proceedings of the National Academy of Sciences. 2012;109(35):14087-91. doi: 10.1073/pnas.1211502109.
19. Ruiz-Pesini E, Mishmar D, Brandon M, Procaccio V, Wallace D. Effects of purifying and adaptive selection on regional variation in human mtDNA. Science. 2004;303(5655):223 - 6. PubMed PMID: doi:10.1126/science.1088434.
20. Stewart JB, Freyer C, Elson JL, Wredenberg A, Cansu Z, Trifunovic A, Larsson N-G. Strong Purifying Selection in Transmission of Mammalian Mitochondrial DNA. PLoS Biol. 2008;6(1):e10. doi: 10.1371/journal.pbio.0060010.
21. Crick FHC. Codon—anticodon pairing: The wobble hypothesis. Journal of molecular biology. 1966;19(2):548-55. doi: http://dx.doi.org/10.1016/S0022-2836(66)80022-0.
22. Brandon M, Baldi P, Wallace D. Mitochondrial mutations in cancer. Oncogene. 2006;25(34):4647 - 62. PubMed PMID: doi:10.1038/sj.onc.1209607.
23. Shidara Y, Yamagata K, Kanamori T, Nakano K, Kwong J, Manfredi G, Oda H, Ohta S. Positive contribution of pathogenic mutations in the mitochondrial genome to the promotion of cancer by prevention from apoptosis. Cancer research. 2005;65(5):1655 - 63. PubMed PMID: doi:10.1158/0008-5472.CAN-04-2012.
24. Gasparre G, Hervouet E, de Laplanche E, Demont J, Pennisi L, Colombel M, Mege-Lechevallier F, Scoazec J, Bonora E, Smeets R. Clonal expansion of mutated mitochondrial DNA is associated with tumor formation and complex I deficiency in the benign renal oncocytoma. Hum Mol Genet. 2008;17(7):986 - 95.
25. Mishmar D, Ruiz-Pesini E, Golik P, Macaulay V, Clark A, Hosseini S, Brandon M, Easley K, Chen E, Brown M. Natural selection shaped regional mtDNA variation in humans. Proc Natl Acad Sci USA. 2003;100(1):171 - 6. PubMed PMID: doi:10.1073/pnas.0136972100.
26. Stafford P, Chen-Quin E. The pattern of natural selection in somatic cancer mutations of human mtDNA. J Hum Genet. 2010;55(9):605 - 12. PubMed PMID: doi:10.1038/jhg.2010.76.
27. Nie H, Shu H, Vartak R, Milstein AC, Mo Y, Hu X, Fang H, Shen L, Ding Z, Lu J, Bai Y. Mitochondrial common deletion, a potential biomarker for cancer occurrence, is selected against in cancer background: a meta-analysis of 38 studies. PloS one. 2013;8(7):e67953. Epub 2013/07/19. doi: 10.1371/journal.pone.0067953. PubMed PMID: 23861839; PMCID: PMC3701633.
28. Chen T, He J, Shen L, Fang H, Nie H, Jin T, Wei X, Xin Y, Jiang Y, Li H, Chen G, Lu J, Bai Y. The mitochondrial DNA 4,977-bp deletion and its implication in copy number alteration in colorectal cancer. BMC medical genetics. 2011;12:8. Epub 2011/01/15. doi: 10.1186/1471-2350-12-8. PubMed PMID: 21232124; PMCID: PMC3025938.
29. Park JS, Sharma LK, Li H, Xiang R, Holstein D, Wu J, Lechleiter J, Naylor SL, Deng JJ, Lu J, Bai Y. A heteroplasmic, not homoplasmic, mitochondrial DNA mutation promotes tumorigenesis via alteration in reactive oxygen species generation and apoptosis. Hum Mol Genet. 2009;18(9):1578-89. Epub 2009/02/12. doi: 10.1093/hmg/ddp069. PubMed PMID: 19208652; PMCID: PMC2733816.

30. Elliott HR, Samuels DC, Eden JA, Relton CL, Chinnery PF. Pathogenic Mitochondrial DNA Mutations Are Common in the General Population. The American Journal of Human Genetics. 2008;83(2):254-60. doi: 10.1016/j.ajhg.2008.07.004.
31. Nekhaeva E, Bodyak ND, Kraytsberg Y, McGrath SB, Van Orsouw NJ, Pluzhnikov A, Wei JY, Vijg J, Khrapko K. Clonally expanded mtDNA point mutations are abundant in individual cells of human tissues. Proceedings of the National Academy of Sciences. 2002;99(8):5521-6. doi: 10.1073/pnas.072670199.
32. Coller H, Khrapko K, Bodyak N, Nekhaeva E, Herrero-Jimenez P, Thilly W. High frequency of homoplasmic mitochondrial DNA mutations in human tumors can be explained without selection. Nature genetics. 2001;28(2):147 - 50. PubMed PMID: doi:10.1038/88859.
33. Taylor RW, Barron MJ, Borthwick GM, Gospel A, Chinnery PF, Samuels DC, Taylor GA, Plusa SM, Needham SJ, Greaves LC, Kirkwood TBL, Turnbull DM. Mitochondrial DNA mutations in human colonic crypt stem cells. The Journal of Clinical Investigation. 2003;112(9):1351-60. doi: 10.1172/JCI19435.
34. Gekeler J, Zsurka G, Kunz WS, Preuss SF, Klussmann JP, Guntinas-Lichius O, Wiesner RJ. Clonal expansion of different mtDNA variants without selective advantage in solid tumors. Mutation research. 2009;662(1-2):28-32. Epub 2008/12/31. doi: 10.1016/j.mrfmmm.2008.11.020. PubMed PMID: 19114048.
35. McMahon S, LaFramboise T. Mutational patterns in the breast cancer mitochondrial genome, with clinical correlates. Carcinogenesis. 2014;35(5):1046-54. Epub 2014/01/21. doi: 10.1093/carcin/bgu012. PubMed PMID: 24442641; PMCID: PMC4004206.
36. Ju YS, Alexandrov LB, Gerstung M, Martincorena I, Nik-Zainal S, Ramakrishna M, Davies HR, Papaemmanuil E, Gundem G, Shlien A, Bolli N, Behjati S, Tarpey PS, Nangalia J, Massie CE, Butler AP, Teague JW, Vassiliou GS, Green AR, Du M-Q, Unnikrishnan A, Pimanda JE, Teh BT, Munshi N, Greaves M, Vyas P, El-Naggar AK, Santarius T, Collins VP, Grundy R, Taylor JA, Hayes DN, Malkin D, Foster CS, Warren AY, Whitaker HC, Brewer D, Eeles R, Cooper C, Neal D, Visakorpi T, Isaacs WB, Bova GS, Flanagan AM, Futreal PA, Lynch AG, Chinnery PF, McDermott U, Stratton MR, Campbell PJ. Origins and functional consequences of somatic mitochondrial DNA mutations in human cancer. Golub T, editor2014 2014-10-01 15:55:06.
37. Frederico LA, Kunkel TA, Shaw BR. A sensitive genetic assay for the detection of cytosine deamination: determination of rate constants and the activation energy. Biochemistry. 1990;29(10):2532-7. Epub 1990/03/13. PubMed PMID: 2185829.
38. Backer JM, Weinstein IB. Mitochondrial DNA Is a Major Cellular Target for a Dihydrodiol-Epoxide Derivative of Benzo[a]pyrene. Science. 1980;209:297-9.
39. Backer JM, Weinstein IB. Interaction of Benzo(a)pyrene and Its Dihydrodiol-Epoxide Derivative with Nuclear and Mitochondrial DNA in C3H10T½ Cell Cultures. Cancer research. 1982;42(7):2764-9.
40. LeDoux SP, Wilson GL, Beecham EJ, Stevnsner T, Wassermann K, Bohr VA. Repair of mitochondrial DNA after various types of DNA damage in Chinese hamster ovary cells. Carcinogenesis. 1992;13(11):1967-73. doi: 10.1093/carcin/13.11.1967.
41. Murata T, Hibasami H, Maekawa S, Tagawa T, Nakashima K. Preferential binding of cisplatin to mitochondrial DNA and suppression of ATP generation in human malignant melanoma cells. Biochemistry international. 1990;20(5):949-55. Epub 1990/01/01. PubMed PMID: 2112385.
42. Wisnovsky SP, Wilson JJ, Radford RJ, Pereira MP, Chan MR, Laposa RR, Lippard SJ, Kelley SO. Targeting mitochondrial DNA with a platinum-based anticancer agent. Chemistry & biology. 2013;20(11):1323-8. Epub 2013/11/05. doi: 10.1016/j.chembiol.2013.08.010. PubMed PMID: 24183971; PMCID: PMC4082333.
43. Yang Z, Schumaker LM, Egorin MJ, Zuhowski EG, Guo Z, Cullen KJ. Cisplatin preferentially binds mitochondrial DNA and voltage-dependent anion channel protein in the mitochondrial membrane of head and neck squamous cell carcinoma: possible role in apoptosis. Clinical cancer research : an official journal of the American Association for Cancer Research. 2006;12(19):5817-25. Epub 2006/10/06. doi: 10.1158/1078-0432.ccr-06-1037. PubMed PMID: 17020989.
44. Gogvadze V, Orrenius S, Zhivotovsky B. Mitochondria as targets for cancer chemotherapy. Seminars in Cancer Biology. 2009;19(1):57-66. doi: http://dx.doi.org/10.1016/j.semcancer.2008.11.007.
45. Tan D, Goerlitz DS, Dumitrescu RG, Han D, Seillier-Moiseiwitsch F, Spernak SM, Orden RA, Chen J, Goldman R, Shields PG. Associations between cigarette smoking and mitochondrial DNA abnormalities in buccal cells. Carcinogenesis. 2008;29(6):1170-7. doi: 10.1093/carcin/bgn034.
46. Prior SL, Griffiths AP, Baxter JM, Baxter PW, Hodder SC, Silvester KC, Lewis PD. Mitochondrial DNA mutations in oral squamous cell carcinoma. Carcinogenesis. 2006;27(5):945-50. Epub 2006/01/13. doi: 10.1093/carcin/bgi326. PubMed PMID: 16407369.
47. Bandelt H, Salas A. Contamination and sample mix-up can best explain some patterns of mtDNA instabilities in buccal cells and oral squamous cell carcinoma. BMC Cancer. 2009;9:113. PubMed PMID: doi:10.1186/1471-2407-9-113.
48. Lai CH, Huang SF, Liao CT, Chen IH, Wang HM, Hsieh LL. Clinical significance in oral cavity squamous cell carcinoma of pathogenic somatic mitochondrial mutations. PloS one. 2013;8(6):e65578. Epub 2013/06/27. doi: 10.1371/journal.pone.0065578. PubMed PMID: 23799027; PMCID: PMC3683038.
49. Berneburg M, Grether-Beck S, Kürten V, Ruzicka T, Briviba K, Sies H, Krutmann J. Singlet Oxygen Mediates the UVA-induced Generation of the Photoaging-associated Mitochondrial Common Deletion. Journal of Biological Chemistry. 1999;274(22):15345-9.
50. Jandova J, Shi M, Norman KG, Stricklin GP, Sligh JE. Somatic alterations in mitochondrial DNA produce changes in cell growth and metabolism supporting a tumorigenic phenotype. Biochimica et Biophysica Acta (BBA) - Molecular Basis of Disease. 2012;1822(2):293-300. doi: http://dx.doi.org/10.1016/j.bbadis.2011.11.010.
51. Mambo E, Gao X, Cohen Y, Guo Z, Talalay P, Sidransky D. Electrophile and oxidant damage of mitochondrial DNA leading to rapid evolution of homoplasmic mutations. Proceedings of the National Academy of Sciences. 2003;100(4):1838-43. doi: 10.1073/pnas.0437910100.
52. Stumpf JD, Copeland WC. MMS Exposure Promotes Increased MtDNA Mutagenesis in the Presence of Replication-Defective Disease-Associated DNA Polymerase γ Variants. PLoS Genet. 2014;10(10):e1004748. doi: 10.1371/journal.pgen.1004748.
53. Mita S, Monnat RJ, Jr., Loeb LA. Resistance of HeLa cell mitochondrial DNA to mutagenesis by chemical carcinogens. Cancer research. 1988;48(16):4578-83. Epub 1988/08/15. PubMed PMID: 3135115.
54. Bielas JH, Loeb KR, Rubin BP, True LD, Loeb LA. Human cancers express a mutator phenotype. Proceedings of the National Academy of Sciences. 2006;103(48):18238-42. doi: 10.1073/pnas.0607057103.
55. Wang D, Kreutzer DA, Essigmann JM. Mutagenicity and repair of oxidative DNA damage: insights from studies using defined lesions. Mutation research. 1998;400(1-2):99-115. Epub 1998/08/01. PubMed PMID: 9685598.
56. Yu M, Shi Y, Wei X, Yang Y, Zang F, Niu R. Mitochondrial DNA depletion promotes impaired oxidative status and adaptive resistance to apoptosis in T47D breast cancer cells. European journal of cancer prevention : the official journal of the European Cancer Prevention Organisation (ECP). 2009;18(6):445-57.
57. Warburg OP, K.; Negelein, E. Ueber den Stoffwechsel der Tumoren. Biochemische Zeitschrift. 1930;152:319-44.

58. Harman D. The biologic clock: the mitochondria? Journal of the American Geriatrics Society. 1972;20(4):145-7. Epub 1972/04/01. PubMed PMID: 5016631.
59. Jacobs HT. The mitochondrial theory of aging: dead or alive? Aging cell. 2003;2(1):11-7. Epub 2003/07/29. PubMed PMID: 12882330.
60. Vermulst M, Bielas JH, Kujoth GC, Ladiges WC, Rabinovitch PS, Prolla TA, Loeb LA. Mitochondrial point mutations do not limit the natural lifespan of mice. Nature genetics. 2007;39(4):540-3. doi: http://www.nature.com/ng/journal/v39/n4/suppinfo/ng1988_S1.html.
61. Kennedy SR, Salk JJ, Schmitt MW, Loeb LA. Ultra-Sensitive Sequencing Reveals an Age-Related Increase in Somatic Mitochondrial Mutations That Are Inconsistent with Oxidative Damage. PLoS Genet. 2013;9(9):e1003794. doi: 10.1371/journal.pgen.1003794.
62. Itsara LS, Kennedy SR, Fox EJ, Yu S, Hewitt JJ, Sanchez-Contreras M, Cardozo-Pelaez F, Pallanck LJ. Oxidative Stress Is Not a Major Contributor to Somatic Mitochondrial DNA Mutations. PLoS Genet. 2014;10(2):e1003974. doi: 10.1371/journal.pgen.1003974.
63. Ravanat JL, Cadet J, Douki T. Oxidatively generated DNA lesions as potential biomarkers of in vivo oxidative stress. Current molecular medicine. 2012;12(6):655-71. Epub 2012/02/02. PubMed PMID: 22292434.
64. Kauppila JH, Stewart JB. Mitochondrial DNA: Radically free of free-radical driven mutations. Biochim Biophys Acta. 2015;1847(11):1354-61. Epub 2015/06/09. doi: 10.1016/j.bbabio.2015.06.001. PubMed PMID: 26050972.
65. Pinz KG, Shibutani S, Bogenhagen DF. Action of mitochondrial DNA polymerase gamma at sites of base loss or oxidative damage. The Journal of biological chemistry. 1995;270(16):9202-6. Epub 1995/04/21. PubMed PMID: 7721837.
66. Thiviyanathan V, Somasunderam A, Volk DE, Hazra TK, Mitra S, Gorenstein DG. Base-pairing properties of the oxidized cytosine derivative, 5-hydroxy uracil. Biochemical and biophysical research communications. 2008;366(3):752-7. Epub 2007/12/15. doi: 10.1016/j.bbrc.2007.12.010. PubMed PMID: 18078807; PMCID: Pmc2262052.
67. Anson RM, Senturker S, Dizdaroglu M, Bohr VA. Measurement of oxidatively induced base lesions in liver from Wistar rats of different ages. Free radical biology & medicine. 1999;27(3-4):456-62. Epub 1999/09/01. PubMed PMID: 10468222.
68. Lim KS, Jeyaseelan K, Whiteman M, Jenner A, Halliwell B. Oxidative damage in mitochondrial DNA is not extensive. Annals of the New York Academy of Sciences. 2005;1042:210-20. Epub 2005/06/21. doi: 10.1196/annals.1338.023. PubMed PMID: 15965065.
69. Kreutzer DA, Essigmann JM. Oxidized, deaminated cytosines are a source of C → T transitions in vivo. Proceedings of the National Academy of Sciences of the United States of America. 1998;95(7):3578-82. PubMed PMID: PMC19878.
70. Lee HR, Johnson KA. Fidelity of the human mitochondrial DNA polymerase. The Journal of biological chemistry. 2006;281(47):36236-40. doi: 10.1074/jbc.M607964200. PubMed PMID: 17005554.
71. Alexeyev M, Shokolenko I, Wilson G, LeDoux S. The maintenance of mitochondrial DNA integrity--critical analysis and update. Cold Spring Harbor perspectives in biology. 2013;5(5):a012641. Epub 2013/05/03. doi: 10.1101/cshperspect.a012641. PubMed PMID: 23637283; PMCID: Pmc3632056.
72. Johnson AA, Johnson KA. Exonuclease proofreading by human mitochondrial DNA polymerase. The Journal of biological chemistry. 2001;276(41):38097-107. Epub 2001/07/31. doi: 10.1074/jbc.M106046200. PubMed PMID: 11477094.
73. Graziewicz MA, Bienstock RJ, Copeland WC. The DNA polymerase γ Y955C disease variant associated with PEO and parkinsonism mediates the incorporation and translesion synthesis opposite 7,8-dihydro-8-oxo-2′-deoxyguanosine. Human Molecular Genetics. 2007;16(22):2729-39. doi: 10.1093/hmg/ddm227.
74. Halliwell B, Aruoma OI. DNA damage by oxygen-derived species. Its mechanism and measurement in mammalian systems. FEBS Lett. 1991;281(1-2):9-19. Epub 1991/04/09. PubMed PMID: 1849843.
75. Feig DI, Sowers LC, Loeb LA. Reverse chemical mutagenesis: identification of the mutagenic lesions resulting from reactive oxygen species-mediated damage to DNA. Proceedings of the National Academy of Sciences of the United States of America. 1994;91(14):6609-13. Epub 1994/07/05. PubMed PMID: 7517554; PMCID: Pmc44252.
76. Samson-Thibault F, Madugundu GS, Gao S, Cadet J, Wagner JR. Profiling Cytosine Oxidation in DNA by LC-MS/MS. Chemical Research in Toxicology. 2012;25(9):1902-11. doi: 10.1021/tx300195f.
77. Schon EA, DiMauro S, Hirano M. Human mitochondrial DNA: roles of inherited and somatic mutations. Nature reviews Genetics. 2012;13(12):878-90.
78. Bender A, Krishnan KJ, Morris CM, Taylor GA, Reeve AK, Perry RH, Jaros E, Hersheson JS, Betts J, Klopstock T, Taylor RW, Turnbull DM. High levels of mitochondrial DNA deletions in substantia nigra neurons in aging and Parkinson disease. Nature genetics. 2006;38(5):515-7. doi: http://www.nature.com/ng/journal/v38/n5/suppinfo/ng1769_S1.html.
79. Trifunovic A, Wredenberg A, Falkenberg M, Spelbrink JN, Rovio AT, Bruder CE, Bohlooly YM, Gidlof S, Oldfors A, Wibom R, Tornell J, Jacobs HT, Larsson NG. Premature ageing in mice expressing defective mitochondrial DNA polymerase. Nature. 2004;429(6990):417-23. Epub 2004/05/28. doi: 10.1038/nature02517. PubMed PMID: 15164064.
80. Kujoth GC, Hiona A, Pugh TD, Someya S, Panzer K, Wohlgemuth SE, Hofer T, Seo AY, Sullivan R, Jobling WA, Morrow JD, Van Remmen H, Sedivy JM, Yamasoba T, Tanokura M, Weindruch R, Leeuwenburgh C, Prolla TA. Mitochondrial DNA mutations, oxidative stress, and apoptosis in mammalian aging. Science. 2005;309(5733):481-4. Epub 2005/07/16. doi: 10.1126/science.1112125. PubMed PMID: 16020738.
81. Schriner SE, Linford NJ, Martin GM, Treuting P, Ogburn CE, Emond M, Coskun PE, Ladiges W, Wolf N, Van Remmen H, Wallace DC, Rabinovitch PS. Extension of murine life span by overexpression of catalase targeted to mitochondria. Science. 2005;308(5730):1909-11. doi: 10.1126/science.1106653. PubMed PMID: 15879174.
82. Imanishi H, Hattori K, Wada R, Ishikawa K, Fukuda S, Takenaga K, Nakada K, Hayashi J. Mitochondrial DNA mutations regulate metastasis of human breast cancer cells. PloS one. 2011;6(8):e23401. Epub 2011/08/20. doi: 10.1371/journal.pone.0023401. PubMed PMID: 21853128; PMCID: PMC3154938.
83. Lee H-C, Chang C-M, Chi C-W. Somatic mutations of mitochondrial DNA in aging and cancer progression. Ageing Research Reviews. 2010;9, Supplement(0):S47-S58. doi: http://dx.doi.org/10.1016/j.arr.2010.08.009.
84. Yakes FM, Van Houten B. Mitochondrial DNA damage is more extensive and persists longer than nuclear DNA damage in human cells following oxidative stress. Proceedings of the National Academy of Sciences. 1997;94(2):514-9.
85. Hunter SE, Jung D, Di Giulio RT, Meyer JN. The QPCR assay for analysis of mitochondrial DNA damage, repair, and relative copy number. Methods. 2010;51(4):444-51. doi: 10.1016/j.ymeth.2010.01.033. PubMed PMID: 20123023; PMCID: 2912960.
86. Hunter SE, Gustafson MA, Margillo KM, Lee SA, Ryde IT, Meyer JN. In vivo repair of alkylating and oxidative DNA damage in the mitochondrial and nuclear genomes of wild-type and glycosylase-deficient Caenorhabditis elegans. DNA Repair (Amst). 2012;11(11):857-63. Epub 2012/09/11. doi: 10.1016/j.dnarep.2012.08.002. PubMed PMID: 22959841; PMCID: PMC3484215.

87. Le Goff J, Gallois J, Pelhuet L, Devier MH, Budzinski H, Pottier D, Andre V, Cachot J. DNA adduct measurements in zebra mussels, Dreissena polymorpha, Pallas. Potential use for genotoxicant biomonitoring of fresh water ecosystems. Aquatic toxicology. 2006;79(1):55-64. doi: 10.1016/j.aquatox.2006.05.002. PubMed PMID: 16780971.
88. Guliaeva NA, Kuznetsova EA, Gaziev AI. [Proteins associated with mitochondrial DNA protect it against the action of X-rays and hydrogen peroxide]. Biofizika. 2006;51(4):692-7. Epub 2006/08/17. PubMed PMID: 16909848.
89. Canugovi C, Maynard S, Bayne AC, Sykora P, Tian J, de Souza-Pinto NC, Croteau DL, Bohr VA. The mitochondrial transcription factor A functions in mitochondrial base excision repair. DNA Repair (Amst). 2010;9(10):1080-9. Epub 2010/08/27. doi: 10.1016/j.dnarep.2010.07.009. PubMed PMID: 20739229; PMCID: PMC2955416.
90. Huang JC, Zamble DB, Reardon JT, Lippard SJ, Sancar A. HMG-domain proteins specifically inhibit the repair of the major DNA adduct of the anticancer drug cisplatin by human excision nuclease. Proceedings of the National Academy of Sciences of the United States of America. 1994;91(22):10394-8. Epub 1994/10/25. PubMed PMID: 7937961; PMCID: PMC45026.
91. Marcelino LA, Thilly WG. Mitochondrial mutagenesis in human cells and tissues. Mutation Research/DNA Repair. 1999;434(3):177-203. doi: http://dx.doi.org/10.1016/S0921-8777(99)00028-2.
92. Niranjan BG, Bhat NK, Avadhani NG. Preferential attack of mitochondrial DNA by aflatoxin B1 during hepatocarcinogenesis. Science. 1982;215(4528):73-5. Epub 1982/01/01. PubMed PMID: 6797067.
93. Wunderlich V, Schutt M, Bottger M, Graffi A. Preferential alkylation of mitochondrial deoxyribonucleic acid by N-methyl-N-nitrosourea. The Biochemical journal. 1970;118(1):99-109. Epub 1970/06/01. PubMed PMID: 5472159; PMCID: PMC1179086.
94. Guzzella L, Monarca S, Zani C, Feretti D, Zerbini I, Buschini A, Poli P, Rossi C, Richardson SD. In vitro potential genotoxic effects of surface drinking water treated with chlorine and alternative disinfectants. Mutation Research/Genetic Toxicology and Environmental Mutagenesis. 2004;564(2):179-93. doi: http://dx.doi.org/10.1016/j.mrgentox.2004.08.006.
95. Berneburg M, Plettenberg H, Medve-Konig K, Pfahlberg A, Gers-Barlag H, Gefeller O, Krutmann J. Induction of the Photoaging-Associated Mitochondrial Common Deletion In Vivo in Normal Human Skin. J Investig Dermatol. 2004;122(5):1277-83.
96. Gebhard D, Mahler B, Matt K, Burger K, Bergemann J. Mitochondrial DNA copy number – but not a mitochondrial tandem CC to TT transition – is increased in sun-exposed skin. Experimental Dermatology. 2014;23(3):209-11. doi: 10.1111/exd.12327.
97. Kraytsberg Y, Nicholas A, Caro P, Khrapko K. Single molecule PCR in mtDNA mutational analysis: Genuine mutations vs. damage bypass-derived artifacts. Methods. 2008;46(4):269-73. doi: 10.1016/j.ymeth.2008.10.005. PubMed PMID: 18955147; PMCID: 2654379.
98. Rothfuss O, Gasser T, Patenge N. Analysis of differential DNA damage in the mitochondrial genome employing a semi-long run real-time PCR approach. Nucleic acids research. 2010;38(4):e24. doi: 10.1093/nar/gkp1082. PubMed PMID: 19966269; PMCID: 2831309.
99. Brault D, Renault D, Tombolan F, Thybaud V. Kinetics of induction of DNA damage and lacZ gene mutations in stomach mucosa of mice treated with beta-propiolactone and N-methyl-N'-nitro-N-nitrosoguanidine, using single-cell gel electrophoresis and MutaMouse models. Environmental and molecular mutagenesis. 1999;34(2-3):182-9. Epub 1999/10/26. PubMed PMID: 10529742.
100. Lemieux CL, Douglas GR, Gingerich J, Phonethepswath S, Torous DK, Dertinger SD, Phillips DH, Arlt VM, White PA. Simultaneous measurement of benzo[a]pyrene-induced Pig-a and lacZ mutations, micronuclei and DNA adducts in Muta Mouse. Environmental and molecular mutagenesis. 2011;52(9):756-65. doi: 10.1002/em.20688. PubMed PMID: 21976233; PMCID: 3258540.
101. Douglas GR, Gingerich JD, Gossen JA, Bartlett SA. Sequence spectra of spontaneous lacZ gene mutations in transgenic mouse somatic and germline tissues. Mutagenesis. 1994;9(5):451-8. Epub 1994/09/01. PubMed PMID: 7837979.
102. Vijg JD, G. Bacteriophage lambda and plasmid LacZ transgenic mice for studying mutations in vivo. Pfeifer G, editor. New York: Plenum Press; 1996.
103. Ye J, Coulouris G, Zaretskaya I, Cutcutache I, Rozen S, Madden TL. Primer-BLAST: a tool to design target-specific primers for polymerase chain reaction. BMC bioinformatics. 2012;13:134. Epub 2012/06/20. doi: 10.1186/1471-2105-13-134. PubMed PMID: 22708584; PMCID: PMC3412702.
104. Pinheiro LB, Coleman VA, Hindson CM, Herrmann J, Hindson BJ, Bhat S, Emslie KR. Evaluation of a Droplet Digital Polymerase Chain Reaction Format for DNA Copy Number Quantification. Analytical Chemistry. 2011;84(2):1003-11. doi: 10.1021/ac202578x.
105. Hindson BJ, Ness KD, Masquelier DA, Belgrader P, Heredia NJ, Makarewicz AJ, Bright IJ, Lucero MY, Hiddessen AL, Legler TC, Kitano TK, Hodel MR, Petersen JF, Wyatt PW, Steenblock ER, Shah PH, Bousse LJ, Troup CB, Mellen JC, Wittmann DK, Erndt NG, Cauley TH, Koehler RT, So AP, Dube S, Rose KA, Montesclaros L, Wang S, Stumbo DP, Hodges SP, Romine S, Milanovich FP, White HE, Regan JF, Karlin-Neumann GA, Hindson CM, Saxonov S, Colston BW. High-Throughput Droplet Digital PCR System for Absolute Quantitation of DNA Copy Number. Analytical Chemistry. 2011;83(22):8604-10. doi: 10.1021/ac202028g.
106. Bielas JH. Non-transcribed strand repair revealed in quiescent cells. Mutagenesis. 2006;21(1):49-53. doi: 10.1093/mutage/gei073. PubMed PMID: 16394029.
107. Furda A, Santos JH, Meyer JN, Van Houten B. Quantitative PCR-Based Measurement of Nuclear and Mitochondrial DNA Damage and Repair in Mammalian Cells. Methods in molecular biology (Clifton, NJ). 2014;1105:419-37. doi: 10.1007/978-1-62703-739-6_31. PubMed PMID: PMC4407362.
108. Long AS, Lemieux CL, Arlt VM, White PA. Tissue-specific in vivo genetic toxicity of nine polycyclic aromatic hydrocarbons assessed using the Muta™Mouse transgenic rodent assay. Toxicology and Applied Pharmacology. 2016;290:31-42. doi: http://dx.doi.org/10.1016/j.taap.2015.11.010.
109. Miller KP, Ramos KS. Impact of cellular metabolism on the biological effects of benzo[a]pyrene and related hydrocarbons. Drug metabolism reviews. 2001;33(1):1-35. Epub 2001/03/29. doi: 10.1081/dmr-100000138. PubMed PMID: 11270659.
110. Choudhary D, Jansson I, Schenkman JB, Sarfarazi M, Stoilov I. Comparative expression profiling of 40 mouse cytochrome P450 genes in embryonic and adult tissues. Arch Biochem Biophys. 2003;414(1):91-100. Epub 2003/05/15. PubMed PMID: 12745259.
111. Karunadharma PP, Basisty N, Dai DF, Chiao YA, Quarles EK, Hsieh EJ, Crispin D, Bielas JH, Ericson NG, Beyer RP, MacKay VL, MacCoss MJ, Rabinovitch PS. Subacute calorie restriction and rapamycin discordantly alter mouse liver proteome homeostasis and reverse aging effects. Aging cell. 2015;14(4):547-57. Epub 2015/03/27. doi: 10.1111/acel.12317. PubMed PMID: 25807975; PMCID: Pmc4531069.
112. Graziewicz MA, Sayer JM, Jerina DM, Copeland WC. Nucleotide incorporation by human DNA polymerase γ opposite benzo[a]pyrene and benzo[c]phenanthrene diol epoxide adducts of deoxyguanosine and deoxyadenosine. Nucleic acids research. 2004;32(1):397-405. doi: 10.1093/nar/gkh213.
113. Krishnan KJ, Reeve AK, Samuels DC, Chinnery PF, Blackwood JK, Taylor RW, Wanrooij S, Spelbrink JN, Lightowlers RN, Turnbull DM. What causes mitochondrial DNA deletions in human cells? Nature genetics. 2008;40(3):275-9. Epub 2008/02/29. doi: 10.1038/ng.f.94. PubMed PMID: 18305478.

114. Tanhauser SM, Laipis PJ. Multiple Deletions Are Detectable in Mitochondrial DNA of Aging Mice. Journal of Biological Chemistry. 1995;270(42):24769-75. doi: 10.1074/jbc.270.42.24769.
115. Jung D, Cho Y, Meyer JN, Di Giulio RT. The long amplicon quantitative PCR for DNA damage assay as a sensitive method of assessing DNA damage in the environmental model, Atlantic killifish (Fundulus heteroclitus). Comparative biochemistry and physiology Toxicology & pharmacology : CBP. 2009;149(2):182-6. doi: 10.1016/j.cbpc.2008.07.007. PubMed PMID: PMC2676791.
116. Lambert IB, Singer TM, Boucher SE, Douglas GR. Detailed review of transgenic rodent mutation assays. Mutation Research/Reviews in Mutation Research. 2005;590(1–3):1-280. doi: http://dx.doi.org/10.1016/j.mrrev.2005.04.002.
117. Gossen JA, de Leeuw WJ, Tan CH, Zwarthoff EC, Berends F, Lohman PH, Knook DL, Vijg J. Efficient rescue of integrated shuttle vectors from transgenic mice: a model for studying mutations in vivo. Proceedings of the National Academy of Sciences. 1989;86(20):7971-5.
118. Hakura A, Tsutsui Y, Sonoda J, Tsukidate K, Mikami T, Sagami F. Comparison of the mutational spectra of the lacZ transgene in four organs of the MutaMouse treated with benzo[a]pyrene: target organ specificity. Mutation research. 2000;447(2):239-47. Epub 2001/02/07. PubMed PMID: 10751607.
119. Justice MJ, Noveroske JK, Weber JS, Zheng B, Bradley A. Mouse ENU Mutagenesis. Human Molecular Genetics. 1999;8(10):1955-63. doi: 10.1093/hmg/8.10.1955.
120. Noveroske JK, Weber JS, Justice MJ. The mutagenic action of N-ethyl-N-nitrosourea in the mouse. Mammalian Genome. 2000;11(7):478-83. doi: 10.1007/s003350010093.
121. Khaidakov M, Heflich RH, Manjanatha MG, Myers MB, Aidoo A. Accumulation of point mutations in mitochondrial DNA of aging mice. Mutation research. 2003;526(1-2):1-7. Epub 2003/04/26. PubMed PMID: 12714177.
122. Chen JZ, Kadlubar FF. Mitochondrial mutagenesis and oxidative stress in human prostate cancer. Journal of environmental science and health Part C, Environmental carcinogenesis & ecotoxicology reviews. 2004;22(1):1-12. Epub 2005/04/23. doi: 10.1081/gnc-120037931. PubMed PMID: 15845219.
123. Friedberg EC, Walker GC, Siede W. DNA Repair and Mutagenesis2006.
124. Greaves LC, Beadle NE, Taylor GA, Commane D, Mathers JC, Khrapko K, Turnbull DM. Quantification of mitochondrial DNA mutation load. Aging cell. 2009;8(5):566-72. doi: 10.1111/j.1474-9726.2009.00505.x. PubMed PMID: PMC2752485.
125. Wright JH, Modjeski KL, Bielas JH, Preston BD, Fausto N, Loeb LA, Campbell JS. A random mutation capture assay to detect genomic point mutations in mouse tissue. Nucleic acids research. 2011;39(11):e73. doi: 10.1093/nar/gkr142.
126. Busbee DL, Joe CO, Norman JO, Rankin PW. Inhibition of DNA synthesis by an electrophilic metabolite of benzo[a]pyrene. Proceedings of the National Academy of Sciences of the United States of America. 1984;81(17):5300-4. Epub 1984/09/01. PubMed PMID: 6089190; PMCID: Pmc391691.
127. Shrivastav N, Li D, Essigmann JM. Chemical biology of mutagenesis and DNA repair: cellular responses to DNA alkylation. Carcinogenesis. 2010;31(1):59-70. doi: 10.1093/carcin/bgp262.
128. Kazak L, Reyes A, Holt IJ. Minimizing the damage: repair pathways keep mitochondrial DNA intact. Nature reviews Molecular cell biology. 2012;13(10):659-71. doi: 10.1038/nrm3439. PubMed PMID: 22992591.
129. Croteau DL, Stierum RH, Bohr VA. Mitochondrial DNA repair pathways. Mutation Research/DNA Repair. 1999;434(3):137-48. doi: http://dx.doi.org/10.1016/S0921-8777(99)00025-7.
130. Mason PA, Matheson EC, Hall AG, Lightowlers RN. Mismatch repair activity in mammalian mitochondria. Nucleic acids research. 2003;31(3):1052-8. doi: 10.1093/nar/gkg167.
131. de Souza-Pinto NC, Mason PA, Hashiguchi K, Weissman L, Tian J, Guay D, Lebel M, Stevnsner TV, Rasmussen LJ, Bohr VA. Novel DNA mismatch-repair activity involving YB-1 in human mitochondria. DNA Repair. 2009;8(6):704-19. doi: http://dx.doi.org/10.1016/j.dnarep.2009.01.021.
132. Stuart JA, Hashiguchi K, Wilson DM, 3rd, Copeland WC, Souza-Pinto NC, Bohr VA. DNA base excision repair activities and pathway function in mitochondrial and cellular lysates from cells lacking mitochondrial DNA. Nucleic acids research. 2004;32(7):2181-92. Epub 2004/04/27. doi: 10.1093/nar/gkh533. PubMed PMID: 15107486; PMCID: PMC407819.
133. Ruchko MV, Gorodnya OM, Zuleta A, Pastukh VM, Gillespie MN. The DNA glycosylase Ogg1 defends against oxidant-induced mtDNA damage and apoptosis in pulmonary artery endothelial cells. Free radical biology & medicine. 2011;50(9):1107-13. Epub 2010/10/26. doi: 10.1016/j.freeradbiomed.2010.10.692. PubMed PMID: 20969951; PMCID: Pmc3033972.
134. van Loon B, Samson LD. Alkyladenine DNA glycosylase (AAG) localizes to mitochondria and interacts with mitochondrial single-stranded binding protein (mtSSB). DNA Repair. 2013;12(3):177-87. doi: http://dx.doi.org/10.1016/j.dnarep.2012.11.009.
135. Bess AS, Crocker TL, Ryde IT, Meyer JN. Mitochondrial dynamics and autophagy aid in removal of persistent mitochondrial DNA damage in Caenorhabditis elegans. Nucleic acids research. 2012;40(16):7916-31. doi: 10.1093/nar/gks532. PubMed PMID: 22718972; PMCID: 3439916.
136. Shokolenko I, Venediktova N, Bochkareva A, Wilson GL, Alexeyev MF. Oxidative stress induces degradation of mitochondrial DNA. Nucleic acids research. 2009;37(8):2539-48. Epub 2009/03/07. doi: 10.1093/nar/gkp100. PubMed PMID: 19264794; PMCID: PMC2677867.
137. Zheng W, Khrapko K, Coller HA, Thilly WG, Copeland WC. Origins of human mitochondrial point mutations as DNA polymerase γ-mediated errors. Mutation Research/Fundamental and Molecular Mechanisms of Mutagenesis. 2006;599(1–2):11-20. doi: http://dx.doi.org/10.1016/j.mrfmmm.2005.12.012.
138. Bailey LJ, Cluett TJ, Reyes A, Prolla TA, Poulton J, Leeuwenburgh C, Holt IJ. Mice expressing an error-prone DNA polymerase in mitochondria display elevated replication pausing and chromosomal breakage at fragile sites of mitochondrial DNA. Nucleic acids research. 2009;37(7):2327-35. Epub 2009/02/27. doi: 10.1093/nar/gkp091. PubMed PMID: 19244310; PMCID: PMC2673436.
139. Vermulst M, Wanagat J, Kujoth GC, Bielas JH, Rabinovitch PS, Prolla TA, Loeb LA. DNA deletions and clonal mutations drive premature aging in mitochondrial mutator mice. Nature genetics. 2008;40(4):392-4. doi: http://www.nature.com/ng/journal/v40/n4/suppinfo/ng.95_S1.html.
140. Stevnsner T, Thorslund T, de Souza-Pinto NC, Bohr VA. Mitochondrial repair of 8-oxoguanine and changes with aging. Experimental gerontology. 2002;37(10–11):1189-96. doi: http://dx.doi.org/10.1016/S0531-5565(02)00142-0.
141. Dai DF, Santana LF, Vermulst M, Tomazela DM, Emond MJ, MacCoss MJ, Gollahon K, Martin GM, Loeb LA, Ladiges WC, Rabinovitch PS. Overexpression of catalase targeted to mitochondria attenuates murine cardiac aging. Circulation. 2009;119(21):2789-97. Epub 2009/05/20. doi: 10.1161/circulationaha.108.822403. PubMed PMID: 19451351; PMCID: Pmc2858759.
142. Muftuoglu M, Mori MP, Souza-Pinto NCd. Formation and repair of oxidative damage in the mitochondrial DNA. Mitochondrion. 2014;17:164-81. doi: http://dx.doi.org/10.1016/j.mito.2014.03.007.

143. Dizdaroglu M, Holwitt E, Hagan MP, Blakely WF. Formation of cytosine glycol and 5,6-dihydroxycytosine in deoxyribonucleic acid on treatment with osmium tetroxide. The Biochemical journal. 1986;235(2):531-6. Epub 1986/04/15. PubMed PMID: 3741404; PMCID: Pmc1146717.
144. Masaoka A, Terato H, Kobayashi M, Ohyama Y, Ide H. Oxidation of thymine to 5-formyluracil in DNA promotes misincorporation of dGMP and subsequent elongation of a mismatched primer terminus by DNA polymerase. The Journal of biological chemistry. 2001;276(19):16501-10. Epub 2001/03/30. doi: 10.1074/jbc.M008598200. PubMed PMID: 11278425.
145. Jaruga P, Dizdaroglu M. Repair of products of oxidative DNA base damage in human cells. Nucleic acids research. 1996;24(8):1389-94. PubMed PMID: PMC145821.
146. Spelbrink JN, Toivonen JM, Hakkaart GAJ, Kurkela JM, Cooper HM, Lehtinen SK, Lecrenier N, Back JW, Speijer D, Foury F, Jacobs HT. In Vivo Functional Analysis of the Human Mitochondrial DNA Polymerase POLG Expressed in Cultured Human Cells. Journal of Biological Chemistry. 2000;275(32):24818-28. doi: 10.1074/jbc.M000559200.
147. Kasiviswanathan R, Minko IG, Lloyd RS, Copeland WC. Translesion synthesis past acrolein-derived DNA adducts by human mitochondrial DNA polymerase γ. Journal of Biological Chemistry. 2013. doi: 10.1074/jbc.M113.458802.
148. Wallace DC. Mitochondria and cancer. Nature reviews Cancer. 2012;12(10):685-98. doi: 10.1038/nrc3365. PubMed PMID: 23001348.
149. Vander Heiden MG, Cantley LC, Thompson CB. Understanding the Warburg Effect: The Metabolic Requirements of Cell Proliferation. Science. 2009;324(5930):1029-33. doi: 10.1126/science.1160809.
150. Christianson DW. Structural chemistry and biology of manganese metalloenzymes. Progress in Biophysics and Molecular Biology. 1997;67(2–3):217-52. doi: http://dx.doi.org/10.1016/S0079-6107(97)88477-5.
151. Glasauer A, Chandel NS. Targeting antioxidants for cancer therapy. Biochemical Pharmacology. 2014;92(1):90-101. doi: http://dx.doi.org/10.1016/j.bcp.2014.07.017.
152. Wheaton WW, Chandel NS. Hypoxia. 2. Hypoxia regulates cellular metabolism2011 2011-03-01 00:00:00. C385-C93 p.
153. Bjelakovic G, Nikolova D, Gluud LL, Simonetti RG, Gluud C. Mortality in randomized trials of antioxidant supplements for primary and secondary prevention: systematic review and meta-analysis. Jama. 2007;297(8):842-57. Epub 2007/03/01. doi: 10.1001/jama.297.8.842. PubMed PMID: 17327526.
154. The effect of vitamin E and beta carotene on the incidence of lung cancer and other cancers in male smokers. The Alpha-Tocopherol, Beta Carotene Cancer Prevention Study Group. The New England journal of medicine. 1994;330(15):1029-35. Epub 1994/04/14. doi: 10.1056/nejm199404143301501. PubMed PMID: 8127329.
155. Hanahan D, Weinberg Robert A. Hallmarks of Cancer: The Next Generation. Cell. 2011;144(5):646-74. doi: 10.1016/j.cell.2011.02.013.
156. Angelica Trejo GN. Phoenix helper-free retrovirus producer lines https://web.stanford.edu/group/nolan/_OldWebsite/retroviral_systems/phx.html.
157. Darzynkiewicz Z, Galkowski D, Zhao H. Analysis of apoptosis by cytometry using TUNEL assay. Methods (San Diego, Calif). 2008;44(3):250-4. doi: 10.1016/j.ymeth.2007.11.008. PubMed PMID: PMC2295206.
158. Dickinson BC, Lin VS, Chang CJ. Preparation and use of MitoPY1 for imaging hydrogen peroxide in mitochondria of live cells. Nature protocols. 2013;8(6):1249-59. Epub 2013/06/01. doi: 10.1038/nprot.2013.064. PubMed PMID: 23722262; PMCID: PMC4096497.
159. Paterson JK, Gottesman MM. P-Glycoprotein is not present in mitochondrial membranes. Exp Cell Res. 2007;313(14):3100-5. Epub 2007/05/22. doi: 10.1016/j.yexcr.2007.04.019. PubMed PMID: 17512524; PMCID: PMC2075362.
160. Rho J-h, Lampe PD. High-Throughput Screening for Native Autoantigen–Autoantibody Complexes Using Antibody Microarrays. Journal of Proteome Research. 2013;12(5):2311-20. doi: 10.1021/pr4001674.
161. Ramirez AB, Lampe PD. Discovery and validation of ovarian cancer biomarkers utilizing high density antibody microarrays. Cancer biomarkers : section A of Disease markers. 2010;8(4-5):293-307. Epub 2010/01/01. doi: 10.3233/cbm-2011-0215. PubMed PMID: 22045360.
162. Smyth GK, Speed T. Normalization of cDNA microarray data. Methods. 2003;31(4):265-73. doi: https://doi.org/10.1016/S1046-2023(03)00155-5.
163. Solan JL, Marquez-Rosado L, Sorgen PL, Thornton PJ, Gafken PR, Lampe PD. Phosphorylation at S365 is a gatekeeper event that changes the structure of Cx43 and prevents down-regulation by PKC. The Journal of Cell Biology. 2007;179(6):1301-9. doi: 10.1083/jcb.200707060. PubMed PMID: PMC2140020.
164. Gujral TS, Karp RL, Finski A, Chan M, Schwartz PE, MacBeath G, Sorger P. Profiling phospho-signaling networks in breast cancer using reverse-phase protein arrays. Oncogene. 2012;32:3470. doi: 10.1038/onc.2012.378 https://www.nature.com/articles/onc2012378#supplementary-information.
165. Zheng GXY, Terry JM, Belgrader P, Ryvkin P, Bent ZW, Wilson R, Ziraldo SB, Wheeler TD, McDermott GP, Zhu J, Gregory MT, Shuga J, Montesclaros L, Underwood JG, Masquelier DA, Nishimura SY, Schnall-Levin M, Wyatt PW, Hindson CM, Bharadwaj R, Wong A, Ness KD, Beppu LW, Deeg HJ, McFarland C, Loeb KR, Valente WJ, Ericson NG, Stevens EA, Radich JP, Mikkelsen TS, Hindson BJ, Bielas JH. Massively parallel digital transcriptional profiling of single cells. Nature Communications. 2017;8:14049. doi: 10.1038/ncomms14049 https://www.nature.com/articles/ncomms14049#supplementary-information.
166. Trapnell C, Cacchiarelli D, Grimsby J, Pokharel P, Li S, Morse M, Lennon NJ, Livak KJ, Mikkelsen TS, Rinn JL. The dynamics and regulators of cell fate decisions are revealed by pseudotemporal ordering of single cells. Nature biotechnology. 2014;32:381. doi: 10.1038/nbt.2859
https://www.nature.com/articles/nbt.2859#supplementary-information.
167. Michelakis ED, Sutendra G, Dromparis P, Webster L, Haromy A, Niven E, Maguire C, Gammer T-L, Mackey JR, Fulton D, Abdulkarim B, McMurtry MS, Petruk KC. Metabolic Modulation of Glioblastoma with Dichloroacetate. Science Translational Medicine. 2010;2(31):31ra4. doi: 10.1126/scitranslmed.3000677.
168. Korsmeyer SJ, Shutter JR, Veis DJ, Merry DE, Oltvai ZN. Bcl-2/Bax: a rheostat that regulates an anti-oxidant pathway and cell death. Seminars in cancer biology. 1993;4(6):327-32. PubMed PMID: 8142617.
169. Bhola Patrick D, Letai A. Mitochondria—Judges and Executioners of Cell Death Sentences. Molecular Cell. 2016;61(5):695-704. doi: http://dx.doi.org/10.1016/j.molcel.2016.02.019.
170. Liu J, Yoshida Y, Yamashita U. DNA-binding activity of NF-kappaB and phosphorylation of p65 are induced by N-acetylcysteine through phosphatidylinositol (PI) 3-kinase. Molecular immunology. 2008;45(15):3984-9. Epub 2008/07/29. doi: 10.1016/j.molimm.2008.06.012. PubMed PMID: 18657320.

171. Schurmann A, Mooney AF, Sanders LC, Sells MA, Wang HG, Reed JC, Bokoch GM. p21-activated kinase 1 phosphorylates the death agonist bad and protects cells from apoptosis. Mol Cell Biol. 2000;20(2):453-61. Epub 1999/12/28. PubMed PMID: 10611223; PMCID: PMC85099.
172. Hockenbery DM. Targeting mitochondria for cancer therapy. Environmental and molecular mutagenesis. 2010;51(5):476-89. doi: 10.1002/em.20552.
173. Ferrin G, Linares CI, Muntane J. Mitochondrial drug targets in cell death and cancer. Current pharmaceutical design. 2011;17(20):2002-16. Epub 2011/07/02. PubMed PMID: 21718250.
174. Nair VS, Gevaert O, Davidzon G, Napel S, Graves EE, Hoang CD, Shrager JB, Quon A, Rubin DL, Plevritis SK. Prognostic PET 18F-FDG Uptake Imaging Features Are Associated with Major Oncogenomic Alterations in Patients with Resected Non–Small Cell Lung Cancer. Cancer research. 2012;72(15):3725-34. doi: 10.1158/0008-5472.can-11-3943.
175. Montero J, Letai A. Dynamic BH3 profiling-poking cancer cells with a stick. Molecular & cellular oncology. 2016;3(3):e1040144. Epub 2016/06/18. doi: 10.1080/23723556.2015.1040144. PubMed PMID: 27314085; PMCID: PMC4909438.
176. Storz G, Christman MF, Sies H, Ames BN. Spontaneous mutagenesis and oxidative damage to DNA in Salmonella typhimurium. Proceedings of the National Academy of Sciences. 1987;84(24):8917-21.
177. Schaaper RM, Danforth BN, Glickman BW. Mechanisms of spontaneous mutagenesis: an analysis of the spectrum of spontaneous mutation in the Escherichia coli lacI gene. Journal of molecular biology. 1986;189(2):273-84. Epub 1986/05/20. PubMed PMID: 3018259.
178. Kohler SW, Provost GS, Fieck A, Kretz PL, Bullock WO, Sorge JA, Putman DL, Short JM. Spectra of spontaneous and mutagen-induced mutations in the lacI gene in transgenic mice. Proceedings of the National Academy of Sciences. 1991;88(18):7958-62.
179. Hoekstra JG, Hipp MJ, Montine TJ, Kennedy SR. Mitochondrial DNA mutations increase in early stage Alzheimer disease and are inconsistent with oxidative damage. Annals of neurology. 2016;80(2):301-6. doi: 10.1002/ana.24709.
180. Takemoto K, Matsuda T, Sakai N, Fu D, Noda M, Uchiyama S, Kotera I, Arai Y, Horiuchi M, Fukui K, Ayabe T, Inagaki F, Suzuki H, Nagai T. SuperNova, a monomeric photosensitizing fluorescent protein for chromophore-assisted light inactivation. Scientific Reports. 2013;3:2629. doi: 10.1038/srep02629
https://www.nature.com/articles/srep02629#supplementary-information.
181. Haskew-Layton RE, Payappilly JB, Smirnova NA, Ma TC, Chan KK, Murphy TH, Guo H, Langley B, Sultana R, Butterfield DA, Santagata S, Alldred MJ, Gazaryan IG, Bell GW, Ginsberg SD, Ratan RR. Controlled enzymatic production of astrocytic hydrogen peroxide protects neurons from oxidative stress via an Nrf2-independent pathway. Proceedings of the National Academy of Sciences. 2010;107(40):17385-90. doi: 10.1073/pnas.1003996107.
182. Lee DY, Sugden B. The LMP1 oncogene of EBV activates PERK and the unfolded protein response to drive its own synthesis. Blood. 2008;111(4):2280-9. Epub 2007/11/29. doi: 10.1182/blood-2007-07-100032. PubMed PMID: 18042799; PMCID: PMC2234060.
183. Jay DG. Selective destruction of protein function by chromophore-assisted laser inactivation. Proceedings of the National Academy of Sciences. 1988;85(15):5454-8.
184. Bulina ME, Lukyanov KA, Britanova OV, Onichtchouk D, Lukyanov S, Chudakov DM. Chromophore-assisted light inactivation (CALI) using the phototoxic fluorescent protein KillerRed. Nature protocols. 2006;1:947. doi: 10.1038/nprot.2006.89.
185. OECD. Test No. 488: Transgenic Rodent Somatic and Germ Cell Gene Mutation Assays. Paris: OECD Publishing; 2013.
186. Pollegioni L, Piubelli L, Sacchi S, Pilone MS, Molla G. Physiological functions of D-amino acid oxidases: from yeast to humans. Cellular and molecular life sciences : CMLS. 2007;64(11):1373-94. Epub 2007/03/31. doi: 10.1007/s00018-007-6558-4. PubMed PMID: 17396222.
187. Gutscher M, Sobotta MC, Wabnitz GH, Ballikaya S, Meyer AJ, Samstag Y, Dick TP. Proximity-based Protein Thiol Oxidation by H(2)O(2)-scavenging Peroxidases. The Journal of biological chemistry. 2009;284(46):31532-40. doi: 10.1074/jbc.M109.059246. PubMed PMID: PMC2797222.
188. Hanson GT, Aggeler R, Oglesbee D, Cannon M, Capaldi RA, Tsien RY, Remington SJ. Investigating mitochondrial redox potential with redox-sensitive green fluorescent protein indicators. The Journal of biological chemistry. 2004;279(13):13044-53. Epub 2004/01/15. doi: 10.1074/jbc.M312846200. PubMed PMID: 14722062.
189. Michikawa Y, Mazzucchelli F, Bresolin N, Scarlato G, Attardi G. Aging-dependent large accumulation of point mutations in the human mtDNA control region for replication. Science. 1999;286(5440):774-9. Epub 1999/10/26. PubMed PMID: 10531063.
190. Wanagat J, Ahmadieh N, Bielas JH, Ericson NG, Van Remmen H. Skeletal muscle mitochondrial DNA deletions are not increased in CuZn-superoxide dismutase deficient mice. Experimental gerontology. 2015;61:15-9. Epub 2014/12/03. doi: 10.1016/j.exger.2014.11.012. PubMed PMID: 25449857; PMCID: Pmc4289650.
191. Taghizadeh K, McFaline JL, Pang B, Sullivan M, Dong M, Plummer E, Dedon PC. Quantification of DNA damage products resulting from deamination, oxidation and reaction with products of lipid peroxidation by liquid chromatography isotope dilution tandem mass spectrometry. Nature protocols. 2008;3:1287. doi: 10.1038/nprot.2008.119.
192. Ahn EH, Lee SH, Kim JY, Chang CC, Loeb LA. Decreased Mitochondrial Mutagenesis during Transformation of Human Breast Stem Cells into Tumorigenic Cells. Cancer research. 2016;76(15):4569-78. Epub 2016/05/20. doi: 10.1158/0008-5472.can-15-3462. PubMed PMID: 27197159; PMCID: PMC5004738.
193. Greaves LC, Nooteboom M, Elson JL, Tuppen HAL, Taylor GA, Commane DM, Arasaradnam RP, Khrapko K, Taylor RW, Kirkwood TBL, Mathers JC, Turnbull DM. Clonal Expansion of Early to Mid-Life Mitochondrial DNA Point Mutations Drives Mitochondrial Dysfunction during Human Ageing. PLoS Genet. 2014;10(9):e1004620. doi: 10.1371/journal.pgen.1004620.
194. Pienaar E, Theron M, Nelson M, Viljoen HJ. A quantitative model of error accumulation during PCR amplification. Computational Biology and Chemistry. 2006;30(2):102-11. doi: https://doi.org/10.1016/j.compbiolchem.2005.11.002.
195. Arbeithuber B, Makova KD, Tiemann-Boege I. Artifactual mutations resulting from DNA lesions limit detection levels in ultrasensitive sequencing applications. DNA Research. 2016;23(6):547-59. doi: 10.1093/dnares/dsw038.
196. Halsne R, Esbensen Y, Wang W, Scheffler K, Suganthan R, Bjoras M, Eide L. Lack of the DNA glycosylases MYH and OGG1 in the cancer prone double mutant mouse does not increase mitochondrial DNA mutagenesis. DNA Repair (Amst). 2012;11(3):278-85. Epub 2012/01/03. doi: 10.1016/j.dnarep.2011.12.001. PubMed PMID: 22209780.
197. Anson RM, Croteau DL, Stierum RH, Filburn C, Parsell R, Bohr VA. Homogenous repair of singlet oxygen-induced DNA damage in differentially transcribed regions and strands of human mitochondrial DNA. Nucleic acids research. 1998;26(2):662-8. PubMed PMID: PMC147305.
198. Huang BK, Sikes HD. Quantifying intracellular hydrogen peroxide perturbations in terms of concentration. Redox Biology. 2014;2:955-62. doi: 10.1016/j.redox.2014.08.001. PubMed PMID: PMC4215397.

199. Chen H, Vermulst M, Wang YE, Chomyn A, Prolla TA, McCaffery JM, Chan DC. Mitochondrial Fusion Is Required for mtDNA Stability in Skeletal Muscle and Tolerance of mtDNA Mutations. Cell. 2010;141(2):280-9. doi: http://dx.doi.org/10.1016/j.cell.2010.02.026.
200. Matsuda N, Sato S, Shiba K, Okatsu K, Saisho K, Gautier CA, Sou Y-s, Saiki S, Kawajiri S, Sato F, Kimura M, Komatsu M, Hattori N, Tanaka K. PINK1 stabilized by mitochondrial depolarization recruits Parkin to damaged mitochondria and activates latent Parkin for mitophagy. The Journal of Cell Biology. 2010;189(2):211-21. doi: 10.1083/jcb.200910140.
201. Wagner JR, Cadet J. Oxidation Reactions of Cytosine DNA Components by Hydroxyl Radical and One-Electron Oxidants in Aerated Aqueous Solutions. Accounts of Chemical Research. 2010;43(4):564-71. doi: 10.1021/ar9002637.
202. Hockenbery DM, Oltvai ZN, Yin X-M, Milliman CL, Korsmeyer SJ. Bcl-2 functions in an antioxidant pathway to prevent apoptosis. Cell. 1993;75(2):241-51. doi: http://dx.doi.org/10.1016/0092-8674(93)80066-N.
203. Stockwell BR, Friedmann Angeli JP, Bayir H, Bush AI, Conrad M, Dixon SJ, Fulda S, Gascón S, Hatzios SK, Kagan VE, Noel K, Jiang X, Linkermann A, Murphy ME, Overholtzer M, Oyagi A, Pagnussat GC, Park J, Ran Q, Rosenfeld CS, Salnikow K, Tang D, Torti FM, Torti SV, Toyokuni S, Woerpel KA, Zhang DD. Ferroptosis: A Regulated Cell Death Nexus Linking Metabolism, Redox Biology, and Disease. Cell. 2017;171(2):273-85. doi: 10.1016/j.cell.2017.09.021.
204. Galluzzi L, Kroemer G. Necroptosis: A Specialized Pathway of Programmed Necrosis. Cell. 2008;135(7):1161-3. doi: 10.1016/j.cell.2008.12.004.
205. Fatokun AA, Dawson VL, Dawson TM. Parthanatos: mitochondrial-linked mechanisms and therapeutic opportunities. Br J Pharmacol. 2014;171(8):2000-16. Epub 2014/04/02. doi: 10.1111/bph.12416. PubMed PMID: 24684389; PMCID: PMC3976618.
206. Gregory MT, Bertout JA, Ericson NG, Taylor SD, Mukherjee R, Robins HS, Drescher CW, Bielas JH. Targeted single molecule mutation detection with massively parallel sequencing. Nucleic acids research. 2015. Epub 2015/09/19. doi: 10.1093/nar/gkv915. PubMed PMID: 26384417.

APPENDIX A – CHAPTER 2 SUPPLEMENTAL MATERIAL

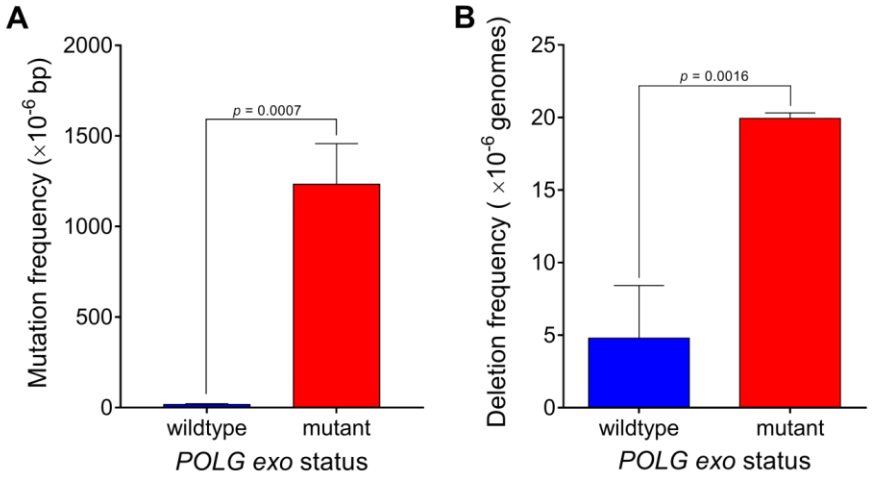

Supplemental Figure A.1 Mouse Embryonic Fibroblasts (MEFs) derived from mice lacking a functional proofreading domain in polymerase γ harbor an increased burden of mtDNA point and deletion mutations. DNA extracted from mouse embryonic fibroblast cells, which are wild-type (WT), or those possessing a homozygous inactivating mutation in the proofreading domain of the mitochondrial DNA polymerase gene, POLG D247A (mutant), were subjected to analysis via A) dRMC at the 12S site ($p = 0.0007$, Welch's t-test, 3 technical replicates) and B) 3D of the 'common deletion' ($p = 0.0016$, Welch's t-test, 3 biological replicates, 2 technical replicates).

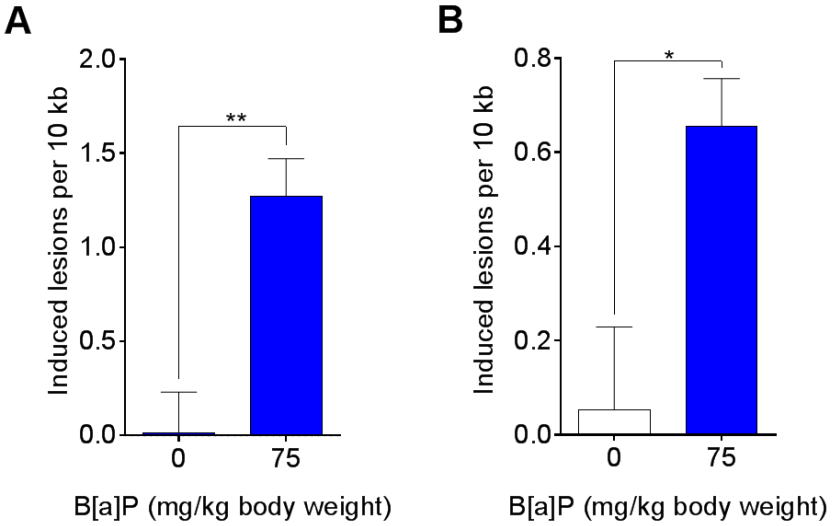

Supplemental Figure A.2 Acute B[a]P exposure induces polymerase blocking lesions in the *LacZ* transgene. Mice were treated with vehicle or a single dose of 75 mg/kg body weight B[a]P. DNA was extracted from bone marrow and liver tissues 24 hours after treatment. The presence of DNA lesions (± s.e.m.) was determined by quantitative PCR in (A) bone marrow and (B) liver. (*$p < 0.05$, ** $p < 0.01$; one-tailed Welch's t-test).

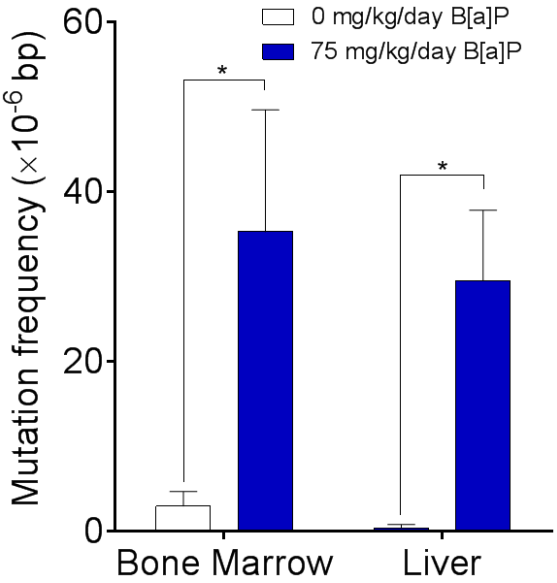

Supplemental Figure A.3 dRMC Detection of B[a]P induced nuclear mutations in bone marrow and liver tissue. Mice were treated daily with B[a]P or vehicle for 28 consecutive days and then allowed 3 days to recover post-treatment before tissue collection and DNA extraction. Mutation frequency per bp (± s.e.m.) was determined via dRMC within the *lacZ* transgene. B[a]P induced a significant increase in mutations in bone marrow and liver (p = 0.03, 0.01, respectively; Welch's t-test).

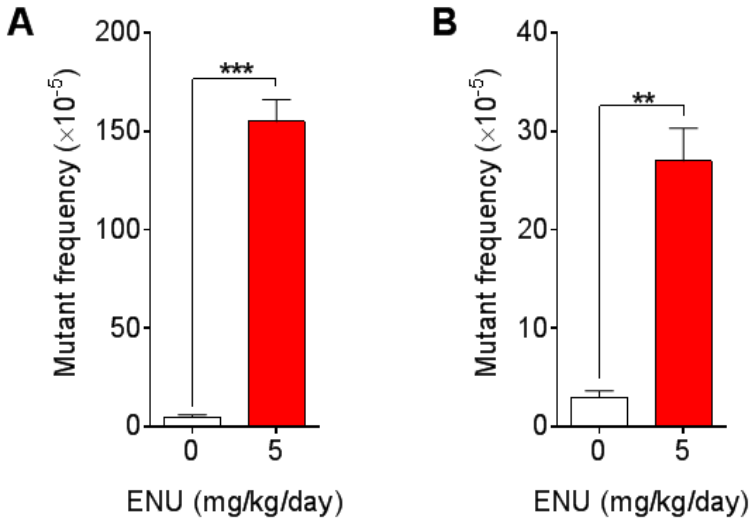

Supplemental Figure A.4 The *lacZ* mutant frequency in mouse nuclear DNA increases after exposure to ENU. Mutant frequency (± s.e.m.) was quantified in bone marrow and liver collected three days after 28 consecutive days of daily ENU exposure (**, $p < 0.01$; ***, $p < 0.001$; two-tailed unpaired Welch's t-test). (A) Bone marrow nuclear DNA mutant frequency ($\chi^2 = 714.8$, $p = < 0.0001$; Fisher's Exact, $p = < 0.0001$). (B) Mutant frequency in liver nDNA ($\chi^2 = 44.62$, $p = < 0.0001$; Fisher's Exact, $p = < 0.0001$).

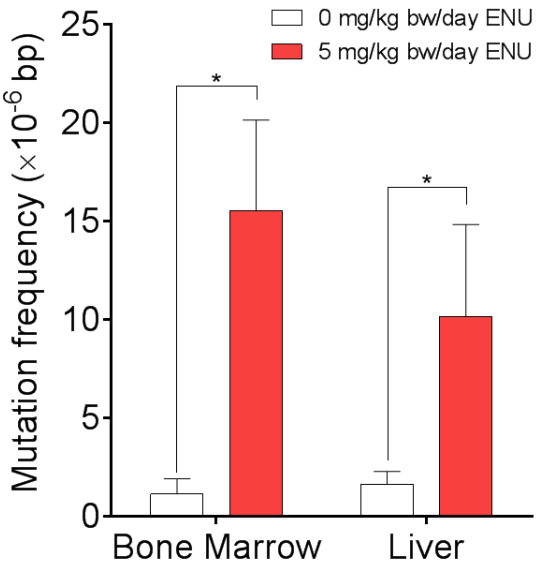

Supplemental Figure A.5 dRMC Detection of nDNA Mutations In Bone Marrow and Liver Following Subchronic ENU Exposure. Mice were treated daily with ENU or vehicle for 28 consecutive days and then allowed 3 days to recover without treatment. After DNA extraction, mutation frequency per bp (± s.e.m.) was determined via dRMC within the *lacZ* transgene in mouse nDNA. ENU induced a significant increase in mutations in mouse bone marrow and liver (p = 0.02, 0.04, respectively; unpaired Welch's t-test).

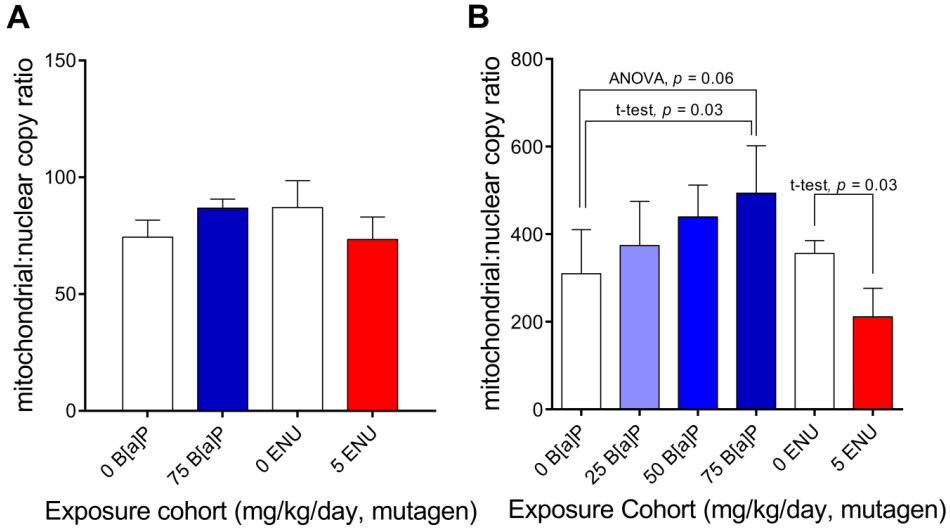

Supplemental Figure A.6 Mitochondrial to nuclear DNA copy number ratio in mice treated with B[a]P or ENU. Mouse tissue DNA from our subchronic B[a]P and ENU cohorts was used to investigate copy number ratio changes in mtDNA and nDNA. ddPCR analysis of mitochondrial and nuclear DNA copy numbers was performed on mouse A) bone Marrow (0 vs 25,50,75, p =0.17, 0.39, 0.37, Welch's t-test) and B) liver (B[a]P ANOVA, p = 0.06; t-test 0 vs 25,50,75, p = 0.6355, 0.1505, 0.0317; ENU, p = 0.03, Welch's t-test) samples.

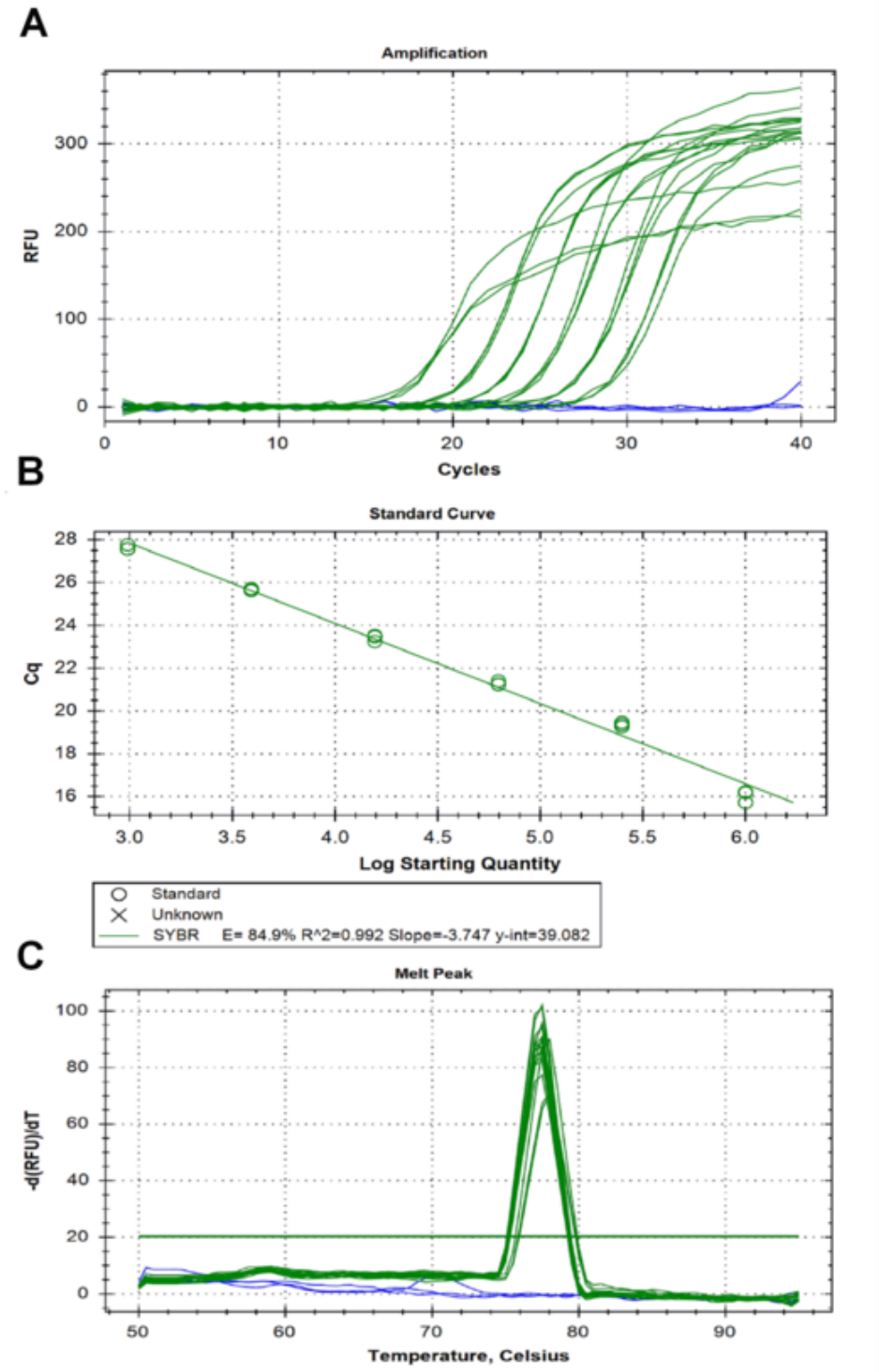

Supplemental Figure A.7 Mouse mtDNA short-range primers. Specificity of primers and the amplified PCR products was examined by raw data (**A**), standard curve (**B**), melt analysis (**C**) and analyzed with CFX Manager Software. PCR efficiencies were calculated from slope, and r^2.

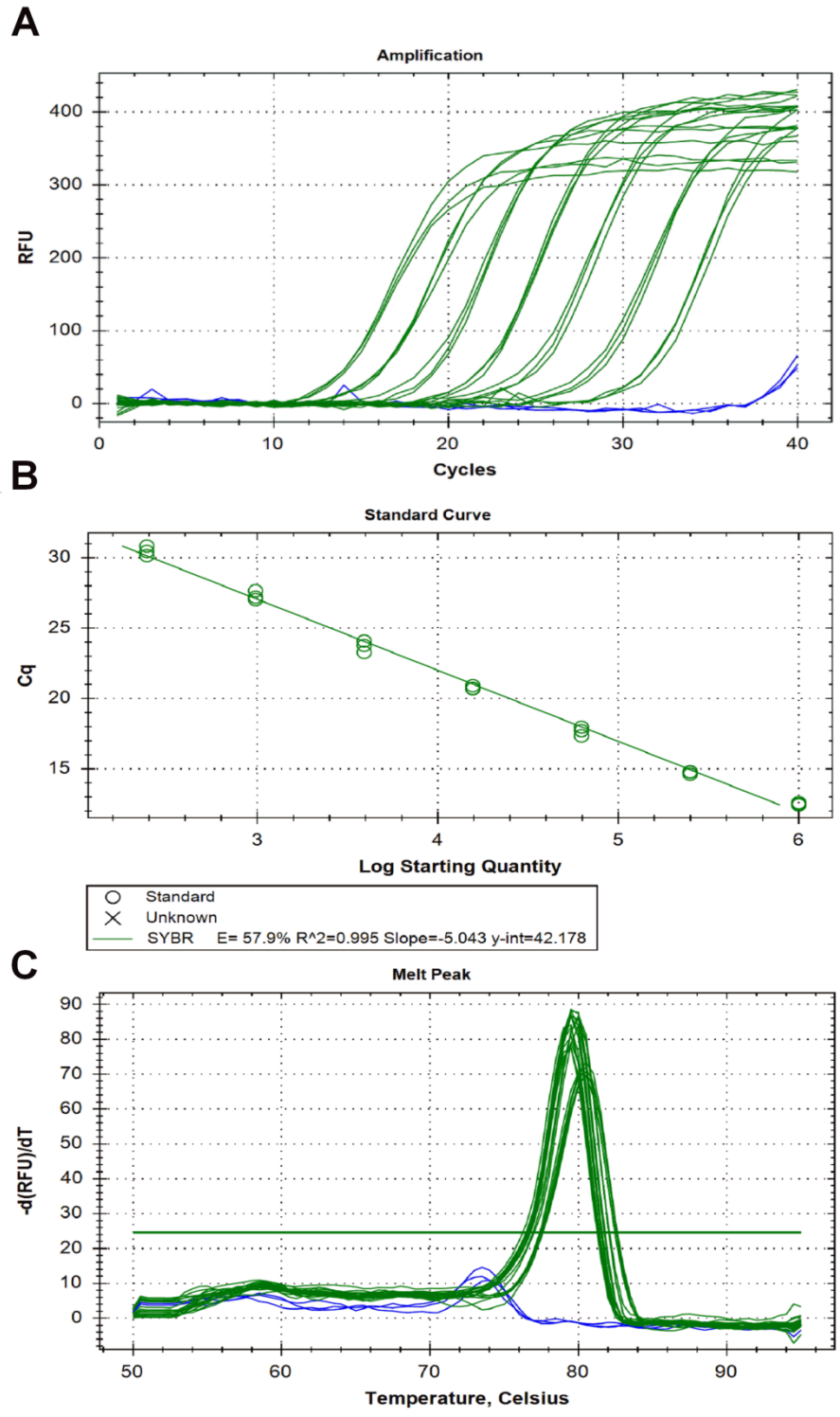

Supplemental Figure A.8 Mouse mtDNA long-range primers. Specificity of primers and the amplified PCR products was examined by raw data (**A**), standard curve (**B**), melt analysis (**C**) and analyzed with CFX Manager Software. PCR efficiencies were calculated from slope, and r^2.

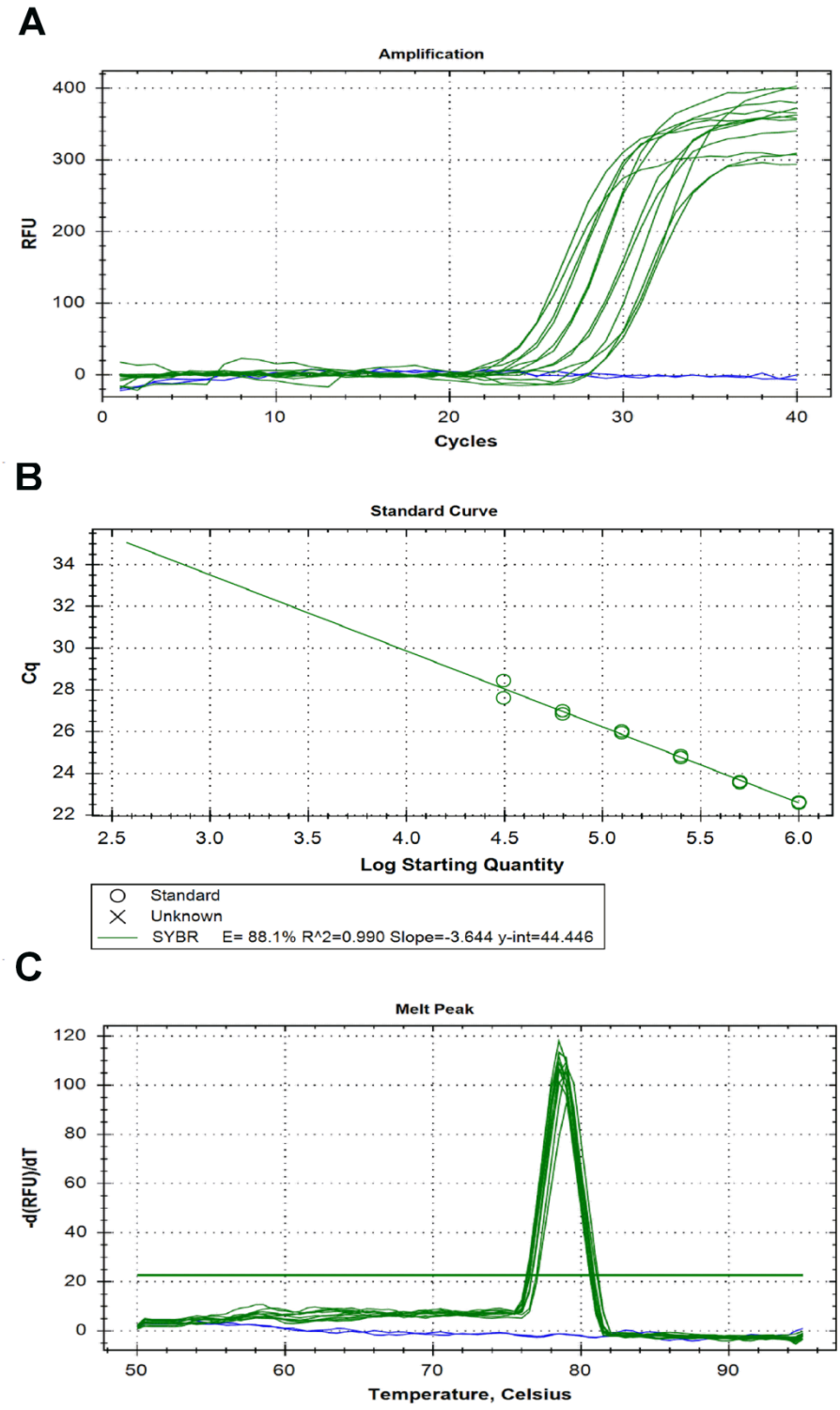

Supplemental Figure A.9 Mouse nDNA short-range primers. Specificity of primers and the amplified PCR products was examined by raw data (**A**), standard curve (**B**), melt analysis (**C**) and analyzed with CFX Manager Software. PCR efficiencies were calculated from slope, and r^2.

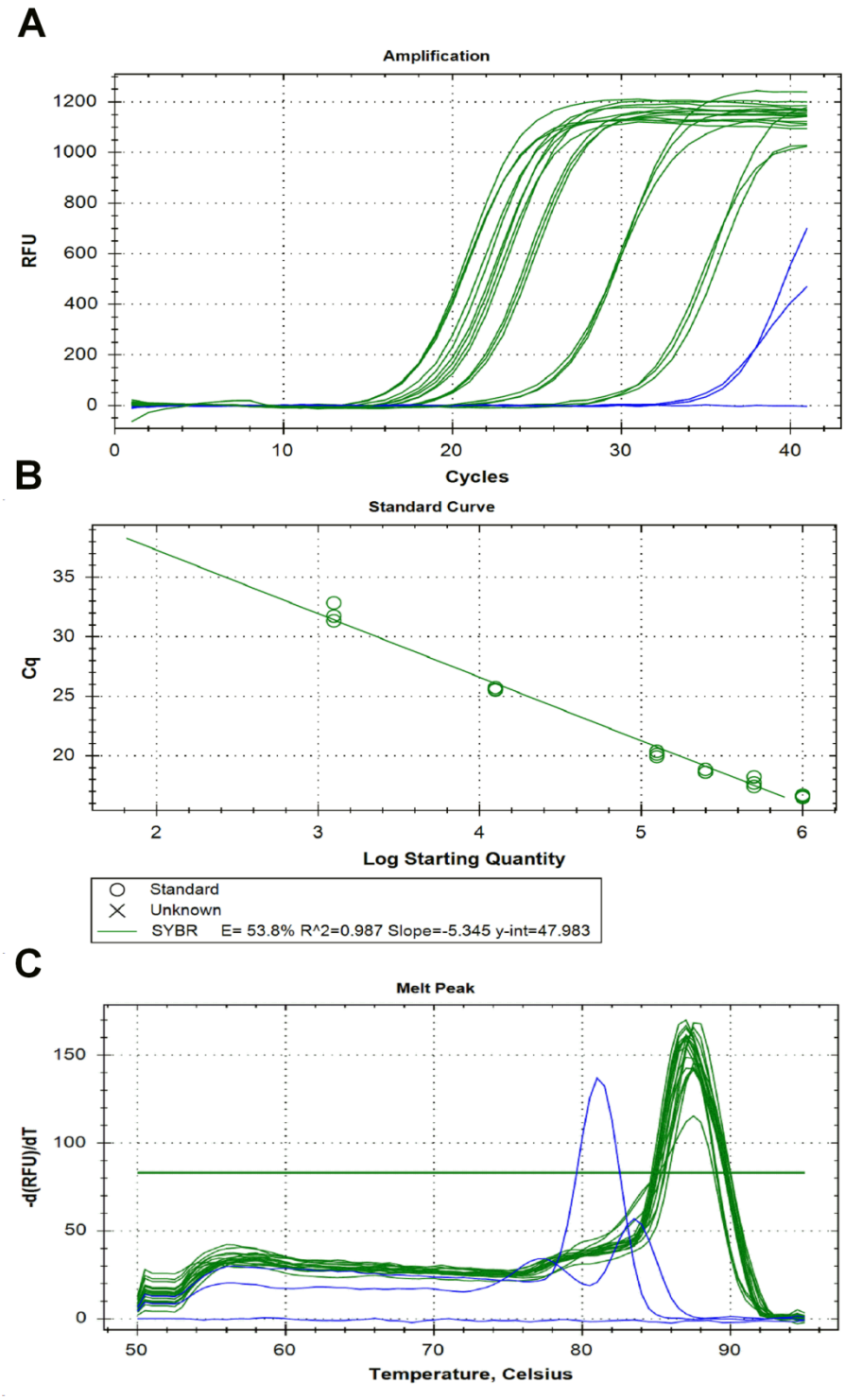

Supplemental Figure A.10 Mouse nDNA short-range primers. Specificity of primers and the amplified PCR products was examined by raw data (**A**), standard curve (**B**), melt analysis (**C**) and analyzed with CFX Manager Software. PCR efficiencies were calculated from slope, and r^2.

APPENDIX B – CHAPTER 3 SUPPLEMENTAL MATERIAL

Supplemental Figure B.1 Localization and activity of mitochondrial targeted catalase in HCT116.
Supplemental Figure B.2 Seahorse XF Analyzer reveals cellular metabolic states.

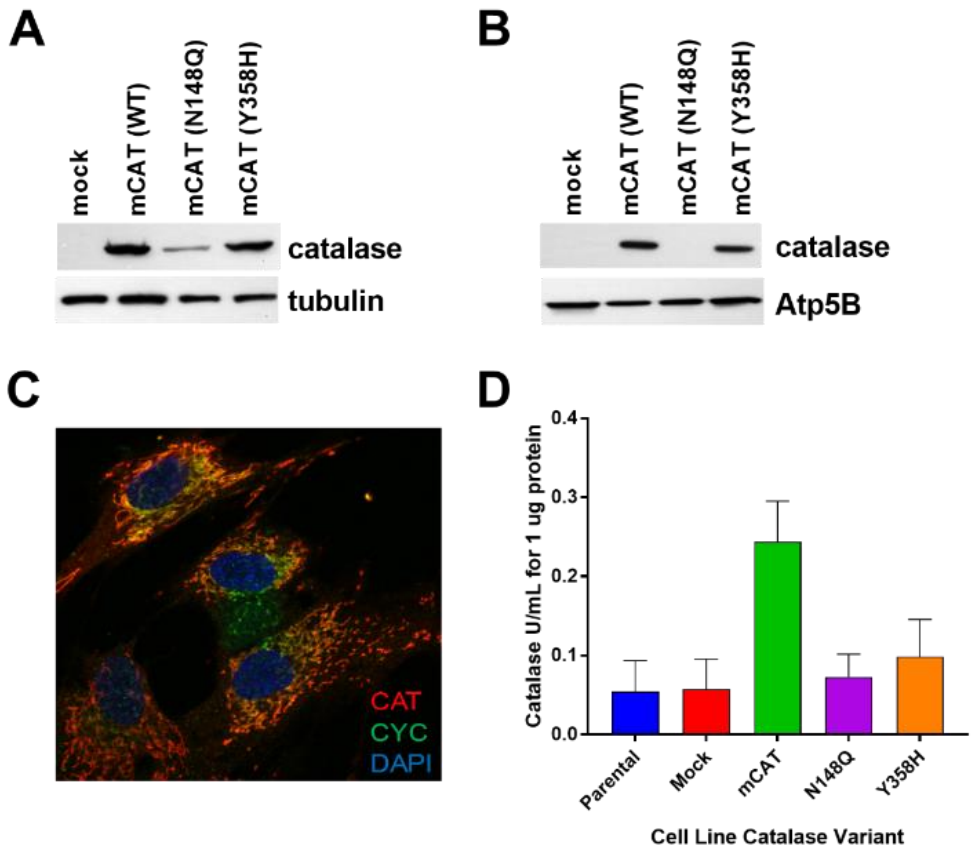

Supplemental Figure B.3 Localization and activity of mitochondrial targeted catalase in HCT116. (A) Western blots for catalase and β-tubulin from whole cell extracts from HCT116 lines transfected with mCAT constructs (N148Q and Y358H ablate catalase activity) or mock, GFP-only insert. (B) Western blots for catalase and mitochondrial ATP synthase subunit 5B from mitochondrial extracts of transfected cell lines. (C) Immunofluorescence imaging of HCT116 cells with fluorescent conjugated antibodies against catalase (CAT, red) or mitochondrial cytochrome c (CYC, green) along with DNA counterstain (DAPI, blue). (D) Catalase activity in whole cell extracts from HCT116 lines with or without transfection.

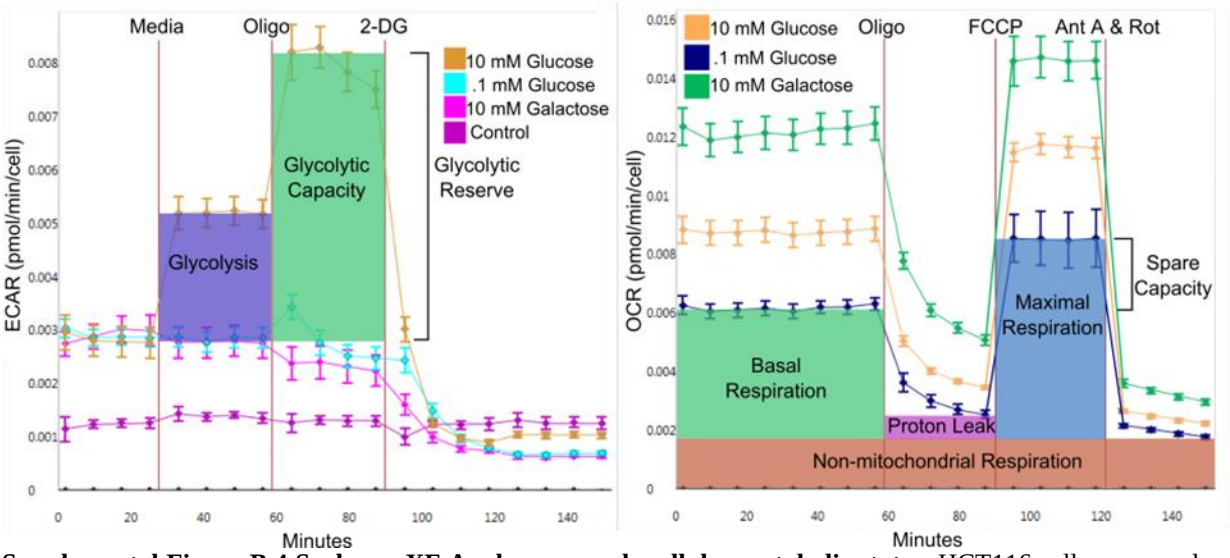

Supplemental Figure B.4 Seahorse XF Analyzer reveals cellular metabolic states. HCT116 cells were analyzed for glycolytic (Left) and respiratory (Right) capacity on glucose or galactose. Values for ECAR and OCR are normalized per cell. A saturating concentration of glucose (10mM) promotes glycolysis, yet galactose cannot support glycolysis to the same degree (Left). With only galactose as a substrate, cell respiration and max capacity are increased relative to glucose-only conditions (Right).

APPENDIX C – CHAPTER 4 SUPPLEMENTAL MATERIAL

Supplemental Figure C.1 Confocal microscopy visualizes SuperNova construct in the mitochondria.**Supplemental Figure C.2** Changes in mitochondrial copy number after

SuperNova and mDAAO treatments.

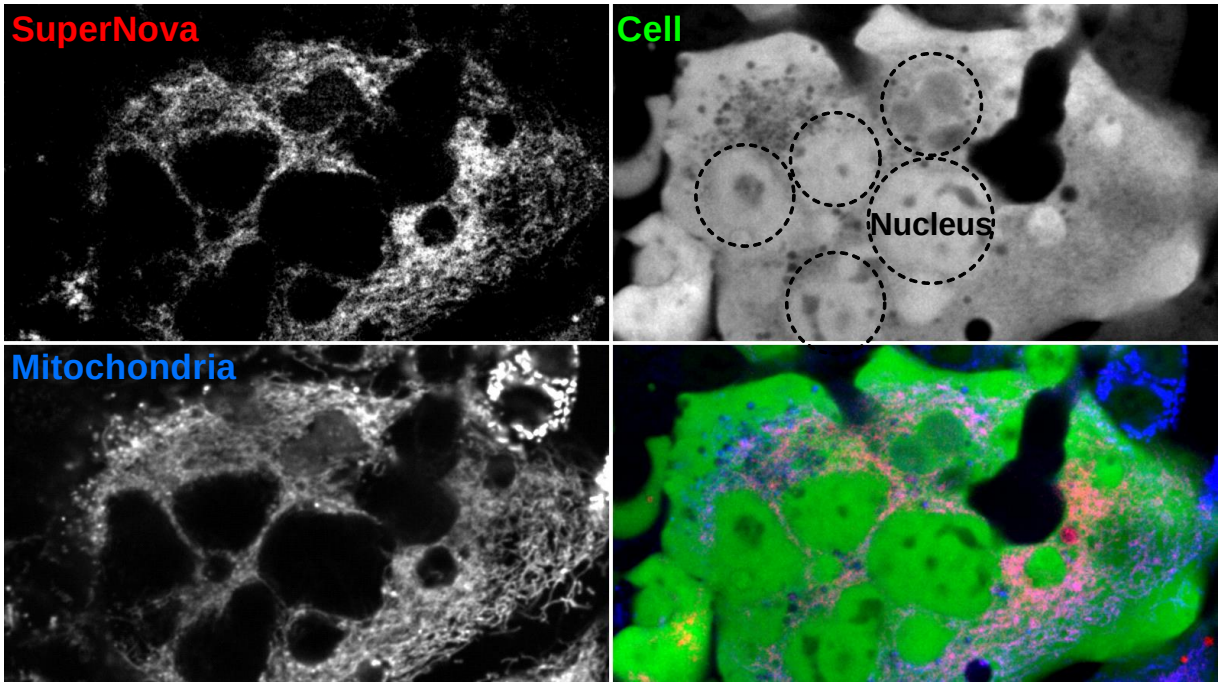

Supplemental Figure C.1 Confocal microscopy visualizes SuperNova construct in the mitochondria. HCT116 cells were transfected with a retroviral vectors consisting of a mitochondrial targeted form of SuperNova (in red) and an untargeted green fluorescent protein (GFP, "Cell"). Mitochondria were stained with MitoTracker Deep Red (blue, "Mitochondria), a dye which is taken up by cells into their mitochondria. The bottom right panel is the merged image. Images were collected using a spinning disc confocal microscope at 40× magnification.

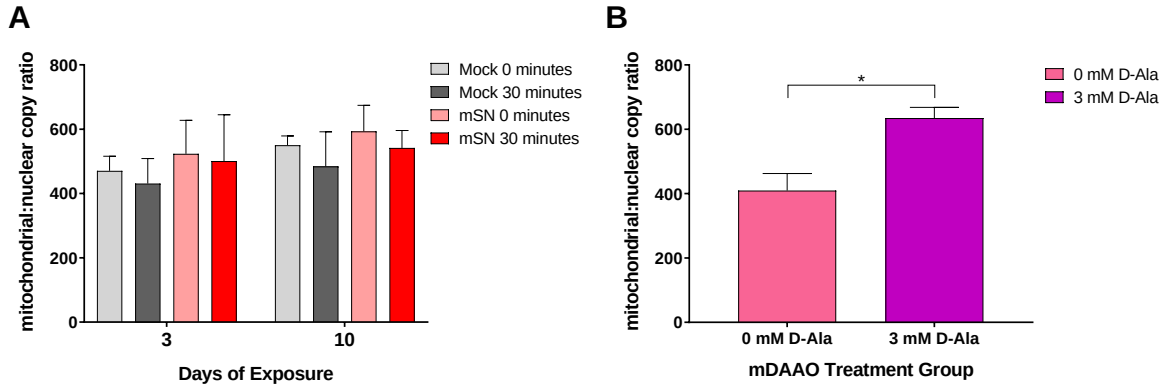

Supplemental Figure C.2 Changes in mitochondrial copy number after SuperNova and mDAAO treatments. (A) Mito-SuperNova cells and mock cells were treated for 0 or 30 minutes of amber light for 3 or 10 days. Results obtained from ddPCR quantification using mitochondrial control region and the nuclear RNaseP locus. N = 3 per condition, s.e.m reported. No significant differences by ANOVA. (B) Mitochondrial:nuclear copy number ratio after 26 days treatment and 4 rest days with daily additions of either 0 or 3 mM D-alanine. Results obtained as in (A), demonstrate a significant increase in mtDNA:nDNA (p = 0.0113 by unpaired, two-tailed student's t-test). N = 4 cohorts assayed in technical triplicate.

VITA

William Joseph Valente

Education

- **Medical Scientist Training Program** — *Entered 2011*
  University of Washington *Seattle, Washington*
  School of Medicine, Department of Molecular & Cellular Biology,
  Fred Hutchinson Cancer Research Center
  Anticipated graduation date 2019

  B.A. in Chemistry, B.A. in Spanish Studies — *2011*
  University of Minnesota *Minneapolis, MN*
  Minor in Biology; graduate *cum laude,* G.P.A. 3.72

- **Research History**

  Graduate Research Assistant to Dr. Jason Bielas — *2013 -*
  University of Washington, Fred Hutchinson Cancer Research Center
  Assayed apoptotic resistance in colorectal cancer cell lines to oxidative stress
  Performed measurements of induced mutation in mutagen-treated mice DNA

  Research Rotation with Dr. Jason Bielas — *2012*
  University of Washington, Fred Hutchinson Cancer Research Center
  Designed mitochondrial enrichment protocol using nuclear-specific restriction endonucleases and selective amplification

  Research Rotation with Dr. Antonio Bedalov — *2011*
  University of Washington, Fred Hutchinson Cancer Research Center
  Developed yeast lines for experimental analysis of replicative aging

  Research Assistant to Dr. Natalia Tretyakova — *2009 - 2011*
  University of Minnesota
  Honors Thesis: “Production of a Covalent Crosslink Between 8-Oxo-Guanine and a DNA Repair Enzyme”

  Research Assistant to Dr. Wayland Noland — *2008*
  University of Minnesota
  Developed and maintained reference system for identifying compounds of pharmaceutical interest

  Summer Research Assistant to Dr. Hendrik Viljoen — *2006 -2010*
  University of Nebraska
  Developed research protocol and guidelines in prototype design for point of care diagnostics involved in Mycobacterium tuberculosis detection

- **Awards and Honors**
  - Ruth L. Kirchstein NRSA Individual Predoctoral Fellowship (F30) – 2015 -
  - Genetic Approaches to Aging Training Grant Trainee (T32) – 2014 - 2015
  - Fellowship, Achievement Rewards for College Scientists (ARCS) Foundation – 2013 -
  - Member, Phi Beta Kappa Honor Society – 2010
  - Certification, Nationally Registered Emergency Medical Technician – 2009
  - National Scholarship Award - 2007
  - Presidential Scholars Award – University of Minnesota - 2007
  - Boy Scouts of America Eagle Scout Award - 2007

- **Peer-Reviewed Articles**

J Rose, J Stephany, WJ Valente, B Trevillian, H Dang, J Bielas, D Maly, D Fowler. Rapidly inducible Cas9 and DSB-ddPCR to probe editing kinetics. **Nature Methods**. 2017 September, 14(9):891-896.

G. Zheng, J. Terry, P. Belgrader, P. Ryvkin, Z. Bent, R. Wilson, S. Ziraldo, T. Wheeler, G. McDermott, J. Zhu, M. Gregory, J. Shuga, L. Montesclaros, J. Underwood, D. Masquelier, S. Nishimura, M. Schnall-Levin, P. Wyatt, C. Hindson, R. Bharadwaj, A. Wong, K. Ness, L. Beppu, H. Deeg, C. McFarland, K. Loeb, W.J. Valente, N. Ericson, E. Stevens, J. Radich, T. Mikkelsen, B. Hindson & J. Bielas. Massively parallel digital transcriptional profiling of single cells. **Nature Communications**. 2017 January; 8:14049.

W.J. Valente, N. Ericson, A. Long, P. White, F. Marchetti, J. Bielas. Mitochondrial DNA exhibits resistance to induced point and deletion mutations. **Nucleic Acids Research**. 2016 October; 44(18): 8513-8524.
* *NAR "Breakthrough Article"*

W.J. Valente, E. Pienaar, A. Fast, A. Fluitt, S.E. Whitney, R.J. Fenton, R.G. Barletta, O. Chacon, H.J. Viljoen. A kinetic study of in vitro lysis of mycobacterium smegmatis. **Chemical Engineering Science.** 2009 May; 63(9): 1944-1952.

Chapters

W.J. Valente and J. Bielas. "Deciphering the Role of Mitochondrial DNA Mutations in Cancer" in Mitochondria and Cancer, Elsevier Academic Press Inc., 2014.

Posters and Presentations

W.J. Valente, N. Ericson, A. Long, P. White, F. Marchetti, J. Bielas. "Mitochondrial DNA exhibits resistance to induced point and deletion mutations". Presented at the Environmental and Molecular Mutagenesis Society conference on September 25th, 2016.

W.J Valente, N. Ericson, K. Sheahan, M. Kulawiec, J. O'Sullivan, J. Salk, M. Vermulst, J. Bielas. "The Role of Cancer Metabolism in Mitochondrial DNA Mutagenesis and Chemoresistance". Presented at the Keystone Symposium: Integrating Metabolism and Tumor Biology January 16, 2015.

W.J. Valente, N. Ericson, P. White, F. Marchetti, J. Bielas. Induced Mutation in Mitochondria and Nuclear DNA. Presented at the Seattle Genetic Instability and Cancer Symposium April 23rd, 2014.